EUROPEAN COMMISSION
5th EURATOM FRAMEWORK PROGRAMME 1998-2002
KEY ACTION : NUCLEAR FISSION

HTR–M

European Project for the development of HTR Technology - Materials for the HTR

CONTRACT N°
FIKI-CT-2000-00032
&
FIKI-CT-2001-00135

Materials for Turbine: Synthesis of materials database

D. E. Buckthorpe
C. J. Earl

NNC

UK

Dissemination level : CO
Document Number: HTR-M-02/7-D-2-1-39
Deliverable 2.7

Materials for the Turbine: Synthesis of Materials Database

by

D. E. Buckthorpe

&

C. J. Earl

C6463/TR/013
Issue 02
August 2004

DOCUMENT ISSUE RECORD
(engineering documents)

Adding value through knowledge

Document Title :	Materials for the Turbine: Synthesis of materials database
Project Reference:	64631

Purpose of Issue : Initial version

Security Class : Commercial-in-Confidence

Issue	Description of Amendment	Originator/ Author	Checker	Approver	Date
01	First issue	D.E.Buckthorpe C.J.Earl	R.D.W.Bestwick	T. Lennox	July 2002
02	Final Issue including comments from HTR-M partners	D.E.Buckthorpe	R.D.W.Bestwick	T. Lennox	August 2004

Total number of pages:	Intro:	vi	Text	26	Tables	4	Figures	6	Appendices	A39, B16

Previous issues of this document shall be destroyed or marked **SUPERSEDED**

Distribution: S. Casalta (EU), SINTER, D. E. Buckthorpe, C.J Earl, A.A. Braithwaite, R.D.W. Bestwick, EDMS

3050aJan01 Controlling procedure - QP11, QP40 *Docprodref*

Table of Contents

List of Tables

List of Figures

Summary

This document contributes to the 5th Framework Project HTR-M, Work Package 2.2 and provides a summary of the results of a technical synthesis of the materials and the materials data for the turbine of the High Temperature Reactor accumulated over the first eighteen months if the project. As specified in the technical descriptions of the project the main aim is to review the materials and materials data for the discs and blades. The work is seen as a first step in supporting the decisions made on selection of materials for the evaluation and testing phases of the project.

1. Introduction

This document contributes to the 5th Framework Project HTR-M, Work Package 2.2 and represents a summary of the results of a technical synthesis of the materials and the materials data for the turbine of the High Temperature Reactor. The main purpose of the study is to review the materials and materials data for the discs and blades. The document summarises the results obtained during the first eighteen months of the HTR-M project and the collection of material information from published papers and other sources, plus, a first step in supporting the decisions made on material selection for the evaluation and testing phases of the work.

For the turbine components, especially the turbine discs and blades, criteria for material selection have been developed in Ref. 2. Candidate alloys for the disc must have a sound industrial base and be capable of production of large defect free ingots with good forging properties and proven thermal stability. For the turbine blade failure modes such as creep rupture strength, high cycle fatigue and low cycle fatigue have to be considered. Corrosion can cause a significant shortening of material creep life and acceleration of creep crack growth rates and issues that affect material behaviour as a result of the environment are also considered. The work involved a review of candidate alloys for the components along with descriptions of available properties.

For the database a limited number of materials has been chosen. The selected materials along with their properties are summarised in sections 4 to 6. The summary of materials property data identified in the literature search has been collated and produced in table form in Appendix A. This and further data collected as the project progresses is to be transferred into the required format for inclusion into the overall project database.

2. Turbine Material Considerations & Requirements

The turbine is housed within the power conversion system of the HTR and used to convert the thermal energy of the primary coolant into mechanical energy for power generation and other purposes. A synthesis of design use and specifications for the GT-MHR turbine is given in Ref. 1, which also provides available information on loading conditions and environment. An initial list of material requirements based on experience from aero-engine turbines has been developed by CEA in Ref. 2.

The current PBMR uses cooled discs and blades and has nominal first row temperatures of around 670-715^{o}C. Present versions of GT-MHR show no cooling with a nominal first row temperature of 850^{o}C. The operating temperatures of the two turbines therefore differ considerably although the stresses in the discs and blades are expected to be of a similar order (160 MPa) (Ref 46). The materials for the current versions of PBMR and GT-MHR are discussed furthering section 2.1.2.

2.1 Criteria for material selection

For the turbine components, especially the turbine discs and blades, the criteria for material selection are based on a safe operation period of 60,000 h at 3000 r.p.m. (50 Hz), with upper temperature limits in the range 850 to 950^{o}C. The main material considerations are those concerned with creep and environment. Two basic requirements dictate the design of gas turbine blades and discs, the cycle temperature and the maintenance of critical dimensions (clearances) throughout the service life. For turbine discs it is necessary to limit the permanent growth and distortion to within typical design life targets. This is usually achieved by maintaining a greater part of the disc cross section within elastic limits. Critical regions for the disc from the point of view of potential creep and fatigue failure are invariably the hottest parts. These are at the disc neck because of unrelieved high localised stresses giving rise to undetected growth, and at the rim, due to the additional geometric effects of the blade root slots and possibly cooling holes. Careful material selection or control of localised stress and temperature conditions can avoid creep-fatigue interaction problems in these areas.

The selection of turbine blade designs is limited by the high temperature creep properties of the material (i.e. non-cooled blade). For the turbine blades gas radial temperature variation often peaks typically in the middle third of the blade with steep temperature gradients across the blade section which vary according to the transient and steady state conditions. All regions of the blade profile therefore undergo complex stress-strain cycling with reversed plasticity in some areas. For material selection a close understanding of some important parameters such as creep rupture, creep ductility and creep rate are needed. Typically for nickel based super-alloys time dependent effects induced by creep and oxidation on cyclic crack growth rates are important for design, and hence an understanding of creep crack growth behaviour and the interaction between creep and fatigue with tensile and compressive dwells is needed. The awareness of the role of grain boundaries in high temperature fracture was important for the development of single crystal super-alloys that can give beneficial an-isotropic material properties. However for the HTR turbine blades such advanced blades are not thought to be necessary.

2.1.1 Initial review and database (Ref. 3)

A first attempt to clarify the selection criteria was made (Ref. 3). This identified several materials based on strength and creep rupture properties and discussed the effects of operation in a helium environment. A key issue for the disc is the potential for manufacturing suitably sized blanks for large discs such as for the GT-MHR design. Large ingots are needed (~10 tons) without solidification defects and attention must be paid to the amount of and the forging process used. Considered materials for the turbine disc include: A286 (Cr Ni Fe), Waspaloy, IN706, IN718, UDIMET 720 and an oxide dispersion alloy MA6000. Waspaloy, used extensively in the past is now being replaced by IN718 and UDIMET 720. Segregation problems during casting can occur with IN718, also because of low castability the production of large ingots has not so far been possible. IN706 with additional Mo and Nb allows for the manufacture of large discs but the process is very complex. The introduction of Hot Isostatically Pressed (HIP) material currently being investigated for the Fusion Reactor also offers the possibility of producing near finished sized components. There is some interest in ceramic forgings in Japan but tests have shown poor rotating properties. The most likely grades to be considered from this survey were IN718 and UDIMET 720 and these are the materials in which the main effort is currently being placed by turbine manufacturers.

For the turbine blade Ref. 3 investigated some nickel based and Molybdenum based alloys. Possible Nickel based alloys included 713LC, M21, MAR-M 004. Other alloys mentioned in the review included IN100, the current material for the PBMR, Nimonic 80A, Nimonic 90, 105 and 115, Udimet 520 & 700, IN591, IN738, IN792, Rene 80, M22, MAR-M 247, Nx 188 and FIS 145. The direction solidified (DS) grade allows blades to operate at higher temperatures, with still higher levels achieved through use of single crystal (SC) materials. A comparison of the creep rupture strength of several blade materials is shown in Fig. 1. For the Molybdenum based alloys TZM offered the highest strength but has not been used in industrial gas turbines and has poor corrosion resistance in air. German experience in helium showed some promise however its notch sensitivity (Fig. 2) and corrosion potential make it a less likely choice.

The effect of impurities within the helium environment is a critical issue that affects both the blades and the disc. The main concerns were corrosion effects on strength. Corrosion can cause a significant shortening of the material creep life and acceleration of creep crack growth rates. Helium impurities can influence creep properties due to oxidation and carburisation mechanisms. Below 577^{o}C corrosion of such alloys is limited. Between 577 & 900^{o}C chromium rich oxide scale can form, also carburisation and de-carburisation due to chemical action. For such temperatures there is a need to consider optimisation of alloy composition and coatings to limit damage to the blades. Application of suitable coatings can arrest creep reduction tendencies, however their use requires an understanding of the potential for interfacial cracking at the coating layer to avoid the development of more significant cracking from the interface. Use of coated materials can potentially allow a comparatively larger increase in operating temperature for a chosen blade material.

2.1.2 HTR Turbine candidate materials (Ref. 4)

A further review of possible materials has been made in Ref. 4. This document looks at candidate materials for discs, blades and the first stage stator. Included in the review are Russian material proposals for the GT-MHR disc (Zh56F & V2HL12U). The first contains more tungsten and niobium and the second more chromium, cobalt, molybdenum and titanium but less tungsten (see Table 2). The western material proposed for the GT-MHR is alloy MA 6000 which has a high strength at temperature. For the PBMR disc IN100 remains possible using powder metallurgy and the HIP process. With regard to the manufacturing process, the general recommendation is to go for a forged disc option rather than cast one.

For the turbine blades, the Russian proposal for GT-MHR is alloy Ch120M cast as a single crystal. If this proves to be unacceptable E929, E1893 and EP800 are proposed as a backup. E1893 does not contain any cobalt. The US equivalent of Ch120M is CMSX2 single crystal. The PBMR uses IN100, the same as for the disc. Other proposals for blade materials that are considered worthy of study include IN738 and IN792, CMSX4 and PWA1483 for single crystals and SC16 as a cobalt free single crystal blade. With regard to the manufacturing process, the improvement in properties provided by DS and SC blades comes from solidification under large thermal gradients. There is a degree of anisotropy in properties with both processes. The single crystal process is more difficult as the size and complexity of the blades increases.

For the turbine stator the Russian proposal for GT-MHR is ChS57. This may need to be classified as an ODS alloy. The Western equivalent is Hastelloy X. The low cobalt version is called Hastelloy XR (in Japan), and should offer similar mechanical properties.

The manufacturing implications of ODS material, also powder metallurgy and HIPing were reviewed. Single crystals, directionally and conventionally cast alloys should be hot isostatically pressed and characterised.

With regard to environment, the resistance of the materials to hot corrosion and oxidation were considered. The Al+Ti content are important also the quality of the oxide layer (Cr_2O_3 or Al_2O_3) depending on the Al/Cr in the materials. Al oxide formers (CMSX2, CMSX4, MAR M247DS, MAR M004) should be considered where carburising or de-carburising atmospheres can be completely excluded, and Cr formers (PWA 1483, IN792, SC16) where they cannot. Coatings were initially used to protect the hot sections from oxidation and corrosion. For the same considerations as the base material Cr rich coatings are preferred for situations were there is a potential for carburising and decarburising atmospheres, it is also much easier to achieve than Al rich coatings. Recent developments include a thermal barrier coating, achieved through vapour deposition or plasma spray, which allows a less heat resistant base material to be used.

The presence of cobalt and tantalum was discussed. For the disc there are no cobalt free materials proposed except MA6000 which may show fabrication difficulties with large diameters. Hastelloy XR which has a reduced cobalt content should also be considered as a possible candidate for a lower temperature disc application. For the turbine blades the number of cobalt free materials is very limited. The potential materials to study are MAR M004 (low Cr) or SC16 (high Cr). If the blades are coated the base material does not need to be cobalt free.

The report concludes by categorising the materials into four areas.

3. Candidate materials and properties

For the material selection, the key points are the first stage turbine discs and blades where the stresses and temperatures are the highest. Helium gas temperatures for the GT-MHR and PBMR industrial projects in these areas are of the order of 850-900^{o}C. The materials selected for these components should ensure a safe operation for at least 60000 hours. As discussed above the selection of high strength alloys to fulfil these requirements must take into account the corrosive actions of the environment as well as the need for high temperature strength. The materials listed in section 6 are those considered as potential candidates and for which some experimental experience at long endurance times exists (e.g. IN 617). Hastalloy X has also been included which is a favoured alloy for the turbine stator. Tables of properties for the materials have been assembled in Appendix A from the list of references investigated.

3.1 Turbine disc

Candidate alloys for the disc include A286 (Cr Ni Fe), IN706, IN718 and UDIMET 720. The introduction of HIP material currently being investigated for the Fusion Reactor also offers the possibility of producing near finished sized components suitable for turbine discs. Creep resistance is important.

A non-cooled disc operating at 850^{o}C may be too ambitious, therefore materials for a cooled design are also considered. Currently the best candidate material for the disc was thought to be UDIMET 720 although this is still under development. R&D work is ongoing to look at its production with coarse homogeneous grain size and appropriate heat treatment for creep. The maximum anticipated temperature for this material is thought to be around 700^{o}C. IN706 on the other hand operates successfully at temperatures of 600^{o}C (steam turbines). IN718, a further possible material, is near to commercial production but R& D is still required in order to control the grain size.

3.2 Turbine blade

Candidate alloys for the blade materials include Inconel MA 6000, DS IN792, DS CM 247 LC, etc. Materials for cooled and non-cooled blades are investigated (although the former clearly offers cost advantages) also materials with Al and Cr oxide formers because of the importance of environmental protection against the atmosphere (Ref. 3). The potential for using a Molybdenum based alloy (L-TZM) has also been considered. This material was investigated during the German HTR programme. The review includes available published properties for DS IN792, DS CM 247 LC, which are the candidate materials chosen for the blade tests.

3.3 Turbine Stator

Hastalloy X has been included which is a favoured alloy for the turbine stator, also IN617 which has an extensive library of material data archived from the German HTR programme.

4 Materials for the disc

At this stage, alloys containing substantial additions of cobalt or tantalum are included in the selection. Many of the high temperature alloys with these elements have the highest mechanical properties.

4.1 UDIMET 720

Udimet 720 is a material that combines high temperature strength with large diameter manufacturing potential. Udimet 720 is a nickel base alloy (commercial designation of Aubert et Duval the French producer of the alloy is PER 72) that achieves its strength due to its γ' $Ni_3(Al,Ti)$ precipitate duplex microstructure (coarse and fine) obtained by heat treatment (Ref. 7). Billets of up to 250 mm diameter have been produced by forging also the material can be processed by powder metallurgy and hot isostatic pressing (HIP) which is expected to be required to produce larger diameter discs.

Ref. 19 considers the tensile and creep properties of the material when applied to the hub of an advanced turbine disc as part of a series of bonding trials for dual alloy discs. The rim alloy used in this case was Mar M 247 LC. The billets were produced using the HIP process with grain sizes of ASTM 9 to 10. The materials were subjected to additional heat treatments to access the effect of thermal cycle exposure and to two HIP bonding cycles a) 2050°F/15ksi/4h and b) 2165°F/25ksi/4h, the latter producing better properties. A tenfold increase was reported in creep rupture life (15h v 160h) and a fourfold increase in elongation (6% v 23%) at 1300oF/ 100ksi. The material received a 2050°F/4h solution and 1400°F/8h + 1200oF/24h age cycles. Hafnium oxide formation in the diffusion-bonded region, which resulted in decreased ductility and planar failures, remains to be addressed for this type of disc.

A comparison of material and industrial capability alongside other potential alloys IN718 & IN706 is shown in Table 1. This alloy is considered the most promising of the Ni based super-alloys for the turbine disc application. Only the oxide dispersion strengthened (ODS) material (such as MA 6000) offers greater potential strength at higher temperatures (945°C/140 MPa for 1000 h). The manufacturing route of UDIMET 720 is however significantly more mature than MA 6000, which requires much work to produce large ingots with homogeneous mechanical properties.

4.2 IN 718

Incoloy 718 (IN718) is a precipitation-strengthened nickel based super-alloy with additions of Cr, Fe, Co, Mo, Ti and Al. It is extensively used for gas turbine discs, which experience long periods at high temperature in an oxidising environment. Its main precipitation strengthening constituent is γ" Ni_3 (Nb, Al, Ti,) with some additional strengthening provided by γ' Ni_3(Al, Ti, Nb). Its deformation under tensile and fatigue loading is therefore quite different from γ' strengthened alloys. It has good oxidation and creep resistance at temperatures up to 650°C, plus high strength and fatigue resistance.

Results at temperatures below 700°C have been generally reported. Some service failures are known to be have resulted from the formation of inhomogeneous deformation bands (mechanical twins) during creep rupture at temperatures below 650°C. Such failures were also observed at higher temperature. Ref. 68 reports results of creep rupture and creep deformation tests between 704 and 871°C in the stress range 80-520 MPa. Deformation bands were shown to be responsible for crystallographic failures during creep rupture up to 760°C whereas above 816°C grain boundary failure plus creep voiding at grain boundaries occurs. Scatterband of creep rupture data at 650 and 850°C is given in Ref. 45 for times up to 10^4 h and compared with results for brazed and welded specimens.

A study on the role of (Nb, Ti) C carbides on fatigue crack initiation has been made in Ref. 69. Oxidised sub-surface carbides were thought to be a major cause of crack initiation at 600°C. Room temperature tests suggest that the cause may be due to local straining causing a rupture of the matrix. Fatigue tests in air at 600°C also showed a beneficial effect of dwell time on fatigue life.

The effect of oxygen and water vapour on the time dependent crack propagation behaviour of the material is investigated in Ref. 18. Both oxygen and water can accelerate crack growth. Their effects however appear to be largely independent of one another. For H_2/ H_2O/inert gas environments a transition from fast to slow crack growth rates is associated with the formation of oxides at the crack tip. Co and Ni rich oxides form at higher crack growth rates and Cr rich oxides at lower crack growth rates. Such oxides are similarly expected to form under cycle dependent loading conditions. In environments containing very small quantities of oxygen and water vapour, the Cr rich oxide phase at the crack tip is expected to remain stable even under high local deformation.

4.3 IN 706

Incoloy 706 is an age hardened Ni-Fe-Cr super alloy developed from IN718. It has reduced Ni, Nb and Mo and is more easily forged, welded and machined than IN718. Ref. 20 proposes two heat treatments to attain optimum stress to rupture properties and tensile properties. Elevated temperature tensile and fracture test were carried out at 538 and 649°C. Fatigue crack growth tests were performed (10 Hz, R= 0.1) with the specimens pre-cracked at room temperature, heated to the test temperature, soaked and then tested. The intermediate step of 843°C for 3 h with an air cool for improved stress rupture properties reduced the static crack growth rates at 649°C by more than 15 times. The fatigue crack growth rates were however shown to be similar at the two temperatures. Further investigation of heat treatments is given in Ref. 21. This looks at the effect of ageing treatments on fatigue properties in air and in a vacuum. No environmental effect was observed. The fatigue tests were performed at 399^{o}C. Rapid cooling rates appear to be the most effective in improving low cycle fatigue when carried out in conjunction with shorter solution times however the latter had a possible negative effect on dislocation density with respect to the ageing treatment.

4.4 IN 100

IN100 is the reference material for the current PBMR design of the turbine disc and blades. The material is a γ' Ni_3 (Al, Ti,) strengthened nickel based super-alloy with good carburisation resistance. It can be easily forged or cast to form components such as turbine discs, blades and vanes. The material forms a thin protective aluminium oxide surface scale on exposure to HTRG helium. As with other similar Ni based super-alloys low cycle fatigue cracking is appreciably enhanced by oxidation both in terms of numbers of cracks and cycles. Ref. 44 gives results for 0.3mm deep cracks in which the initiation is enhanced by an order of magnitude at 1000^{o}C. Ref. 9 reports results for bulk carbon changes after exposure up to 4000h at 900^{o}C.

Low cycle fatigue behaviour of the material when used as a disc alloy is investigated at 649^{o}C in Ref. 29 as part of a study into the applicability of strain range partitioning (SRP). The material is produced in the forged condition (Gatorised). Heat treatment consisted of solution treatment, stabilisation and precipitation hardening. Tests were performed over a range of frequencies and with tensile holds. Another application of the method at 760^{o}C (Gatorised) and 925^{o}C (cast) is reported in Ref. 28. A further application of the SRP method to IN100 turbine blade material (alumina coating) at 900 and 1000^{o}C is given in Ref. 30 together with results for the continuous damage approach. The 1000h rupture stress at 649, 900, 925 and 1000^{o}C are given as 880, 187, 158.6 and 82 MPa respectively in the three documents. Tabulated results from the SRP programme (including raw data) are given in Ref. 8. Ref. 42 also reports results at 800^{o}C in air and contaminated gases.

4.5 Inconel MA6000

Inconel MA6000 is an oxide dispersion and γ' strengthened nickel based alloy with good oxidation resistance. It has good high temperature strength, and its rupture strength decreases slowly with increasing temperature suggesting a levelling off of the Larson-Miller curve (Ref. 13-which shows stress to rupture results at temperatures between 750 and 950^{o}C). It also has excellent corrosion/oxidation resistance. Ref. 5 compares the 10,000h rupture strength with IN738 at temperatures up to 1050^{o}C suggesting an operating temperature advantage of 160^{o}C.

Low cycle fatigue properties are investigated in Refs. 32 & 33, which provide tabulated results at temperatures of 750 to 1050^{o}C. Its cyclic life is comparable or better than IN738 LC. During the tests the material did not cyclically harden or soften giving near constant stress-deformation curves with failure preceded by a sudden drop in the stress range. Assessment of the fracture behaviour however showed the material to be rather brittle with evidence in Ref. 33 that the grain boundaries had been torn apart at failure. Further fatigue lives at 850^{o}C are given in Ref. 32. The effect of varying the strain rate was small at this temperature suggesting the effect of time dependent damage at this temperature is also small (transgrannular cracking). At 1050^{o}C there is a marked dependence of strain rate on life suggesting that the interaction of fatigue with creep, oxidation or degradation is more likely (mixed intergrannular/ transgrannular cracking). The initiation phase of failure takes up a significant proportion of the fatigue life with subsequent crack growth at a very high rate.

4.6 ZhS6F

Ni based precision investment cast alloy proposed by OKBM for the GT-MHR turbine disc (Ref. 46). The alloy contains chromium, cobalt, molybdenum, tungsten, titanium, aluminium, niobium, vanadium and hafnium. Cast parts are not used for large disks in aero-engines and consideration must be given to the viability of manufacturing a large disc in this way.

4.7 VZhL12U

VZhL12U is also proposed for GTMHR by OKBM. This material has more chromium, cobalt, molybdenum and titanium but less tungsten than ZhS6f and no hafnium.

4.8 Ceramics

Strength and fabricability of ceramics has considerably improved in recent years, with much of the progress being made in Japan. Ceramic blades and vanes have been studied with most progress being made on vanes, demonstrating that Si_3N_4 vanes are capable of operation at temperatures of 1300^{o}C for several hours. This appears to be an upper temperature because of oxidation resistance and strength. Conservative comparisons of rupture strength with MA 6000 and IN738 material are made in Ref. 5 suggesting a 10000h rupture stress in excess of 200Mpa is achievable at temperatures of 1150^{o}C. Fibre reinforced ceramics are also under investigation in Japan (SiC fibres) to improve toughness.

5 Materials for the blade

5.1 DS IN 792

The chemical analysis of IN792 is very similar to IN738. Developed for higher strength at the expense of corrosion, IN792 contains higher amounts of niobium, tantalum, cobalt, tungsten and titanium with slightly lower chromium content than IN738 and additions of hafnium. Ref. 7 suggests an advantage of 30°C in high temperature strength for IN792 (10°C over IN100) and that the directionally solidified (DS) version of IN792 produces a further improvement in high temperature strength of around 25°C.

Creep and crack growth behaviour of IN792 has been investigated in Ref. 17 at a temperature of 927^{o}C. The tests were done in air, vacuum and impure helium. Generally crack growth behaviour for IN792 was similar to IN738. IN792 had the best resistance to crack growth in air and IN738 the worst. The crack growth resistance in a vacuum and in helium were similar and showed a similar crack growth resistance for both materials.

5.2 DS CM 247 LC

MAR M 247 the material from which CM 247 LC alloy is derived, is an aluminium oxide former with low values of Ti/Al ratio (Ti/Al < 0.2). The CM 247 LC alloy designed for blades and vanes of aeroturbines has reduced carbon (approximately one half), improved stability and alloy ductility plus reductions of Zr and Ti to improve grain boundary cracking without sacrificing strength. The W and Mo levels are reduced to minimise the formation of undesirable effects resulting from carbide degeneration (Ref. 36). The material has been used successfully in industrial turbines with a ductile high chromium coating for resistance to hot corrosion attack. It offers better castability, higher strength, improved oxidation resistance and greater process flexibility than IN738 or IN792. In terms of metal temperature capability the DS CM 247 LC version of the material is expected to provide a 50°C greater temperature at stress levels of 138-207 MPa (20-30 ksi) compared with IN 738.

Ref. 19 considers the use of Mar M 247 LC the material in spraycast-X form for the rim of a turbine disc bonded on to a hub manufactured from Udimet 720. Results from mechanical test (tensile and stress rupture) in a solution treated and aged condition showed higher strength than conventionally cast material because of the inherent fine grain structure. The average stress to rupture life was however slightly lower but it was considered that a higher temperature solution and age treatment would improve this.

Low cycle fatigue tension-torsion multiaxial results for MAR 247LC DS are given in Ref. 79 at 900°C along with IN738 LC, DS Rene 80 and SC CMSX-2.

5.3 L- TZM

Investigation of TZM material was carried out within the HHT materials programme (Refs. 10, 15). This is a Molybdenum based alloy that has excellent creep strength at high temperatures but is known to be brittle at temperatures up to 360-440°C. Its notch sensitivity remains high at HTGR service temperature (figure 2). It is considered unsuitable for oxidising atmospheres because of the volatility of Molybdenum oxide however in HTRG helium atmospheres such a risk is expected to be negligible (up to 1000°C) except in the case of massive air ingress.

Its high melting point (2607°C) contributes to a very flat creep rupture strength curve compared with other Ni based turbine blade materials (Fig. 1) and therefore makes it a potential candidate for service periods in excess of 60000h (Ref. 10). Its corrosion behaviour within a HTRG atmosphere has been studied using HHT test impurity levels and these were not sufficient to form surface oxides (impurity levels in μbar: $50H_2$, $5H_2O$, 50CO, $5CO_2$, $5CH_4$ and $5N_2$). Fatigue tests at Room temperature and 850°C (between 10 and 50Hz) for different levels of coldwork suggest a similar scatter band to IN713 LC. The less worked TZM is at the lower end of the scatter band and the highly worked material at the upper end. When introducing the effects of hold time, the TZM alloy reaches a higher lifetime than IN713 LC under similar conditions.

Creep rupture and corrosion testing of vacuum arc-melted Mo-TZM , 53% worked, in simulated helium environment is reported in Ref. 58. Its extrapolated 100000h creep rupture strength of 340 MPa at 850°C was more than three times higher than that of IN738 LC. Microstructure analysis identified the Mo_2C layer on the surface however this did not initiate failures under steady state conditions. Experiments after 36000h creep testing showed a reduction in plastic strain to failure although widespread cracking of the gauge length was not found. Tensile test at 500°C on a 35000h creep tested specimen showed that initiated cracks stopped at the metal-carbide interface.

Ref. 12 reports on the results from a powder metallurgy (PM) produced Mo-TZM blade. Hardness, tensile strength and ductility, impact energy, fatigue and creep rupture behaviour were all measured for different parts of the blade. Also some pullout tests were carried out on the blade fastenings. Certain weak points were identified in the case of large forgings: insufficient strength in the air foil/root transition zone, too high a ductile brittle transition temperature, insufficient fatigue strength under reversed bending fatigue in the air/foil transition zone. Further work was done to improve the quality of the starting material and an improved version was found which was considered to give acceptable properties in these areas. However due to shortage of material for testing further evaluation was not done. It was recommended that testing was carried out to quantify and substantiate improvements particularly in the ductile-brittle transition temperature.

5.3 IN713

Alloy 713LC is a chromium molybdenum aluminium and niobium nickel base alloy with a low cobalt content. The material has been extensively tested over the years and has become almost a reference material for comparing against new and developing alloys for turbine applications. It also has the advantage of a wide industrial experience in conventional gas turbines. The lack of Co and Ta means it should not present any activation problems when used in HTGR atmospheres, it can however be susceptible to carburisation and sulfidation and may therefore require coating (Ref. 46). The DS or SC versions overcome this but contain more cobalt (10%). IN713 C also suffers from over-temperature damage (occurs in aero-engines during startup) which can blister the coating and substantially alter the creep behaviour (removal of tertiary creep phase). Such effects cannot be reversed by heat treatment and the blades have to be rejected (Ref. 38).

Inconel 713 was one of the turbine blade reference alloys selected for testing within the Dragon metals programme of the 1970's and has been used for the fabrication of blades for the German project HHV (a full scale test turbine driven by HTGR – type helium). During the short high temperature lifetime experienced by the blades (325h at 850^{o}C) no problems were encountered.

Creep and long term stress to rupture properties have been investigated in Ref. 16 as part of the NRIM data sheet programme. Several super alloys were sampled in the programme with data points beyond 50000h (Fig. 3), for IN713 C the longest data point available is for 52149h at a temperature of 850^{o}C (S-108Mpa). Results are available for multiple heats (8) and temperatures between 850-1000^{o}C. The paper looks at the time temperature parameter (TTP) and the Larson-Miller methods of correlation and extrapolation of data. The temperature dependence of 100000 rupture strength for IN713 C against other alloys is given in Fig. 3. As shown by Fig.1 a rapid fall off in strength occurs with temperature for this alloy (Ref. 15).

Creep rupture tests were also carried out in air and an HHT helium atmosphere (Ref.10, 58). Test results of five heats are shown in Figure 4. The effect of the helium atmosphere was not found to be significant and for the period reviewed. Creep rupture strength decrease sharply with temperature, and the rupture ductility drops to just a few percent between 500-750^{o}C. Test durations of about 44000h in air and 37000h in impure helium were achieved. Results of low cycle fatigue tests are also reported at room temperature, 650 and 750^{o}C with and without hold times of up to 20min at the tensile and compressive maximum. The effect of the 20min hold times at 750^{o}C was to reduce the fatigue life by more than an order of magnitude due to the effects of creep.

5.4 IN 738

IN 738 LC has been widely used for large land based gas turbine blade applications. The effect of environment on creep and fatigue behaviour plus crack growth rates has been studied by numerous authors (Refs. 7, 17, 23-27, 37, 39, 42-45, 76) through tests in air, vacuum and hot corrosive environments. Crack growth rates (927^{o}C) were generally higher in air than a vacuum (Ref. 17). Tests in air and vacuum were also conducted at 900^{o}C (Ref. 76) and Ref. 26 discusses results at 850^{o}C for different strain rates. The higher strain rate gave a longer life in air, but the strain rate influence disappeared under a vacuum, also the fatigue life is greater. The effect of different cyclic wave forms was investigated in Ref. 23 from tests in air at 850^{o}C. Generally shorter lives to crack initiation were experienced by wave shapes with the dwells/slow strain rates in compression or tension. Tests in impure helium suggest fatigue results should not differ markedly from those for a vacuum. (Ref. 17).

5.5 M 21

Alloy M21 chosen as one of the reference blade alloys for the Dragon project, its a cobalt free low chromium high aluminium nickel based alloy that combines precipitation hardening with solid solution hardening (~10% addition of Tungsten). Its corrosion in HTRG helium is not as good as IN713 LC or IN738 (the ratio of Al/Ti is <1).

5.6 SC 16

SC16 is a cobalt free γ' hardened high chromium turbine blade material, its Ti/Al ratio is close to unity making it a chromium former (i.e. produces a chromium oxide layer in HTRG helium) material. Proposed as a single crystal (SC) alloy (Ref. 4) it's expected to provide an increase in temperature of up to 60^{o}C compared with IN738, potentially a similar temperature capability (in terms of creep rupture strength over 10000h) as DS CM 247 LC (Ref. 5).

5.7 MAR M 004

MAR M 004 is developed from IN713 LC and has a similar creep rupture strength (Fig. 5). The alloy is a cobalt free aluminium oxide former alloy (Ti/Al < 0.2), which has a good resistance to corrosion in a HTRG helium environment (Fig. 3) and includes hafnium for better toughness.

5.8 Nimonic 80A

Nimonic 80A has relatively lower creep rupture strength than for example IN713 LC and is only suitable for lower service temperature operation (Fig. 5) but could be considered for the last row of blades. Data in the form of uni-axial creep strain curves at 650 & 750^{o}C (currently available on Alloys-DB) have been provided by FZJ (see typically Fig. 6). Creep rupture values at 10000, 30000 and 100000h are also available from the German standard (DIN 17240) for heat-resisting materials used for bolts and nuts.

5.9 Ch120M

This is a Russian proposed nickel based alloy used in casting or single crystal form. The single crystal alloy is close to the CSMX-2 grade (Ref. 46).

5.10 E1929, E1893, EP800

Three forged materials proposed by OKBM for GT-MHR as a backup if Ch120M is not accepted. They are nickel base alloys with chromium, molybdenum tungsten and aluminium. E1893 is cobalt free and EP800 has niobium instead of titanium (Ref. 4).

6. Materials for the Stator & other components

6.1 Hastelloy XR

Hastelloy X is a well established Ni based alloy for ducts, casings and linings. A low Co version of the alloy has been developed in Japan (called Hastelloy XR) for application to HTRG and is used as the structural material for the HTTR. Information on most properties is available, also for weldments. Data has also been produced under irradiated conditions (Ref. 49). Fig. 10 shows a comparison of creep rupture results under thermal fluence between Hastelloy X and Alloy 800. Extensive work has also been done of the effects of environment, including simulated HTGR environments which demonstrates the superiority of iron-based alloys compared with Ni rich alloys. From the testing of the alloy for the HTR reactor application the following key issues were identified as requiring further work:

Excessive loss of toughness and ductility that occurs due to thermal aging
Significant creep at high temperature
Effect of creep on fatigue
Strain softening at high temperature
Mechanical properties in the weld zone
Effect of corrosion on mechanical properties in HTR environments

6.2 Chs57

This is Russian proposed material for GTMHR turbine stator which compares favourably with Hastalloy X. It's a chromium tungsten molybdenum base nickel alloy which may also contain amounts of zirconium (0-15 %) and ytrium (0.05 %). It is not clear whether this is an (Oxide Dispersion Strengthened) ODS alloy.

6.3 IN 617

Developed in the early 1970's this alloy was used for combustion components, transition ducting and exhaust system components of aircraft and land based turbines. It was also considered for use in the high temperature ducts and casings of the primary circuit of the Dragon and HHT projects. It has good structural high temperature stability, fatigue strength and long term strength. It shows excellent resistance to corrosion/oxidation and is easily formed and welded (Ref. 40).

A Ni-Cr-Co-Mo alloy with ~1.2% Al, the material has been extensively tested within the German HTR programme (Ref. 51) and a comprehensive set of material information and data has been established up to temperatures of around 1000^{o}C. This includes physical and mechanical properties, isocronous curves, fatigue and creep rupture data (Ref. 78). Fig.7 compares 60000h creep rupture strength with comparable results for some turbine blade alloys (Ref. 78). The test work on IN617 includes results in an impure helium environment plus creep rupture test results that extend up to 64000h (Fig. 8).

7. Main Findings

7.1 Review

This review of candidate materials for the turbine has been performed as a first step towards selection of materials for the disc and blades of future HTRs. The most notable alloys from the review are to be considered for inclusion in the materials database. Additional review documents are also available (Refs. 2 to 4) prepared by HTR-M partners that discuss some of the issues in more detail.

The review has considered eight potential materials for the turbine disc, thirteen for the blade (including the Russian backup options) and three structural materials for the stator and ducting, etc. Creep resistance and high temperature strength are important requirements and expected to be a main selection criteria.

Discussions with a turbine materials manufacturer Aubert & Duval together with the results from a review of published information identified UDIMET 720 as the best available candidate for the turbine disc. UDIMET 720 is still under development and the current view is that it may not be usefully applicable for discs above 700^{o}C. This suggests that a cooled disc may be necessary.

UDIMET 720 can be processed by powder metallurgy and hot isostatic pressing (HIP), and this is considered necessary to produce larger diameter discs. The literature search produced very few published data on this material. This shortage of data will clearly be addressed during the testing phases of HTR-M/M1. This material has been chosen for short term testing within the HTR-M programme (section 7.7). Of the several materials examined only the oxide dispersion strengthened (ODS) material (MA 6000) looked capable of providing greater strength at higher temperatures (Fig. 11), but its manufacturing route still requires significant work.

From the blade materials investigated the best potential long term creep strength was provided by the Molybdenum based alloy -TZM. This has seen a significant amount of testing within the German HTR programme but its high ductile brittle transition temperature appears to make it a less practical option compared with Ni based alloys. This material is however to be included in the database and its suitability for future application will be assessed as further information is gathered.

From the Ni based super alloys, the most promising in terms of creep strength are the single crystal alloy SC CMSX-4, the direction solidified DS CM 247LC (plus MAR M247), (Fig. 7) and IN100 (Fig. 9). From published data, these are expected to have a creep rupture strength of the order of 150-200Mpa at 850^{o}C after 60, 000h (which compares with the preliminary stress values of 160MPa in section 2 Ref 46). DS IN792 is also included in this group since it is expected to have a 35^{o}C advantage over IN100. A cobalt free option to these materials would be SC 16, which is similar in strength to DS CM247 LC. The Russian alloy Ch120M is comparable to the single crystal CSMX-2 grade and therefore also offers potential. It should be noted however that an additional design margin of around 2.0 on stress would normally be required for nuclear components important to safety. The need for such a factor for the turbine would need to be reviewed. Alloys IN713 LC and IN738 LC although well established as turbine blade materials are expected to have much lower strengths (<100 MPa). These properties will however be included in the database.

For the stator and ducting materials, Hastelloy XR and IN617 are potential materials, being extensively tested in Japanese and German HTR programmes.

7.2 Manufacturing considerations

The manufacturing route and capability has a direct bearing on the material selection and strength. For the disc there is a requirement to produce large ingots without porosity and segregation. Such a process requires the production of around 10 ton ingots with subsequent forging. For aero-engines the manufacturing route includes re-melting technology (vacuum induction melting, vacuum arc re-melting, electro-slag re-melting) in order to produce large diameters however with current alloys discs produced in this way have reached the limit of their performance.

Powder metallurgy offers a route for high quality ingots to be produced. The possibility of producing near-shaped large diameter discs using Hot Isostatic Pressing (HIPping) seems more promising, following the availability of large diameter hipping furnaces (~1.4 m). Examples of discs or parts of discs produced in this way were identified in the references (e.g. UDIMET 520, Ref. 19). Subsequent heat treatments were shown to have a significant effect on the high temperature strength properties.

The future possibility of a bonded disc produced in this way should also not be discounted. HIPping produces materials with design properties different from those of the corresponding forged or cast alloy.

With respect to the manufacture of blades, single crystals offer the highest creep properties but their cost is high, properties can be an-isotropic and they cannot be easily repaired if damaged. Directionally solidified blades are good candidates for non-cooled blades. They offer improved creep properties compared with conventionally cast versions, better repair possibilities and their experience in industrial land-based gas turbines is more extensive. Conventionally cast grades are easy to procure, have extensive industrial experience and the fabrication of HTR blades should be possible. However, the major limitation is the modest creep strength at 850°C.

If a SC blade were chosen the most likely candidates would be PWA 1483 (Cr-oxide former) and CMSX4 (an Al-oxide former). For a DS blade suitable materials would be DS IN 792 LC (Cr-oxide former) and CM 247 LC DS (Al-oxide former). These latter materials were in fact chosen for the HTR-M/M1 tests. In the case of a conventionally cast blade (which could be used if the blade was cooled) IN792 (Cr-oxide former) and MAR M247 (Al-oxide former) are possible candidates.

For the manufacture of a component using an ODS alloy, active co-operation with a producer of the alloy is necessary. It is possible to produce a material that has design material properties quite different from those of the matrix alloy.

7.3 Environment

The corrosion resistance of alloys in HTR helium depends on the levels of minor reactive elements as well as the main alloy constituents. The environment in an HTR is composed of helium with impurities as CH_4, CO, H_2O and H_2 at μbar levels. Depending on the partial pressure of the impurities, the atmosphere can be either oxidising (high P_{O2}, low a_c) or carburising (low P_{O2}, high a_c) for the alloys selected. The carburisation can be limited by a protective Cr-oxide layer, provided that the oxygen partial pressure is sufficiently high for a stable Cr oxide scale to be formed.

The potential for carburisation or decarburisation is an important material selection criteria. Tests in IN617 have shown that the effect of such carbon transfer can have a significant effect on turbine disc and blade alloys and may result in significant reductions in creep strength. Doping the atmosphere with carbon monoxide alleviates the carburising effect.

Experience from the past German projects has shown that the oxygen partial pressure may not, in all cases, be high enough for the formation of a stable Cr-oxide scale. In such a case Al-oxide formers should be considered in the selection of blade alloys since Al-oxide forms even at extremely low oxygen partial pressures.

7.4 Coatings

Coating of the blades is considered necessary for long life. A base material with adequate corrosion resistance is also needed even in the case of a coated blade. Coating must be of the same type (chromium oxide former or aluminium oxide former) as the base alloy.

For turbines aluminide coatings have been developed for resistance to oxidation. Metal, chromium, aluminium and yttrium coatings (MCrAlY, metal M being nickel, cobalt or iron) are used for hot corrosion. Thermal barrier coating (TBC) involving a second porous coating can be used to give an additional temperature advantage (of up to 100°C). Deposition of such coatings is done using vapour deposition (EP-PVD) or plasma spray.

The choice of the best coating remains to be made for HTR helium environment in the 6FP and its durability assessed.

7.5 Alloying elements

The presence of alloying elements in the materials such as cobalt (which is in most of the currently available turbine disc and blade materials) is a further area of investigation. The main issues are the potential for plate out and lift off of particles and their activation and prevention of them flowing through the core. The current view is that the amount of Co present in the alloys should not present any serious drawback towards selection.

In the case of a coated blade the alloying elements in the coating is important and should be confirmed for suitability.

7.6 Materials database

The materials chosen for inclusion in the database are to be taken from the list of materials considered in this report. The review identified general information on tensile, creep and fatigue strength plus results on fracture/crack growth behaviour. Information on physical properties (Young's Modulus, conductivity, etc.) was limited. No information was found for turbine disc and blade materials subjected to low levels of irradiation. The available tabulated data from the review plus graphical information on relative properties is included for each alloy in Appendix A.

The format for the materials database will be as presented in Ref. 80. The system consists of a series of linked Excel worksheets. For a series of test results on a particular material, information on the test material is entered and identified by a unique number. Results from tests on this material are then entered into associated worksheets with each set accompanied by the material unique number so that necessary material information can be retrieved when necessary. The datasheets contain information relating to the material production and compositional information (recorded on a separate sheet). If the test material involves a weldment, then two additional sheets are used to allow details of the weld consumable and of the weldment itself to be entered.

The extent and the precise format of the test worksheets are governed by the requirements of the data. The information includes available data on fracture toughness, creep properties, impact and fatigue crack growth properties and endurance (including specimen details, etc.) where available. For each particular property, it is intended to include a separate sheet on design (or assessment) data, from codes and standards. This would allow comparisons to be made between experimental data recorded on the database and the equivalent design data. The design data would be stored on the sheets as sets of XY pairs and represented by an equation if appropriate. Where only graphical information is available (without data points) the data is to be digitised.

It is proposed to transfer the information on the database Excel sheets on to Alloys-DB in stages throughout the project.

7.7 Material selection for experiments

The choice of the materials for the short and medium experiments of HTR-M & M1 are the following.

Turbine disc:	UDIMET 720
Turbine blade:	IN792 DS
	CM 247 LC DS

The test information gained during the HTR-M & M1 project will be included in the database. For the turbine blade tests direction solidified chromium former and aluminium former materials have been selected. The current view is to avoid single crystal materials if possible at this stage in the development. The basis for the selection plus details of the supporting experimental programme is described in Ref. 81.

8. Conclusions & recommendations

This document provides a review and a first step towards identifying the materials that can be used for turbine discs and blades for future HTRs.

The report considers information from around 80 published sources and presents the available test and graphical data into tabular form for processing and inclusion in the materials database where applicable.

The review has considered eight potential materials for the turbine disc, thirteen for the blade (including the Russian backup options) and three structural materials for the stator and ducting, etc. Creep resistance and high temperature strength are key selection criteria.

For the turbine disc UDIMET 720 is considered the best available candidate. This material is still under development but the current view is that it may not be usefully applicable above 700^{o}C. The literature search produced very few published data on this material. The shortage of data will be addressed during the testing phases of HTR-M/M1.

For the turbine blade material the Ni based super alloys were considered to offer the best all round properties. Directional solidified grades were preferred to single crystals at this stage. The most promising DS grades in terms of creep strength were chosen for the testing phase (DS CM 247LC and DS IN 792 LC). DS CM 247LC is an aluminium oxide former and DS 792 LC a chromium oxide former. Adoption of a cobalt free option (SC 16) was not considered a priority.

Coating of the blades is considered necessary for long life. The choice of coating remains to be made and tested and its durability assessed for the HTR helium environment.

Information on materials data are being assembled in the database during the HTR-M & M1 projects and recommendations for future investigation and tests will be made on completion.

8. References

Reference 1: B. Riou
"HTR-M Design use and Specification for Turbine"
HTR-M Report: HTR-M-01/10-D-2.1.19

Reference 2: R. Couturier
Information needs on "Turbine Design and Operating Conditions" for the choice of high temperature materials and experimental tests conditions,
HTR-M Report : HTR-M-01/3-D-2.0.23.

Reference 3: R. Couturier
"HTR-M WP2, Milestone 2. Materials review and database"
HTR-M Report: HTR-M 01/09 D 2.0.12.

Reference 4: C. Escaravage
HTR: Identification and Review of Turbine Candidate Materials,
HTR-M Report: HTR-M 02/04 D 2.2.32

Reference 5: R.F. Singer
"Advanced Materials and Processes for Land-Based Gas Turbines".
D. Coutsouradis et al (eds.), Materials for Advanced Power Engineering, Part II 1707-1729. Copyright 1994 Kluwer Academic Publishers.
pp 1707 – 1729 (1994)

Reference 6: M.R. Winstone, A. Partridge and J.W Brooks
"The Contribution of Advanced Materials to Future Aeroengines."
Proceedings of the 5th International Charles Parsons Turbine Conference
pp 779 – 797 (2000)

Reference 7: G. Jianting, D. Ranucci and E. Picco
"Low Cycle Fatigue behaviour of Cast Nickel-base Superalloy IN-738LC in Air and in Hot Corrosive Environments."
Materials Science and Engineering 58
pp 127 – 133 (1982)

Reference 8: H Nickel, F. Schubert and H. Schuster
"Evaluation of Alloys for Advanced High-Temperature Reactor Systems"
029-5493/84 Elsevier Science Publishers B.V. (North Holland Physics Publishing Division
pp 251 – 265 (1983)

Reference 9: W.R.Johnson, L.D. Thompson, T. A. Lechtenberg
"Design of Wrought Nickel-Base Alloys for Advanced High-Temperature Gas-Cooled Reactor Applications."
Nuclear Technology Vol. 66
pp 88 – 101 (1984)

Reference 10: W. Jakobeit, J-P. Pfeifer, G Ullrich
"Evaluation of High-Temperature Alloys for Helium Gas Turbines"
Nuclear Technology Vol. 66
pp 195 – 206 (1984)

Reference 11: L.W. Graham
"Materials for Advanced High Temperature Reactors"
Rev. int. High Temp. et Refract., t. 13 No 4
pp 190 – 203 (1976)

Reference 12: W. Jakobeit
“PM Mo-TZM Turbine Blades-Demands on Mechanical Properties R and HM”
Refractory and Hand Metals
pp 133 – 136 (1983)

Reference 13: R.C.Benn and G.M. McColvin
“The Development of ODS Superalloys for Industrial Gas Turbines”
Superalloys 1988 Edited by S. Reichman, D.N. Duhl, G Maurer, S. Antolovich and C. Lund. The Metallurgical Society
pp 73 – 80 (1988)

Reference 14: L.W. Graham
“Corrosion of Metallic Materials in HTR-Helium Environments”
Journal of Nuclear Materials 171
pp 76 – 83 (1989)

Reference 15: H. Schuster and W Jakobeit
“High-temperature Alloys for the Power Conversion Loops of Advanced HTRs”
Proceedings of the symposium "gas-cooled reactors with emphasis on advanced systems"
pp 401 – 419 (1975)

Reference 16: Y. Monma
“Creep and Stress Rupture-Long Term”
Superalloys, Supercomposites and Superceramics. Copyright 1989 by Academic Press, Inc.
pp 339 – 361 (1989)

Reference 17: P.Shahinian and K. Sadananda
“Creep and Fatigue Crack Growth behaviour of Some Cast Nickel-base Alloys”
Materials Science and Engineering, A108 (1989)
pp 131 – 140 (1989)

Reference 18: P.F. Browning, K. Rajan, J.L. Thompson and M.F. Henry
“The Effect of Oxygen and Water Vapour on Time Dependent Crack Propagation and Crack Tip Oxide Scale Formation in Nickel Base Gas Turbine Disk Alloys”
Conference Proceeding from Materials Solutions 1998
pp 35 – 44 (1998)

Reference 19: A.R. Price, T.Tom, M.D. Fitzpatrick
“Sprayformed Materials for Disc Applications”
Conference Proceeding from Materials Solutions 1998
pp 45 – 53 (1998)

Reference 20: H.W Sizek and S.K.Mannon
“High Temperature Static and Fatigue Crack Growth of INCONEL Alloy 706”
Conference Proceeding from Materials Solutions 1998
pp 54 – 61 (1998)

Reference 21: M.M. Morra
“The Effect of Intergranular Eta Phase on LTF in Alloy 706”
Conference Proceeding from Materials Solutions 1998
pp 62 – 69 (1998)

Reference 22: H. van Esch, W. Greaves
“Extending the Limits of Welding Nickel-Based Superalloys”
Conference Proceeding from Materials Solutions 1998
pp 130 – 137 (1998)

Reference 23: M. Y. Nazmy
"High Temperature Low Cycle Fatigue of IN738 and Application of Strain Range Partitioning"
Metallurgical Transactions A Volume 14A
pp 449 – 461 (1983)

Reference 24: G. Jianting, D. Ranucci and E. Picco
"The Effect of Hot Corrosion on Creep and Low-Cycle Fatigue in the Cast Nickel-Base Superalloy IN738LC"
Superalloys 1984
pp 689 – 698 (1984)

Reference 25: F. Jiao, W Chen, D Mukherji, J Zhu and R.P. Wahi
"Deformation behaviour and Microstructural Evolution in IN738LC Under LCF Loading"
Mechanical behaviour of Materials, 6th International Conference 1991
pp 385 – 390 (1991)

Reference 26: M. Marchionni, D. Ranucci, E. Picco
"High-Temperature Low Cycle Fatigue behaviour of IN738LC Alloy in Air and in a Vacuum"
High Temperature Alloys for gas turbines October 1982. Liege Belgium
pp 791 – 804 (1982)

Reference 27: M.F Day and G.B. Thomas
"Prediction of Intergranular Failure in Ni-Cr Based Alloys in Low Cycle Fatigue at High Temperatures"
Crown Copyright 1983 National Physical Laboratories
pp all (1983)

Reference 28: G. R. Halford and A. J. Nachtigall
"Strainrange Partitioning behaviour of the Nickel-Base Superalloys, Rene' 80 and IN 100"
AGARD Conference Proceedings No. 243, Characterization of Low Cycle High Temperature Fatigue by the Strainrange Partitioning Method
pp 2-1 – 2-14 (1978)

Reference 29: M. C. Van Wanderham, R. M. Wallace and C. G. Annis, Jr.
"Low Cycle Fatigue behaviour of IN-100: Strainrange Partitioning Method"
AGARD Conference Proceedings No. 243, Characterization of Low Cycle High Temperature Fatigue by the Strainrange Partitioning Method
pp 3-1 – 3-17 (1978)

Reference 30: J. L. Chaboache, H. Policella and H Kaczmarek
"Applicability of the SRP Method and Creep-Fatigue Damage approach to the LCHTF Life Prediction of IN-100 Alloy"
AGARD Conference Proceedings No. 243, Characterization of Low Cycle High Temperature Fatigue by the Strainrange Partitioning Method
pp 4-1 – 4-20 (1978)

Reference 31: Appendix A1
AGARD Conference Proceedings No. 243, Characterization of Low Cycle High Temperature Fatigue by the Strainrange Partitioning Method
pp A1-1 – A1-43 (1978)

Reference 32: J. Bressers and E. Arzt
"High Temperature Low Cycle Fatigue of INCONEL MA 6000"
High Temperature Alloys for gas turbines and other applications 1986. Proceedings of a Conference held in Liege, Belgium, 6-9 October 1986 vol 2
pp1067 – 1079 (1986)

Reference 33: A. Hynna, V.-T. Kuokkala, T. Lepisto, T. Mantyla, P Kettunen
"High Temperature Low Cycle Fatigue of Superalloy MA 6000"
High Temperature Alloys for gas turbines and other applications 1986. Proceedings of a Conference held in Liege, Belgium, 6-9 October 1986 vol 2
pp 1091 – 1102 (1986)

Reference 34: R. Tanaka and T Kondo
"Research and development on heat resistant alloys for nuclear process heating in Japan"
Nuclear technology vol. 66
pp 75 – 87 (1984)

Reference 35: K. Hada, M. Ohkubo and O. Baba
"Application of new design methodologies to very high temperature metallic components of the HTTR"
Nuclear Engineering and design, vol 132, n°1
pp.13 – 22 (1991)

Reference 36: G. L. Erickson
"Superalloy Developments for Aero and Industrial Gas Turbines"
Advanced Materials and Coatings for Combustion Turbines Proceedings of ASM 1993 Materials Congress
pp 29 – 41 (1993)

Reference 37: Y. Yoshioka, D. Saito, K. Fujiyama and N. Okabe
"Effect of Material Degradation on Mechanical Properties of Cast-Base Superalloy IN738LC"
Advanced Materials and Coatings for Combustion Turbines Proceedings of ASM 1993 Materials Congress
pp 53 – 58 (1993)

Reference 38: A. K. Koul, J. P. Immarigeon, R. V. Dainty and P. C. Patnaik
"Degradation of High Performance Aero-Engine Turbine Blades"
Advanced Materials and Coatings for Combustion Turbines Proceedings of ASM 1993 Materials Congress
pp 69-74 (1993)

Reference 39: A. K. Koul and R. Castillo
"Creep behaviour of Industrial Turbine Blades"
Advanced Materials and Coatings for Combustion Turbines Proceedings of ASM 1993 Materials Congress
pp 75-88 (1993)

Reference 40: D. H. Yates, P. Ganesan and G. D. Smith
"Recent Advances in the Enhancement of Inconel Alloy 617 Properties to Meet the Needs of the Land Based Gas Turbine Industry"
Advanced Materials and Coatings for Combustion Turbines Proceedings of ASM 1993 Materials Congress
pp 89 – 97

Reference 41: G. Y. Lai
"Nitridation of Several Combustor Alloys in a Simulated Gas Turbine Combustion Environment"
Advanced Materials and Coatings for Combustion Turbines Proceedings of ASM 1993 Materials Congress
pp 113-121 (1993)

Reference 42: V. Guttmann and M. Schutze
"Interactions of Corrosion and Mechanical Properties"
High Temperature Alloys for gas turbines and other applications 1986. Proceedings of a Conference held in Liege, Belgium, 6-9 October 1986 vol 1
pp 293-326 (1986)

Reference 43: W. Hoffelner
"Creep Dominated Damage Processes"
High Temperature Alloys for gas turbines and other applications 1986. Proceedings of a Conference held in Liege, Belgium, 6-9 October 1986 vol 1 pp 413-439 (1986)

Reference 44: J. Bressers, L. Remy and W. Hoffelner
"Fatigue Dominated Damage Processes"
High Temperature Alloys for gas turbines and other applications 1986. Proceedings of a Conference held in Liege, Belgium, 6-9 October 1986 vol 1
pp 441-468 (1986)

Reference 45: W. Esser, M. McLean and K. Schneider
"Effect of Fabrication and Repair Procedures on the Performance of IN 738 LC and IN 939"
High Temperature Alloys for gas turbines and other applications 1986. Proceedings of a Conference held in Liege, Belgium, 6-9 October 1986 vol 1 pp 593-622 (1986)

Reference 46: R. Couturier and C. Escaravage
"High Temperature Alloys for the HTGR Gas Turbine: Required Properties and Development Needs"
Gas Turbine Power Conversion Systems for Modular HTGRs. IAEA, Vienna 2001
pp 1 – 12 (2001)

Reference 47: O. F. Kimball
"Thermal Stability and Environmental Compatibility Inconel 617"
High Temperature Metallic Materials for Gas-Cooled Reactors
Proceedings of a Specialists Meeting Organized by the International Atomic Energy Agency and Held in Cracow, 20-23 June 1988
pp 65 – 71 (1988)

Reference 48: W. J. Quadakkers, and H. Schuster
"Corrosion behaviour of High Temperature Alloys in the Cooling Gas of High Temperature Reactors"
High Temperature Metallic Materials for Gas-Cooled Reactors
Proceedings of a Specialists Meeting Organized by the International Atomic Energy Agency and Held in Cracow, 20-23 June 1988
pp 72 – 77 (1988)

Reference 49: H. Tsuji, H. Nakajima and T. Kondo
"Current Status of Studies on High Temperature Metallic Materials for HTGR Applications in JAERI"
High Temperature Metallic Materials for Gas-Cooled Reactors
Proceedings of a Specialists Meeting Organized by the International Atomic Energy Agency and Held in Cracow, 20-23 June 1988
pp 81 – 90 (1988)

Reference 50: K. Nagato, T. Murakami and T. Hashimoto
"High Temperature Low-Cycle Fatigue Strength of Hastelloy-XR"
High Temperature Metallic Materials for Gas-Cooled Reactors
Proceedings of a Specialists Meeting Organized by the International Atomic Energy Agency and Held in Cracow, 20-23 June 1988
pp 91 – 95 (1988)

Reference 51: H. Breitling, W. Dietz and H. J. Penkalla
"Evaluation of Mechanical Properties of the Alloy NiCr22Co12Mo (Alloy 617) for Heat Exchanging Components of HTGRs"
High Temperature Metallic Materials for Gas-Cooled Reactors
Proceedings of a Specialists Meeting Organized by the International Atomic Energy Agency and Held in Cracow, 20-23 June 1988
pp 96 – 104 (1988)

Reference 52: H. J. Penkalla, F Schubert and H. Nickel
"Multiaxial Creep of Tubes of Alloy 800 and Alloy 617 at High Temperature High Temperature Metallic Materials for Gas-Cooled Reactors"
Proceedings of a Specialists Meeting Organized by the International Atomic Energy Agency and Held in Cracow, 20-23 June 1988
pp 105 – 115 (1988)

Reference 53: H. Tsuji and H. Nakajima
"Fatigue Properties of Nickel Base High Temperature Alloys for HTGRs"
High Temperature Metallic Materials for Gas-Cooled Reactors
Proceedings of a Specialists Meeting Organized by the International Atomic Energy Agency and Held in Cracow, 20-23 June 1988"
pp 115 – 128 (1988)

Reference 54: B. Huchtemann
"The New Alloy Thermon 4972 (NiCr22W12Fe) for High Temperature Components of Gas Cooled Reactors"
High Temperature Metallic Materials for Gas-Cooled Reactors
Proceedings of a Specialists Meeting Organized by the International Atomic Energy Agency and Held in Cracow, 20-23 June 1988
pp 159 – 168 (1988)

Reference 55: T. Kondo
"Development and Testing of Alloys for Primary Circuit Structure of a VHTR"
Specialists' Meeting on High Temperature Metallic Materials for Application in Gas-Cooled Reactors Vienna, Austria 4-6 May 1981
pp B1 – B15 (1981)

Reference 56: W. R. Johnson and G. Y. Lai
"Interaction of Metals with Primary Coolant Impurities: Comparison of Steam-Cycle and Advanced HTGRs"
Specialists' Meeting on High Temperature Metallic Materials for Application in Gas-Cooled Reactors Vienna, Austria 4-6 May 1981
pp J1 – J22 (1981)

Reference 57: H. Inouye and P. L. Rittenhouse
"Relationship Between Carburization and Zero-Applied-Stress Creep Dilation in Alloy 800H and Hastelloy X"
Specialists' Meeting on High Temperature Metallic Materials for Application in Gas-Cooled Reactors Vienna, Austria 4-6 May 1981
pp L1 – L12 (1981)

Reference 58: G. Raule and R. Bauer
"Properties of Materials for the High Temperature Helium Turbine Under Mechanical and Thermal Loading"
Specialists' Meeting on High Temperature Metallic Materials for Application in Gas-Cooled Reactors Vienna, Austria 4-6 May 1981
pp O1 – O19 (1981)

Reference 59: J. F. King, H. E. McCoy and P. L. Rittenhouse
"Weldability Evaluations and Weldment Properties of Hastelloy X"
Specialists' Meeting on High Temperature Metallic Materials for Application in Gas-Cooled Reactors Vienna, Austria 4-6 May 1981
pp R1 – R12 (1981)

Reference 60: D. Schuhmacher and U. Bruch
"Materials Behaviour in Methane Reforming Gas"
Specialists' Meeting on High Temperature Metallic Materials for Application in Gas-Cooled Reactors Vienna, Austria 4-6 May 1981
pp S1 – S15 (1981)

Reference 61: J. P. Strizac, C. R. Brinkman and P. L. Rittenhouse
"High Temperature Low Cycle Fatigue and Tensile Properties of Hastelloy X and Alloy 617 in Air and HTGR-Helium"
Specialists' Meeting on High Temperature Metallic Materials for Application in Gas-Cooled Reactors Vienna, Austria 4-6 May 1981
pp T1 – T15 (1981)

Reference 62: H. P. Meurer, H. Breitling and E. D. Grosser
"Fatigue and Creep Fatigue Behaviour of High Temperature Alloys for HTR Application"
Specialists' Meeting on High Temperature Metallic Materials for Application in Gas-Cooled Reactors Vienna, Austria 4-6 May 1981
pp U1 – U12 (1981)

Reference 63: J. F. G. Conde
"Turbines for Motor Vehicles"
Research and Development of High Temperature Materials for Industry. Institute of Advanced Materials Joint Research Centre
pp 437 – 448 (1989)

Reference 64: R. Viswanathan, S. Scheirer and J. Stringer
"Materials Advancements in Land-Based Gas Turbines"
Powergen International Conference Proceedings, Orange County Convention Centre, Orlando, Florida USA, December 9-11 1998
pp all (1998)

Reference 65: G. Harkegard, T. Borvik and R. Buchs
"Ballistic Penetration Testing of the Containment Wall of a Marine Gas Turbine"
Proceedings of the 5th International Charles Parsons Turbine Conference
pp 700 – 709 (2000)

Reference 66: M. Uunonen and P. Kettunen
"Development of Diffusion Barriers for the Superalloy Blades of Gas Turbine"
Proceedings of the 5th International Charles Parsons Turbine Conference
pp 724 – 732 (2000)

Reference 67: R. W. Broomfield
“Development of Brazing Techniques for the Joining of Single Crystal Components”
Proceedings of the 5th International Charles Parsons Turbine Conference
pp 742 – 754 (2000)

Reference 68: C. Y. Jo, D. W. Joo, S. M. Seo, D. H. Kim, J. H. Lee, S. J. Choe and S. K. Oh
“Precipitation and Deformation Behaviour of Cast 718 During Creep and Thermal Exposure”
Proceedings of the 5th International Charles Parsons Turbine Conference
pp 971 – 981 (2000)

Reference 69: T. Connolley, P. A. S. Reed and M. J. Starink
“A Study of the Role of (Nb, Ti)C Carbides in Fatigue Crack Initiation in Inconel 718 at 20°C and 600°C”
Proceedings of the 5th International Charles Parsons Turbine Conference
pp 982 – 998 (2000)

Reference 70: F. Schubert, G. Fleur, T. Steinhaus and P. J. Ennis
“Description of the Mechanical Behaviour of the Single-Crystal Alloy CMS X4”
Proceedings of the 5th International Charles Parsons Turbine Conference
pp 999 – 1011 (2000)

Reference 71: R. Mohrmann and S. Gallet
“Constitutive Modelling of the Single Crystal Superalloy CMSX-4 for Industrial Gas Turbine”
Proceedings of the 5th International Charles Parsons Turbine Conference
pp 1036 – 1048 (2000)

Reference 72: L. W. Wright, D. W. MacLachlan, Q. Chen, S. S. K. Gunturi and D. M. Knowles
“High Temperature Creep of CMSX-4: Effect of Precipitate Orientation and Morphology”
Proceedings of the 5th International Charles Parsons Turbine Conference
pp 1049 – 1062 (2000)

Reference 73: M. Shindo, W. J. Quadakkers and H. Schuster
“Corrosion behaviour of high temperature alloys in impure helium environments”
Journal of Nuclear Materials 140, North-Holland Amsterdam
pp 94 – 104 (1986)

Reference 74: W. J. Quadakkers
“Corrosion of High Temperature Alloys in the Primary Circuit Helium of High Temperature Gas Cooled Reactors. - Part 2: Experimental Results”
Werkstoffe und Korrosion 36
pp 335 - 347 (1985)

Reference 75: A. R. Price & B. A. Mueller
“ATS Land Based Turbine Casting Initiative”
Howmet Research Corporation
pp all (1997)

Reference 76: G. Jianting, D Ranucci, E. Picco and P.M. Strocci
“Effect of Environment on the Low Cycle Fatigue Behaviour of Cast Nickel-Base Superalloy IN738LC.”
Int J Fatigue Vol 6 No2
pp 95 – 99 (1984)

Reference 77: P. Ennis
Attachments 19 – 21 from minutes of HTRM meeting at Grenoble
HTRM 02/1M0026
5 – 7 December 2001

Reference 78: *"Layout Criteria for High Temperature Metallic and Ceramic Components as well as for Pre-Stressed Concrete Pressure Vessels of Future HTR-Plants"*
Volume IIb
Part B: Metallic Components
Final Report for the Utility-Research Project of the BMFT
pp all (1988)

Reference 79: M. Ohnami and Sakane
"High Temperature Multiaxial low-cycle fatigue of Nickel base superalloys"
Sixth International Conference on Creep and Fatigue, London
pp521 – 530 (1996)

Reference 80: A. A. Braithwaite
"Scheme for HTR-M Materials data collection"
HTR-M Report01/11 D0.0.22

Reference 81: R. Couturier
"Materials for turbine: definition of complimentary testing experiments"
HTR-M Report: HTR-M 02/26 D2.2.35

Table 1 Materials for large turbine discs / industrial capabilities

Material Ni based	**Composition** Wt%	**Max use T°**	**Heat Treatment** (ageing)	**Creep** σ_{1000h}	**Max disc size** mm	**Process** mm	**R&D**
IN 706	**16Cr** **0.15Al** **1.7Ti** **3Nb** 38Fe <0.02C	<600°C	620°C + 720°C	580MPa/650°C	ϕ ≤ 2300 e ≤ 400	Ingot ϕ ≤ 1020 VIM + ESR + VAR Pre-form 4500 t press Close die 65000 t press	Fine grains ASTM 3-4
IN 718	**18Cr** **3Mo** **0.5Al** **1Ti** **5Nb** 18Fe <0.03C	<650°C	718°C + 620°C	600MPa/650°C 195MPa/760°C	ϕ ≤ 2000 e ≤ 325	Ingot ϕ ≤ 710 VIM + ESR + VAR Preform 4500 t press Close die 65000 t press	↓ %C for large discs Fine grains ASTM <4
U 720	**16Cr** **15Co** **5Ti** **2.5Al** **1.25W** **3Mo** 0.03Zr 0.018B 0Fe	<680-700°C	650°C + 760°C	700MPa/650°C 480MPa/700°C 175MPa/750°C	ϕ ≤ 500 A&D : 850	VIM + ESR + VAR C&W billet ϕ 100-150 HIP ϕ ≤ 1400 Isothermal forging 45000t press	HIP Hot Extrusion + forge HIP + forge ASTM 11→ ASTM 9 PPB Large forging

Table 2 Candidate materials for turbine discs

(% mass)	C	Cr	Co	Mo	W	Ti	Al	Nb	Ta	Hf	V	B	Zr	Other
Zh56F	$\simeq$ 0.11	$\simeq$ 5.5	$\simeq$ 9.4	$\simeq$ 0.9	$\simeq$ 12	$\simeq$ 1.0	$\simeq$ 5.3	$\simeq$ 1.6	-	$\simeq$ 0.9	$\simeq$ 0.9			
V2HL12U	$\simeq$ 0.17	$\simeq$ 9.5	$\simeq$ 13.5	$\simeq$ 3.1	$\simeq$ 1.4	$\simeq$ 4.4	$\simeq$ 5.4	$\simeq$ 0.75	-	-	$\simeq$ 0.75			
Inconel MA6000 (ODS)	$\simeq$ 0.05	$\simeq$ 15	-	$\simeq$ 2	$\simeq$ 4	$\simeq$ 2.5	$\simeq$ 4.5	-	$\simeq$ 2	-		$\simeq$ 0.01	$\simeq$ 0.15	Y_2O_3 : 1.1
Udimet 720 (F or HIP)	0.03 0.04	17.5 18.5	14 15.5	2.75 3.25	1.1 1.4	4.75 5.25	2.25 2.75	-	-			0.03 0.04	0.025 0.050	
IN 100 (C)	$\simeq$ 0.18	$\simeq$ 10	$\simeq$ 15	$\simeq$ 3	-	$\simeq$ 3	$\simeq$ 4.7	-			$\simeq$ 1	$\simeq$ 0.014	$\simeq$ 0.06	

F : Forged

C : Cast

ODS : Oxide Dispersion Strengthened

HIP : Hot Isostatic Pressed

Udimet : trademark of Special Metals Corporation

Inconel, MA : trademark of Inco group of companies

Table 3 Candidate materials for turbine blades

(% mass)	C	Cr	Co	Mo	W	Ti	Al	Nb	Ta	Hf	V	B	Zr
Ch120M (C or SC)		≃ 11.7	≃ 7.5	≃ 1	≃ 6.5	≃ 4.3	≃ 4	≃ 0.8	-				
EI929 (F)	-	9 12	12 16	4 6	4.5 6.5	1.4 2	3.6 4.6	-	-				
EI893 (F)	-	15 17	-	3.5 4.5	8.5 10	1.2 1.6	1.2 1.6	-	-				
EP800 (F)	-	12 13.5	8.5 10.5	5 6	4 6	-	4.2 4.9	1.5 2	-				
CMSX2 (SC)	≤ 0.03	≃ 8	≃ 4.6	≃ 0.6	≃ 7.9	≃ 1	≃ 5.5	-	5.8				
CMSX4 (SC)		≃ 6.5	≃ 9	≃ 0.6	≃ 6	≃ 1.0	≃ 5.6		≃ 6.5	≃ 0.1			
PWA1480 (SC)		≃ 10	≃ 5		≃ 4	≃ 1.5	≃ 5		≃ 12				
PWA1483 (SC)	≃ 0.080	≃ 12.3	≃ 8.5	≃ 1.9	≃ 3.8	≃ 4	≃ 3.6		≃ 5	< 0.01		< 0.003	< 0.01
SC16 (SC)		≃ 16		≃ 3.0		≃ 3.5	≃ 3.5		≃ 3.5				
MAR M247 (C or DS)	0.13 0.17	8 9	9 11	0.5 0.8	9.5 10	0.9 1.2	5.3 5.7		2.8 3.8	1.2 1.6			
M21 (C)	~ 0.1	~ 6	-	~ 2	~ 10.5	-	~ 6	1.5				~ 0.02	~ 0.1
MAR M004 (C)	≃ 0.065	≃ 11.86	-	≃ 4.42	-	≃ 0.6	≃ 5.95	≃ 1.6	≃ 0.3	≃ 1.3			
713LC (C)	≃ 0.07	≃ 12	≃ 0.04	≃ 4.65	-	≃ 0.74	≃ 5.8	≃ 2				≃ 0.09	≃ 0.1
IN100 (C) or (DS)	≃ 0.18	≃ 10	≃ 15	≃ 3	-	≃ 3	≃ 4.7			-	≃ 1	0.014	0.06
IN792 (C) or (DS)	≃ 0.11	≃ 12.15	≃ 9.25	≃ 1.8	≃ 3.78	≃ 4.10	≃ 3.45	-	≃ 3.75	≃ 0.52		0.01	0.09
IN738LC (C)	0.09 0.13	15.7 16.5	8.0 9.0	1.5 2.0	2.4 2.6	3.2 3.7	3.2 3.7	0.6 1.1	1.5 2.0	-		0.007 0.012	0.03 0.08

(F) : Forged
(C) : Conventionally, cast
(DS) : Directionally solidified

CMSX is a trade name of Cannon Muskegon Corporation
MAR M is a trade name of Martin Marietta Corporation
PWA is a trade name of Pratt and Withney

(SC) : Single crystal

Table 4 Candidate materials for first stage stator / ducting etc.

(% mass)	C	Cr	Co	Mo	W	Ti	Al	Nb	Ta	Hf	V	B	Zr	Fe	Mn	Si
ChS57	≤ 0.05	≃ 19		≃ 6	≃ 2.5		≤ 0.15	-	-	-	-					
Hastelloy X	0.05 0.15	20.5 23	0.5 2.5	8 10	0.2 1.0	≤ 0.15	≤ 0.50	-	-	-	-	≤ 0.01	-	17.0 20.0	0.6 1.1	≤ 1.0
Hastelloy XR	0.05 0.09	20.5 23	≤ 0.10	8 10	0.2 1.0	≤ 0.05	≤ 0.05	-	-	-	-	≤ 0.01	-	17.0 20.0	0.6 1.1	0.2 0.5
Inconel 617	0.04 0.08	20.0 23.0	10.0 13.0	8.0 10.0	-	0.2 0.6	0.6 1.3	-	-	-	-	0.002 0.005	-	<1.5	<0.7	<0.7

Hastelloy is a trademark of Cabot Corporation

Figure 1 Creep rupture design strength in 10^5h for high temperature alloys (Ref 15)

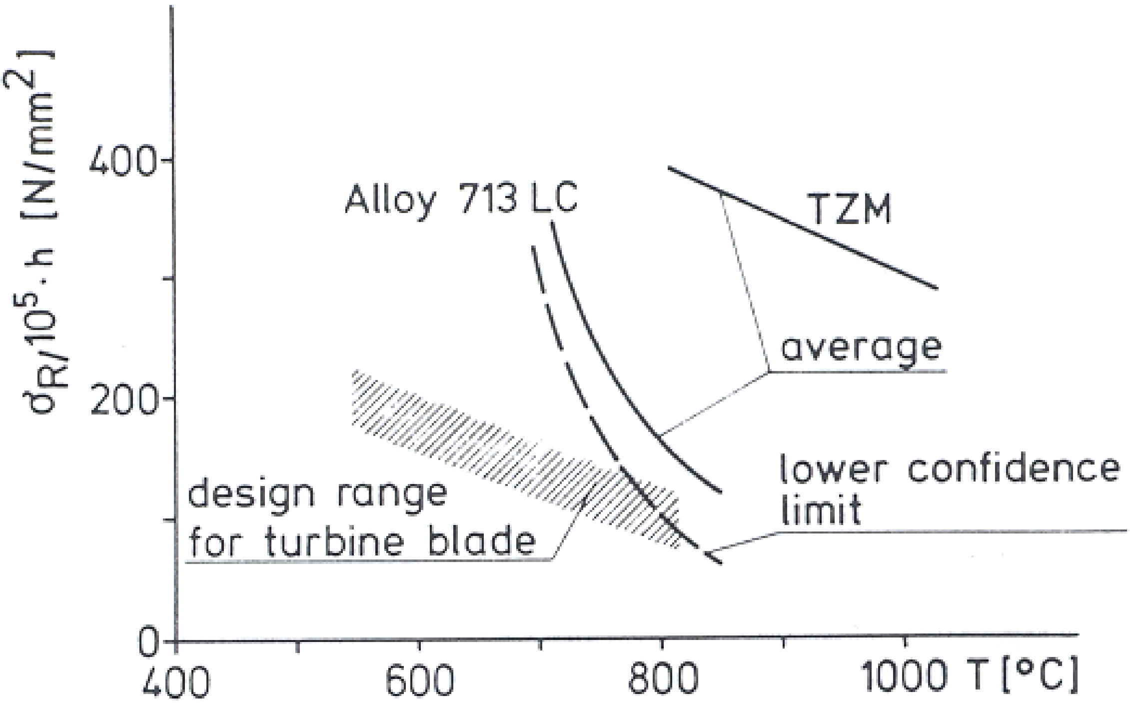

Figure 2 Notch sensitivity of Mo-TZM alloy (Ref 15)

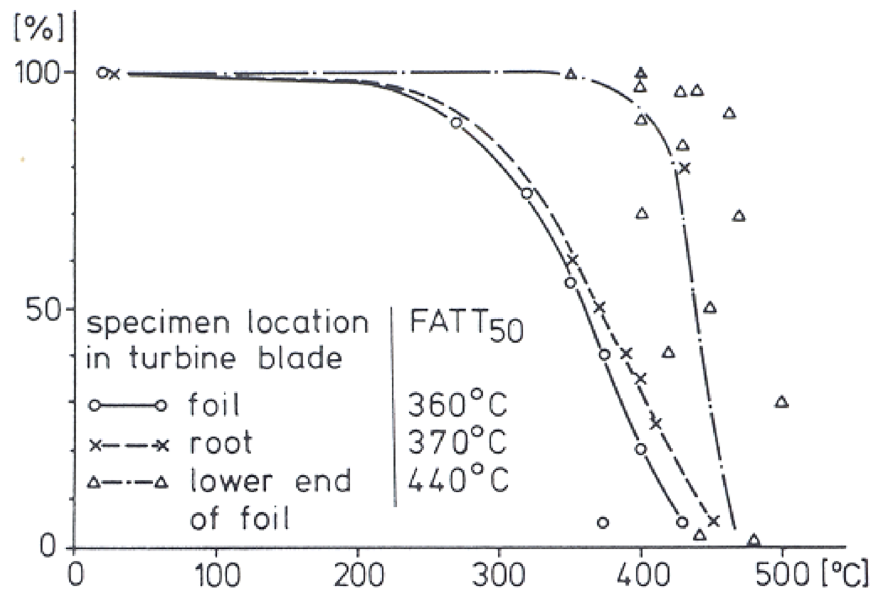

Figure 3 Temperature dependence of 100,000h rupture time (Ref 16)

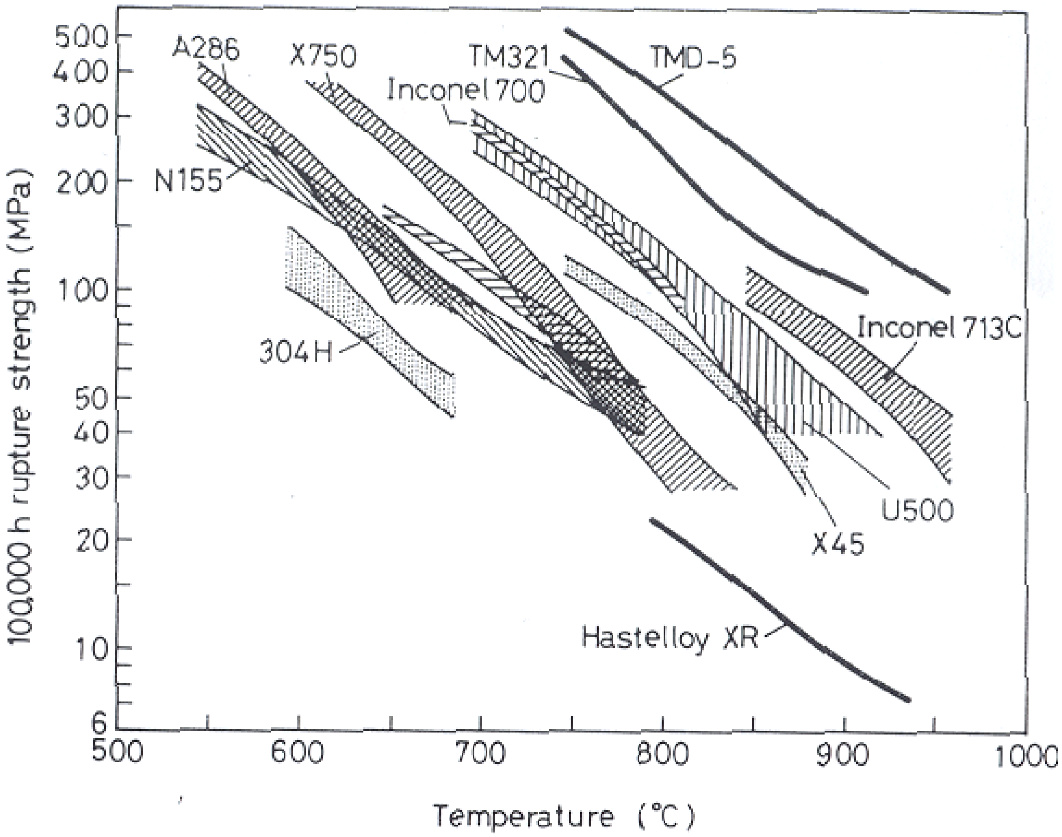

Figure 4 Creep rupture strength of alloy IN713LC between 500 & 850°C (Ref 10)

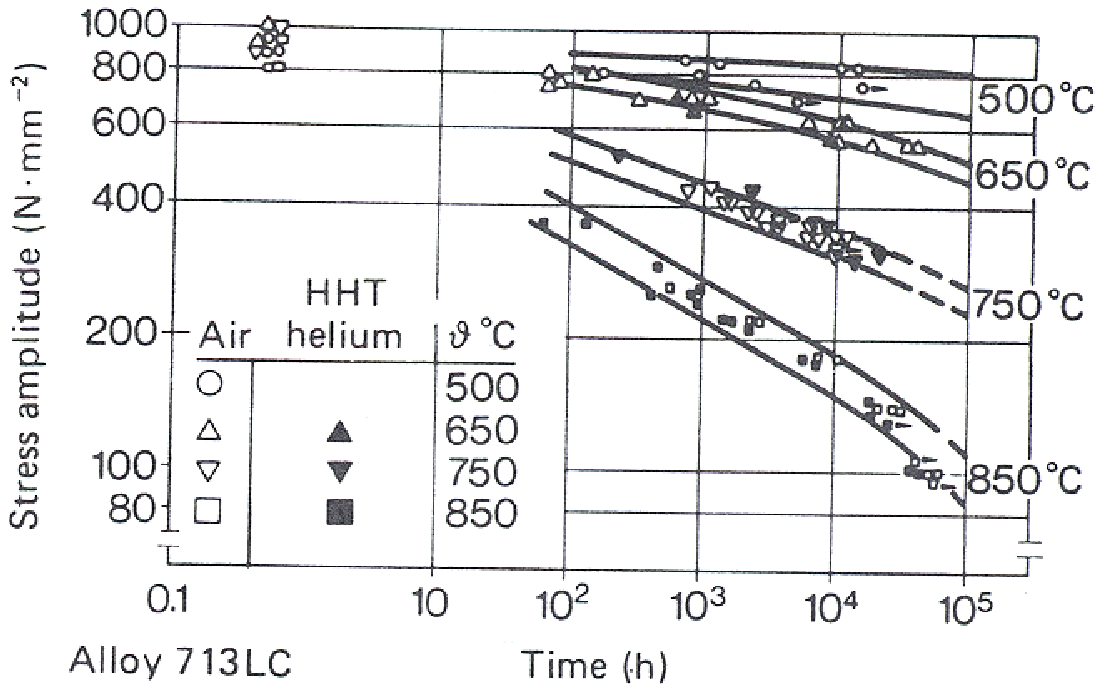

Figure 5 Creep rupture strength of different alloys at 850°C (Ref 10)

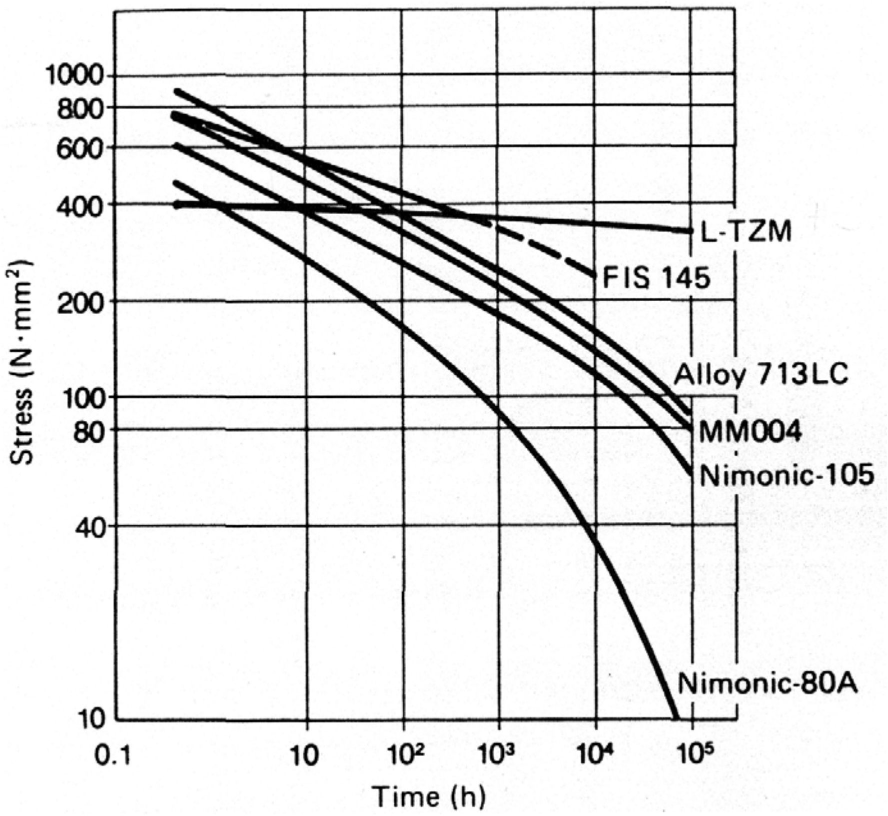

Figure 6 Uni-axial creep curves for Nimonic 80A

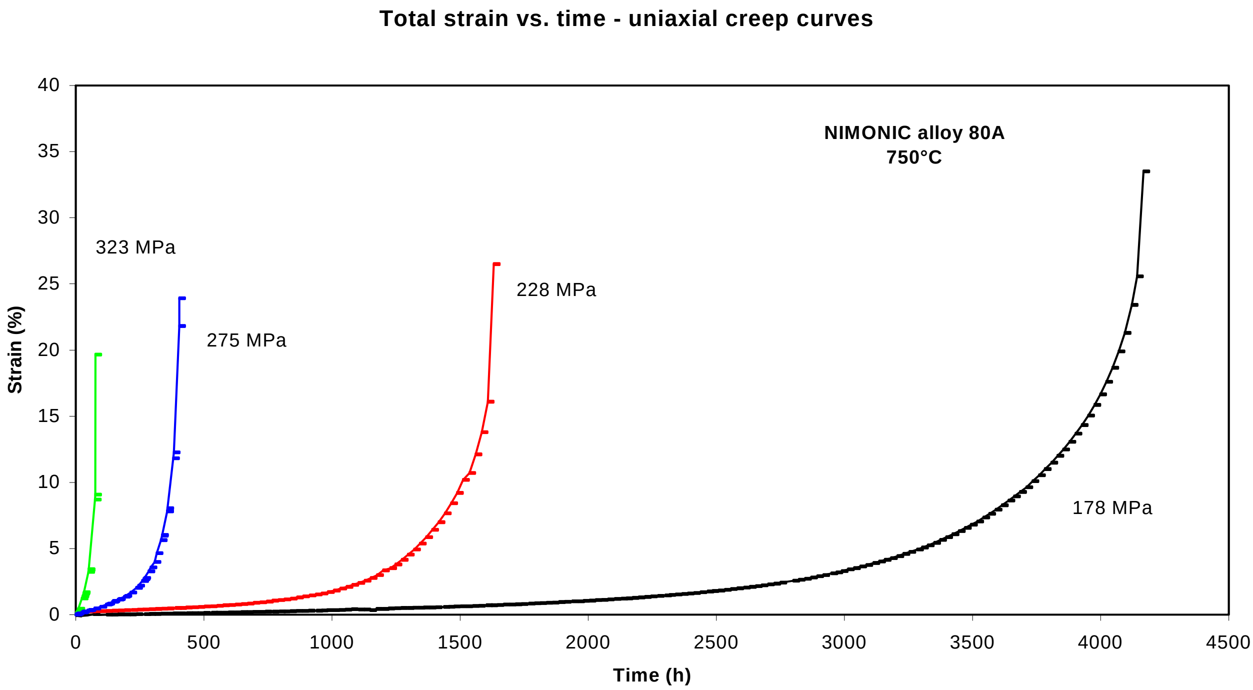

Figure 7 Creep rupture strength of different alloys with temperature

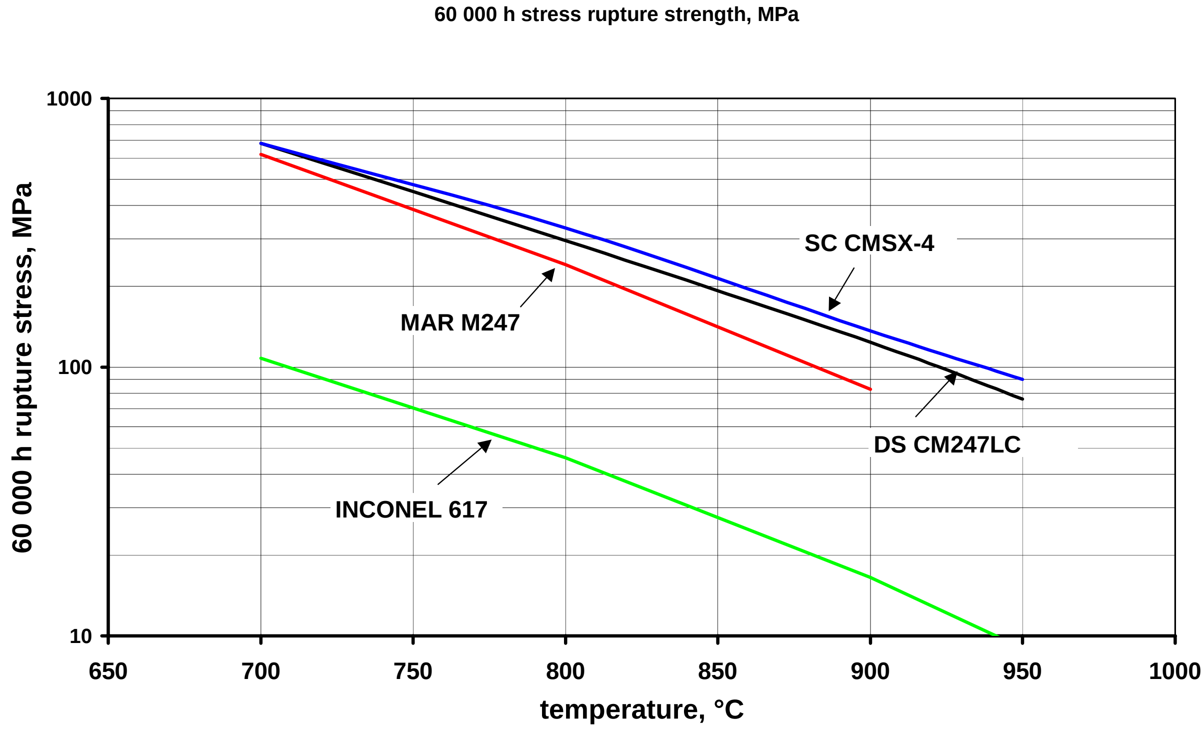

Figure 8 Creep rupture strength of Inconel 617 (550-1100°C)

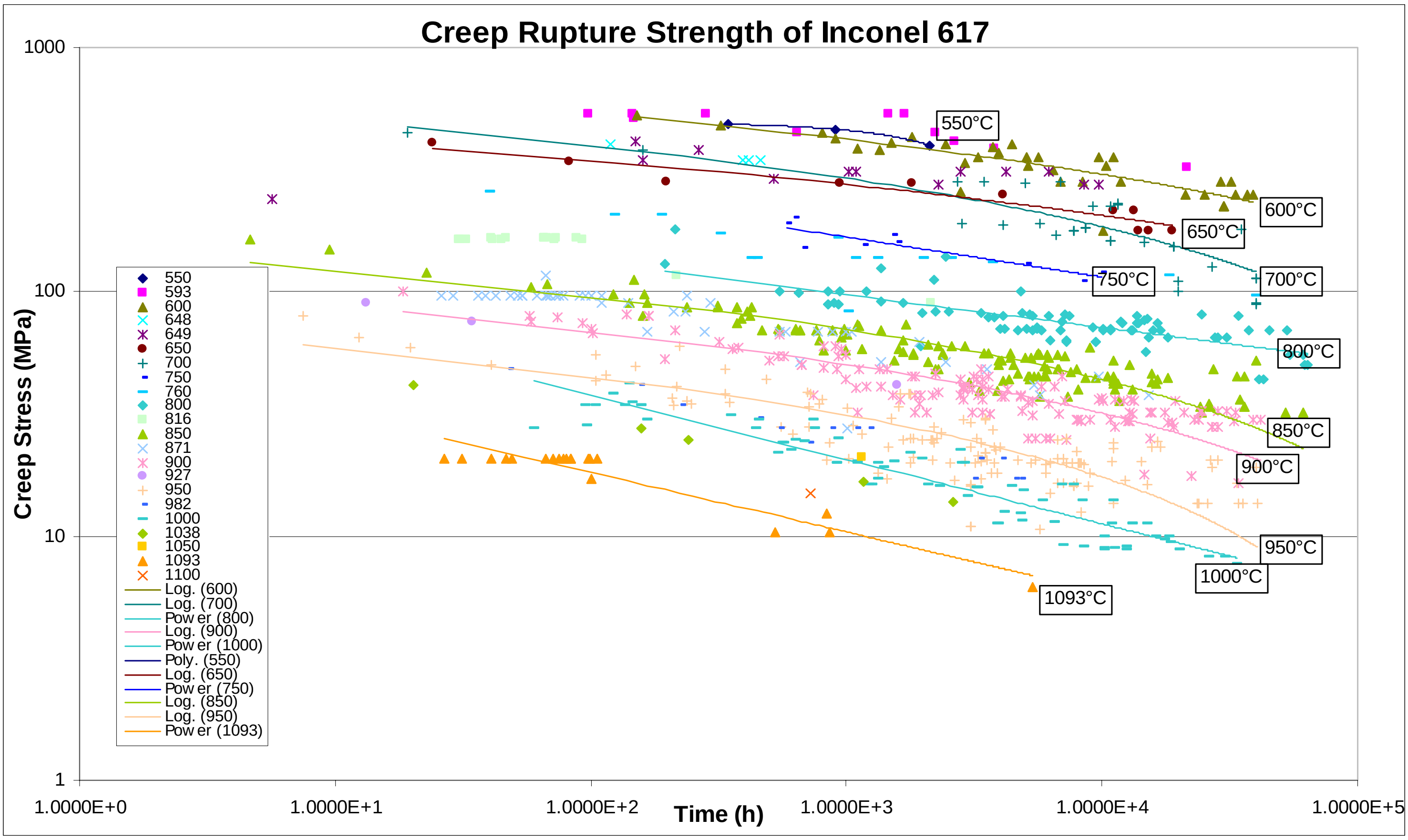

Figure 9 **Comparison of the rupture strength of turbine disc materials (700°C - 1000°C)**

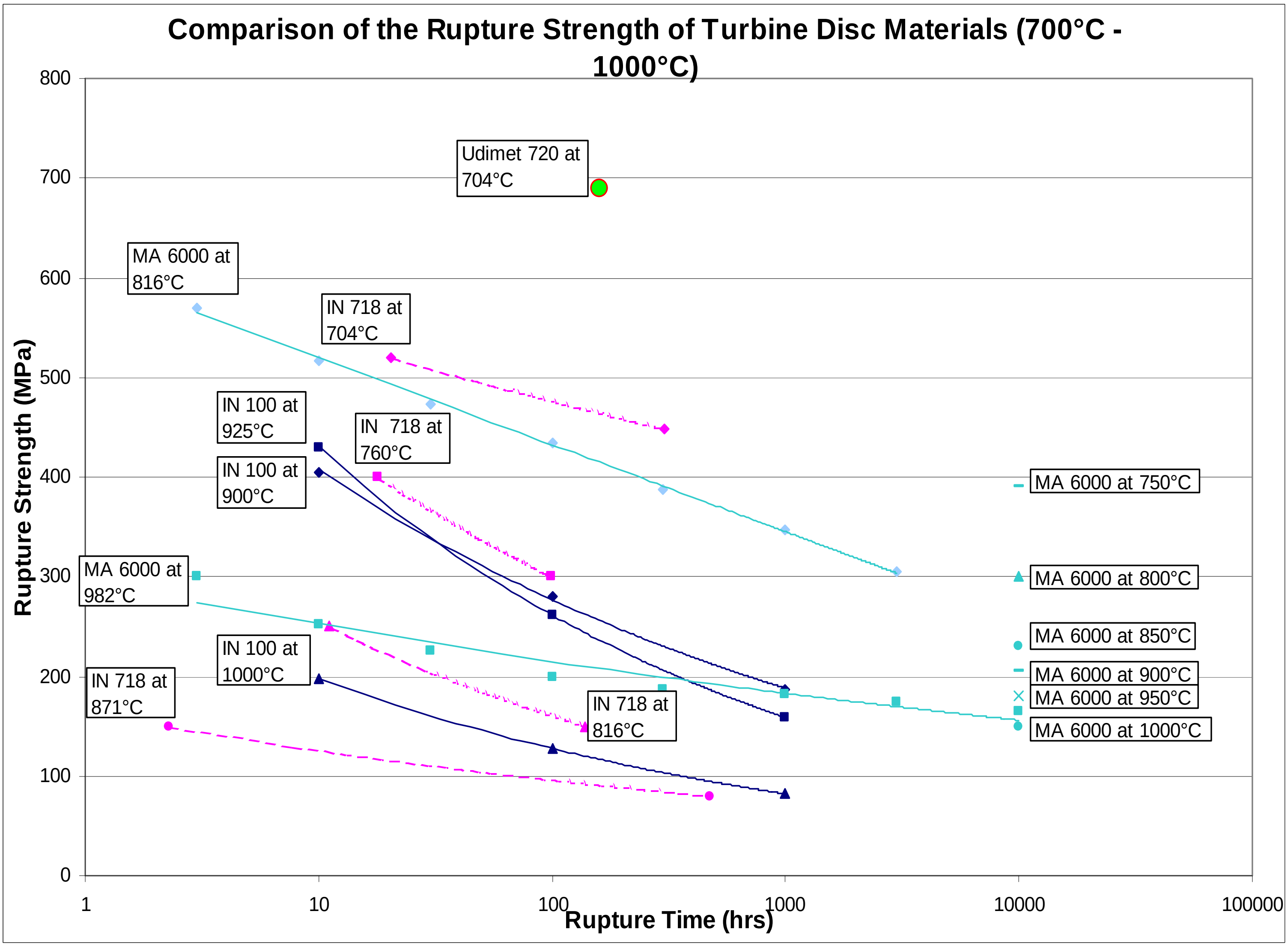

Figure 10 Stress rupture test (tested at 900°C) results for Hastelloy X, unirradiated and irradiated (7.5 x 10^{24} n/m^2, 60°C) and compared to those for Incoloy 800 (Ref. 49)

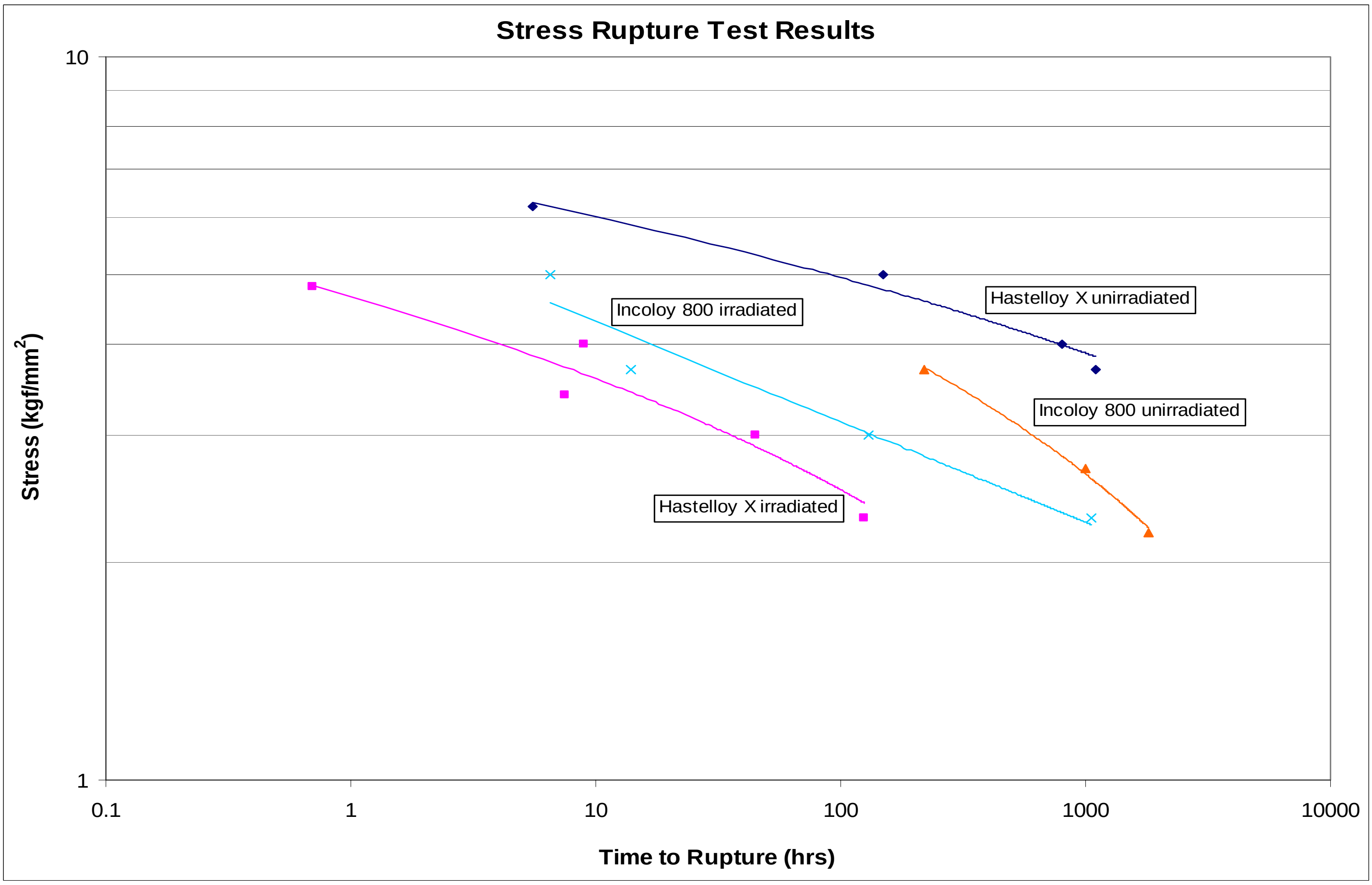

Appendix A - Information Tables

A1 Udimet 720

Mechanical Property	Value	Units	Reference	Notes Sol = 2125°F/2h, DA = 1400°F/8h + 1200°C/24h
0.2% YS	130.6	ksi	19, Table 2, Page 48	DA only condition - 70°F
	125.2	ksi	19, Table 2, Page 48	Sol + DA conditions - 70°F
	119.3	ksi	19, Table 2, Page 48	DA only condition - 1200°F
	118.3	ksi	19, Table 2, Page 48	Sol + DA conditions - 1200°F
	155.3	ksi	19, Table 4, Page 51	HIP condition 2050°F - 70°F
	145.3	ksi	19, Table 4, Page 51	HIP condition 2165°F - 70°F
	142.9	ksi	19, Table 4, Page 51	HIP condition 2050°F - 1200°F
	129.1	ksi	19, Table 4, Page 51	HIP condition 2165°F - 1200°F
EL (Tensile)	28.8	%	19, Table 2, Page 48	DA only condition - 70°F
	29.1	%	19, Table 2, Page 48	Sol + DA conditions - 70°F
	25.3	%	19, Table 2, Page 48	DA only condition - 1200°F
	28.7	%	19, Table 2, Page 48	Sol + DA conditions - 1200°F
	22.8	%	19, Table 4, Page 51	HIP condition 2050°F - 70°F
	23.3	%	19, Table 4, Page 51	HIP condition 2165°F - 70°F
	30.9	%	19, Table 4, Page 51	HIP condition 2050°F - 1200°F
	30.8	%	19, Table 4, Page 51	HIP condition 2165°F - 1200°F
EL (Creep)	9.6	%	19, Table 3, Page 48	DA only condition - 1300°F
	12.0	%	19, Table 3, Page 48	Sol + DA condition - 1300°F
	6.0	%	19, Table 5, Page 51	HIP condition 2050°F - 1300°F
	25.0	%	19, Table 5, Page 51	HIP conditions 2165°F 1300°F
Failure	33.3	h	19, Table 3, Page 48	DA only condition - 1300°F
	45.0	h	19, Table 3, Page 48	Sol + DA condition - 1300°F
	15.1	h	19, Table 5, Page 51	HIP condition 2050°F - 1300°F
	159.9	h	19, Table 5, Page 51	HIP conditions 2165°F 1300°F

Mechanical Property	Value	Units	Reference	Notes Sol = 2125°F/2h, DA = 1400°F/8h + 1200°C/24h
Larson-Miller	37.9		19, Table 3, Page 48	DA only condition - 1300°F
	38.1		19, Table 3, Page 48	Sol + DA condition - 1300°F
	37.3		19, Table 5, Page 51	HIP condition 2050°F - 1300°F
	39.1		19, Table 5, Page 51	HIP conditions 2165°F 1300°F
Tensile Properties			19, Fig 21, Page 52	Graph shows the tensile properties of P/M U720 after different HIP processes and typical published data
UTS	207.9	ksi	19, Table 2, Page 48	DA only condition - 70°F
	203.6	ksi	19, Table 2, Page 48	Sol + DA conditions - 70°F
	179.3	ksi	19, Table 2, Page 48	DA only condition - 1200°F
	182.1	ksi	19, Table 2, Page 48	Sol + DA conditions - 1200°F
	229.2	ksi	19, Table 4, Page 51	HIP condition 2050°F - 70°F
	220.5	ksi	19, Table 4, Page 51	HIP condition 2165°F - 70°F
	193.9	ksi	19, Table 4, Page 51	HIP condition 2050°F - 1200°F
	191.4	ksi	19, Table 4, Page 51	HIP condition 2165°F - 1200°F

A2 IN 718

Mechanical Property	Value	Units	Reference	Notes
AES sputter depth profile			18, Figs 13 & 14, Page 41	Graphs show the AES sputter depth profile of a crack grown in Alloy 718
Average Flow Stress	1100	MPa	65, Table 1, Page 702	Thickness: 9mm, mean diameter: 924mm, Axial length: 180mm
Crack Growth Data			18, Fig 17, Page 42	Graph shows the Alloy 718 crack growth data for all investigated environments
Crack Propagation Rate			18, Fig 1, Page 35	Graph shows the crack propagation rate vs. oxygen partial pressure
			18, Fig 7, Page 38	Graph shows the crack propagation rate per unit time vs. equilibrium oxygen partial pressure
			18, Fig 8, Page 38	Graph shows the crack propagation rate per unit time vs. water vapour partial pressure

Mechanical Property	Value	Units	Reference	Notes
Elongation	6.5	%	68, Table 2, Page 974	704°C, 448 MPa
	6.1	%	68, Table 2, Page 974	704°C, 520 MPa
	10.6	%	68, Table 2, Page 974	760°C, 300 MPa
	10.3	%	68, Table 2, Page 974	760°C, 400 MPa
	28.2	%	68, Table 2, Page 974	816°C, 150 MPa
	22.3	%	68, Table 2, Page 974	816°C, 250 MPa
	9.4	%	68, Table 2, Page 974	871°C, 80 MPa
	49.1	%	68, Table 2, Page 974	871°C, 150 MPa
Fatigue Crack Growth Rate			44, Fig 12, Page 460	Graph shows the fatigue crack growth rates of long cracks
			44, Fig 13, Page 461	Graph shows the effect of test temperature on the fatigue crack growth rates
Fracture Energy	0.52	MJ	65, Table 1, Page 702	Thickness: 9mm, mean diameter: 924mm, Axial length: 180mm
Fracture Strain	10	%	65, Table 1, Page 702	Thickness: 9mm, mean diameter: 924mm, Axial length: 180mm
Rupture Time	302.9	h	68, Table 2, Page 974	704°C, 448 MPa
	20.3	h	68, Table 2, Page 974	704°C, 520 MPa
	99.1	h	68, Table 2, Page 974	760°C, 300 MPa
	17.8	h	68, Table 2, Page 974	760°C, 400 MPa
	139.2	h	68, Table 2, Page 974	816°C, 150 MPa
	11.1	h	68, Table 2, Page 974	816°C, 250 MPa
	476.3	h	68, Table 2, Page 974	871°C, 80 MPa
	2.3	h	68, Table 2, Page 974	871°C, 150 MPa
Short Crack Growth Rates			166, Fig 8, Page 992	Graph shows the room temperature short crack growth rates
Tensile Strength	1200	MPa	65, Table 1, Page 702	Thickness: 9mm, mean diameter: 924mm, Axial length: 180mm
Threshold value for the growth of long cracks			44, Fig 15, Page 463	Graph shows the effect of test temperature on the threshold value for the growth of long cracks
Yield Stress	1000	MPa	65, Table 1, Page 702	Thickness: 9mm, mean diameter: 924mm, Axial length: 180mm

A3 IN 706

Mechanical Property	Value	Units	Reference	Notes
0.2% Y. S.	911	MPa	20, Table 3, Page 55	Heat treatment A (stress rupture properties optimised), 538°C
	873	MPa	20, Table 3, Page 55	Heat treatment A (stress rupture properties optimised), 649°C
	880	MPa	20, Table 3, Page 55	Heat treatment B (tensile properties optimised), 538°C
	810	MPa	20, Table 3, Page 55	Heat treatment B (tensile properties optimised), 649°C
0.2% Y. S.	919	MPa	21, Table 2, Page 64	As received
	577	MPa	21, Table 2, Page 64	As solution heat treated
	927	MPa	21, Table 2, Page 64	621°C/16h
	909	MPa	21, Table 2, Page 64	621°C/16h
	985	MPa	21, Table 2, Page 64	Aging step 1: 704°C/8h; Aging step 2: 621°C/16h
	1023	MPa	21, Table 2, Page 64	Aging step 1: 704°C/8h; Aging step 2: 621°C/8h
	1031	MPa	21, Table 2, Page 64	Aging step 1: 718°C/8h; Aging step 2: 621°C/8h
	1009	MPa	21, Table 2, Page 64	Aging step 1: 732°C/8h; Aging step 2: 621°C/8h
	1045	MPa	21, Table 2, Page 64	Aging step 1: 732°C/8h; Aging step 2: 621°C/8h
	1000	MPa	21, Table 2, Page 64	Aging step 1: 746°C/8h; Aging step 2: 621°C/8h
	1062	MPa	21, Table 3, Page 64	Solution time: 0.25h; Cooling Rate 11°C/min - 988°C
	1027	MPa	21, Table 3, Page 64	Solution time: 2.0h; Cooling Rate 11°C/min - 988°C
	1082	MPa	21, Table 3, Page 64	Solution time: 0.25h; Cooling Rate 55.6°C/min - 971°C
	1062	MPa	21, Table 3, Page 64	Solution time: 0.25h; Cooling Rate 11°C/min - 971°C
	1062	MPa	21, Table 3, Page 64	Solution time: 0.25h; Cooling Rate 8.3°C/min - 971°C
	1000	MPa	21, Table 3, Page 64	Solution time: 0.25h; Cooling Rate 5.5°C/min - 971°C
	1048	MPa	21, Table 3, Page 64	Solution time: 2.0h; Cooling Rate 55.6°C/min - 971°C
	1062	MPa	21, Table 3, Page 64	Solution time: 2.0h; Cooling Rate 11°C/min - 971°C
	1041	MPa	21, Table 3, Page 64	Solution time: 2.0h; Cooling Rate 8.3°C/min - 971°C
	1007	MPa	21, Table 3, Page 64	Solution time: 2.0h; Cooling Rate 5.5°C/min - 971°C
	1048	MPa	21, Table 3, Page 64	Solution time: 0.25h; Cooling Rate 11°C/min - 960°C
	1029	MPa	21, Table 3, Page 64	Solution time: 2.0h; Cooling Rate 11°C/min - 960°C

Mechanical Property	Value	Units	Reference	Notes
399°C Cycles to Failure	6017		21, Table 2, Page 64	As received
	15143		21, Table 2, Page 64	As solution heat treated
	10945		21, Table 2, Page 64	621°C/16h
	12054		21, Table 2, Page 64	621°C/16h
	5541		21, Table 2, Page 64	Aging step 1: 704°C/8h; Aging step 2: 621°C/16h
	7103		21, Table 2, Page 64	Aging step 1: 704°C/8h; Aging step 2: 621°C/8h
	6902		21, Table 2, Page 64	Aging step 1: 718°C/8h; Aging step 2: 621°C/8h
	5330		21, Table 2, Page 64	Aging step 1: 732°C/8h; Aging step 2: 621°C/8h
	4729		21, Table 2, Page 64	Aging step 1: 732°C/8h; Aging step 2: 621°C/8h
	5093		21, Table 2, Page 64	Aging step 1: 746°C/8h; Aging step 2: 621°C/8h
	16300		21, Table 3, Page 64	Solution time: 0.25h; Cooling Rate 11°C/min - 988°C
	8250		21, Table 3, Page 64	Solution time: 2.0h; Cooling Rate 11°C/min - 988°C
	14400		21, Table 3, Page 64	Solution time: 0.25h; Cooling Rate 55.6°C/min - 971°C
	18650		21, Table 3, Page 64	Solution time: 0.25h; Cooling Rate 11°C/min - 971°C
	16000		21, Table 3, Page 64	Solution time: 0.25h; Cooling Rate 8.3°C/min - 971°C
	12750		21, Table 3, Page 64	Solution time: 0.25h; Cooling Rate 5.5°C/min - 971°C
	7950		21, Table 3, Page 64	Solution time: 2.0h; Cooling Rate 55.6°C/min - 971°C
	6800		21, Table 3, Page 64	Solution time: 2.0h; Cooling Rate 11°C/min - 971°C
	7550		21, Table 3, Page 64	Solution time: 2.0h; Cooling Rate 8.3°C/min - 971°C
	9850		21, Table 3, Page 64	Solution time: 2.0h; Cooling Rate 5.5°C/min - 971°C
	16550		21, Table 3, Page 64	Solution time: 0.25h; Cooling Rate 11°C/min - 960°C
	10950		21, Table 3, Page 64	Solution time: 2.0h; Cooling Rate 11°C/min - 960°C
			21 Fig 5, Page 67	Graph shows the cycles to failure vs intergranular η phase
	5034		21, Table 4, Page 67	Air
	3424		21, Table 4, Page 67	Air
	2907		21, Table 4, Page 67	Air
	5407		21, Table 4, Page 67	1.3 x 10^{-3} Pa vacuum
	2802		21, Table 4, Page 67	1.3 x 10^{-3} Pa vacuum

Mechanical Property	Value	Units	Reference	Notes
	3283		21, Table 4, Page 67	1.3 x 10^{-3} Pa vacuum
399°C Cycles to Initiation	4425		21, Table 2, Page 64	As received
	14744		21, Table 2, Page 64	As solution heat treated
	8225		21, Table 2, Page 64	621°C/16h
	9501		21, Table 2, Page 64	621°C/16h
	3620		21, Table 2, Page 64	Aging step 1: 704°C/8h; Aging step 2: 621°C/16h
	4547		21, Table 2, Page 64	Aging step 1: 704°C/8h; Aging step 2: 621°C/8h
	4172		21, Table 2, Page 64	Aging step 1: 718°C/8h; Aging step 2: 621°C/8h
	4949		21, Table 2, Page 64	Aging step 1: 732°C/8h; Aging step 2: 621°C/8h
	2788		21, Table 2, Page 64	Aging step 1: 732°C/8h; Aging step 2: 621°C/8h
	4885		21, Table 2, Page 64	Aging step 1: 746°C/8h; Aging step 2: 621°C/8h
	15181		21, Table 3, Page 64	Solution time: 0.25h; Cooling Rate 11°C/min - 988°C
	6901		21, Table 3, Page 64	Solution time: 2.0h; Cooling Rate 11°C/min - 988°C
	14227		21, Table 3, Page 64	Solution time: 0.25h; Cooling Rate 55.6°C/min - 971°C
	16967		21, Table 3, Page 64	Solution time: 0.25h; Cooling Rate 11°C/min - 971°C
	15884		21, Table 3, Page 64	Solution time: 0.25h; Cooling Rate 8.3°C/min - 971°C
	11767		21, Table 3, Page 64	Solution time: 0.25h; Cooling Rate 5.5°C/min - 971°C
	7490		21, Table 3, Page 64	Solution time: 2.0h; Cooling Rate 55.6°C/min - 971°C
	6778		21, Table 3, Page 64	Solution time: 2.0h; Cooling Rate 11°C/min - 971°C
	4985		21, Table 3, Page 64	Solution time: 2.0h; Cooling Rate 8.3°C/min - 971°C
	9368		21, Table 3, Page 64	Solution time: 2.0h; Cooling Rate 5.5°C/min - 971°C
	15933		21, Table 3, Page 64	Solution time: 0.25h; Cooling Rate 11°C/min - 960°C
	10448		21, Table 3, Page 64	Solution time: 2.0h; Cooling Rate 11°C/min - 960°C
ASTM Grain Size Number	5.4 ± 0.5		21, Table 2, Page 64	As received
	5.5 ± 0.4		21, Table 2, Page 64	As solution heat treated
	5.4 ± 0.4		21, Table 2, Page 64	621°C/16h
	3.8 ± 0.5		21, Table 2, Page 64	621°C/16h
	5.7 ± 0.5		21, Table 2, Page 64	Aging step 1: 704°C/8h; Aging step 2: 621°C/16h

Mechanical Property	Value	Units	Reference	Notes
	4.9 ± 0.5		21, Table 2, Page 64	Aging step 1: 704°C/8h; Aging step 2: 621°C/8h
	5.1 ± 0.6		21, Table 2, Page 64	Aging step 1: 718°C/8h; Aging step 2: 621°C/8h
	5.0 ± 0.3		21, Table 2, Page 64	Aging step 1: 732°C/8h; Aging step 2: 621°C/8h
	4.1 ± 0.4		21, Table 2, Page 64	Aging step 1: 732°C/8h; Aging step 2: 621°C/8h
	4.9 ± 0.4		21, Table 2, Page 64	Aging step 1: 746°C/8h; Aging step 2: 621°C/8h
	5.4		21, Table 3, Page 64	Solution time: 0.25h; Cooling Rate 11°C/min - 988°C
	4.5		21, Table 3, Page 64	Solution time: 2.0h; Cooling Rate 11°C/min - 988°C
	6.2		21, Table 3, Page 64	Solution time: 0.25h; Cooling Rate 55.6°C/min - 971°C
	6.3		21, Table 3, Page 64	Solution time: 0.25h; Cooling Rate 11°C/min - 971°C
	5.9		21, Table 3, Page 64	Solution time: 0.25h; Cooling Rate 8.3°C/min - 971°C
	6.7		21, Table 3, Page 64	Solution time: 0.25h; Cooling Rate 5.5°C/min - 971°C
	4.8		21, Table 3, Page 64	Solution time: 2.0h; Cooling Rate 55.6°C/min - 971°C
	4.3		21, Table 3, Page 64	Solution time: 2.0h; Cooling Rate 11°C/min - 971°C
	4.8		21, Table 3, Page 64	Solution time: 2.0h; Cooling Rate 8.3°C/min - 971°C
	4.7		21, Table 3, Page 64	Solution time: 2.0h; Cooling Rate 5.5°C/min - 971°C
	6.7		21, Table 3, Page 64	Solution time: 0.25h; Cooling Rate 11°C/min - 960°C
	5.7		21, Table 3, Page 64	Solution time: 2.0h; Cooling Rate 11°C/min - 960°C
Elongation	16.4	%	20, Table 3, Page 55	Heat treatment A (stress rupture properties optimised), 538°C
	20	%	20, Table 3, Page 55	Heat treatment A (stress rupture properties optimised), 649°C
	21.6	%	20, Table 3, Page 55	Heat treatment B (tensile properties optimised), 538°C
	26.6	%	20, Table 3, Page 55	Heat treatment B (tensile properties optimised), 649°C
Elongation	14.2	%	21, Table 2, Page 64	As received
	34.0	%	21, Table 2, Page 64	As solution heat treated
	21.5	%	21, Table 2, Page 64	621°C/16h
	32.0	%	21, Table 2, Page 64	621°C/16h
	20.7	%	21, Table 2, Page 64	Aging step 1: 704°C/8h; Aging step 2: 621°C/16h
	23.0	%	21, Table 2, Page 64	Aging step 1: 704°C/8h; Aging step 2: 621°C/8h
	21.5	%	21, Table 2, Page 64	Aging step 1: 718°C/8h; Aging step 2: 621°C/8h

Mechanical Property	Value	Units	Reference	Notes
	16.7	%	21, Table 2, Page 64	Aging step 1: 732°C/8h; Aging step 2: 621°C/8h
	21.5	%	21, Table 2, Page 64	Aging step 1: 732°C/8h; Aging step 2: 621°C/8h
	16.5	%	21, Table 2, Page 64	Aging step 1: 746°C/8h; Aging step 2: 621°C/8h
	20	%	21, Table 3, Page 64	Solution time: 0.25h; Cooling Rate 11°C/min - 988°C
	21	%	21, Table 3, Page 64	Solution time: 2.0h; Cooling Rate 11°C/min - 988°C
	21	%	21, Table 3, Page 64	Solution time: 0.25h; Cooling Rate 55.6°C/min - 971°C
	20	%	21, Table 3, Page 64	Solution time: 0.25h; Cooling Rate 11°C/min - 971°C
	19	%	21, Table 3, Page 64	Solution time: 0.25h; Cooling Rate 8.3°C/min - 971°C
	20	%	21, Table 3, Page 64	Solution time: 0.25h; Cooling Rate 5.5°C/min - 971°C
	20	%	21, Table 3, Page 64	Solution time: 2.0h; Cooling Rate 55.6°C/min - 971°C
	20	%	21, Table 3, Page 64	Solution time: 2.0h; Cooling Rate 11°C/min - 971°C
	20	%	21, Table 3, Page 64	Solution time: 2.0h; Cooling Rate 8.3°C/min - 971°C
	20	%	21, Table 3, Page 64	Solution time: 2.0h; Cooling Rate 5.5°C/min - 971°C
	20	%	21, Table 3, Page 64	Solution time: 0.25h; Cooling Rate 11°C/min - 960°C
	20	%	21, Table 3, Page 64	Solution time: 2.0h; Cooling Rate 11°C/min - 960°C
Fatigue Crack Growth			20, Figs 5 & 6, Page 60	Graphs show the fatigue crack growth of Inconel alloy 706 tested at 538°C and 649°C for both heat treatments
Reduction in Area	46.0	%	20, Table 3, Page 55	Heat treatment A (stress rupture properties optimised), 538°C
	51.5	%	20, Table 3, Page 55	Heat treatment A (stress rupture properties optimised), 649°C
	52.5	%	20, Table 3, Page 55	Heat treatment B (tensile properties optimised), 538°C
	57.9	%	20, Table 3, Page 55	Heat treatment B (tensile properties optimised), 649°C
Reduction in Area	18.4	%	21, Table 2, Page 64	As received
	32.8	%	21, Table 2, Page 64	As solution heat treated
	23.3	%	21, Table 2, Page 64	621°C/16h
	47.8	%	21, Table 2, Page 64	621°C/16h
	26.1	%	21, Table 2, Page 64	Aging step 1: 704°C/8h; Aging step 2: 621°C/16h
	31.9	%	21, Table 2, Page 64	Aging step 1: 704°C/8h; Aging step 2: 621°C/8h
	29.1	%	21, Table 2, Page 64	Aging step 1: 718°C/8h; Aging step 2: 621°C/8h
	22.4	%	21, Table 2, Page 64	Aging step 1: 732°C/8h; Aging step 2: 621°C/8h

Mechanical Property	Value	Units	Reference	Notes
	31.9	%	21, Table 2, Page 64	Aging step 1: 732°C/8h; Aging step 2: 621°C/8h
	20.5	%	21, Table 2, Page 64	Aging step 1: 746°C/8h; Aging step 2: 621°C/8h
	33	%	21, Table 3, Page 64	Solution time: 0.25h; Cooling Rate 11°C/min - 988°C
	32	%	21, Table 3, Page 64	Solution time: 2.0h; Cooling Rate 11°C/min - 988°C
	39	%	21, Table 3, Page 64	Solution time: 0.25h; Cooling Rate 55.6°C/min - 971°C
	33	%	21, Table 3, Page 64	Solution time: 0.25h; Cooling Rate 11°C/min - 971°C
	34	%	21, Table 3, Page 64	Solution time: 0.25h; Cooling Rate 8.3°C/min - 971°C
	33	%	21, Table 3, Page 64	Solution time: 0.25h; Cooling Rate 5.5°C/min - 971°C
	31	%	21, Table 3, Page 64	Solution time: 2.0h; Cooling Rate 55.6°C/min - 971°C
	37	%	21, Table 3, Page 64	Solution time: 2.0h; Cooling Rate 11°C/min - 971°C
	30	%	21, Table 3, Page 64	Solution time: 2.0h; Cooling Rate 8.3°C/min - 971°C
	32	%	21, Table 3, Page 64	Solution time: 2.0h; Cooling Rate 5.5°C/min - 971°C
	35	%	21, Table 3, Page 64	Solution time: 0.25h; Cooling Rate 11°C/min - 960°C
	33	%	21, Table 3, Page 64	Solution time: 2.0h; Cooling Rate 11°C/min - 960°C
Static Crack Growth			20 Fig 1, Page 57	Graph shows the static growth rate for INCONEL alloy 706 tested at 538°C and 649°C in both heat treatment conditions
Ultimate Strength	1112	MPa	20, Table 3, Page 55	Heat treatment A (stress rupture properties optimised), 538°C
	1014	MPa	20, Table 3, Page 55	Heat treatment A (stress rupture properties optimised), 649°C
	1054	MPa	20, Table 3, Page 55	Heat treatment B (tensile properties optimised), 538°C
	983	MPa	20, Table 3, Page 55	Heat treatment B (tensile properties optimised), 649°C
Ultimate Strength	1234	MPa	21, Table 2, Page 64	As received
	980	MPa	21, Table 2, Page 64	As solution heat treated
	1187	MPa	21, Table 2, Page 64	621°C/16h
	1202	MPa	21, Table 2, Page 64	621°C/16h
	1207	MPa	21, Table 2, Page 64	Aging step 1: 704°C/8h; Aging step 2: 621°C/16h
	1225	MPa	21, Table 2, Page 64	Aging step 1: 704°C/8h; Aging step 2: 621°C/8h
	1227	MPa	21, Table 2, Page 64	Aging step 1: 718°C/8h; Aging step 2: 621°C/8h
	1222	MPa	21, Table 2, Page 64	Aging step 1: 732°C/8h; Aging step 2: 621°C/8h
	1252	MPa	21, Table 2, Page 64	Aging step 1: 732°C/8h; Aging step 2: 621°C/8h

Mechanical Property	Value	Units	Reference	Notes
	1222	MPa	21, Table 2, Page 64	Aging step 1: 746°C/8h; Aging step 2: 621°C/8h
	1296	MPa	21, Table 3, Page 64	Solution time: 0.25h; Cooling Rate 11°C/min - 988°C
	1269	MPa	21, Table 3, Page 64	Solution time: 2.0h; Cooling Rate 11°C/min - 988°C
	1317	MPa	21, Table 3, Page 64	Solution time: 0.25h; Cooling Rate 55.6°C/min - 971°C
	1310	MPa	21, Table 3, Page 64	Solution time: 0.25h; Cooling Rate 11°C/min - 971°C
	1303	MPa	21, Table 3, Page 64	Solution time: 0.25h; Cooling Rate 8.3°C/min - 971°C
	1289	MPa	21, Table 3, Page 64	Solution time: 0.25h; Cooling Rate 5.5°C/min - 971°C
	1276	MPa	21, Table 3, Page 64	Solution time: 2.0h; Cooling Rate 55.6°C/min - 971°C
	1282	MPa	21, Table 3, Page 64	Solution time: 2.0h; Cooling Rate 11°C/min - 971°C
	1276	MPa	21, Table 3, Page 64	Solution time: 2.0h; Cooling Rate 8.3°C/min - 971°C
	1276	MPa	21, Table 3, Page 64	Solution time: 2.0h; Cooling Rate 5.5°C/min - 971°C
	1303	MPa	21, Table 3, Page 64	Solution time: 0.25h; Cooling Rate 11°C/min - 960°C
	1276	MPa	21, Table 3, Page 64	Solution time: 2.0h; Cooling Rate 11°C/min - 960°C

A4 IN 100

Mechanical Property	Value	Units	Reference	Notes
0.2% yield strength	1100	MPa	29, Table 1, Page 3-5	Typical properties for IN-100 at 649°C
0.2% yield strength	770	MPa	30, Table, Page 4-3	Typical properties for the coated material at room temperature
	550	MPa	30, Table, Page 4-3	Typical properties for the coated material at 900°C
0.2% yield strength	866.0	MPa	28, Table 3, Page 2-13	Mechanical properties (20°C)
	467.0	MPa	28, Table 3, Page 2-13	Mechanical properties (925°C)
Bulk carbon content			9, Fig 4, Page 95	Graph shows the change in bulk carbon content after exposure in controlled impurity helium at 900°C
			9, Fig 5, Page 95	Graph shows the effect of the exposure temperature on the change in bulk carbon content after exposure in controlled impurity helium
Creep fatigue data			29, Table 2, Page 3-5	Creep fatigue data (tabulated)
Creep fatigue data			31, Table 4,Page A1-18-23	Table shows the creep fatigue data for IN-100 (cast)
Creep fatigue data			28, Table 4, Page 2-14	Creep fatigue data (tabulated)
Creep rupture life 0.2%	900	MPa	29, Table 1, Page 3-5	Typical properties for IN-100 at 649°C (100hr)

Mechanical Property	Value	Units	Reference	Notes
	760	MPa	29, Table 1, Page 3-5	Typical properties for IN-100 at 649°C (1000hr)
Creep rupture properties	430.0	MPa	28, Table 3, Page 2-13	Creep rupture properties (10h)
	262.0	MPa	28, Table 3, Page 2-13	Creep rupture properties (100h)
	158.6	MPa	28, Table 3, Page 2-13	Creep rupture properties (1000h)
Cyclic life			29, Fig 12, Page 3-17	Graph shows the actual vs. calculated cyclic life for IN-100
Cycles to failure Elastic modulus			29, Table 6, Page 4-17	Calculation of number of cycles to failure with the two methods from the measured stabilised loops (tabulated)
	214,000	MPa	30, Table, Page 4-3	Typical properties for the coated material room temperature
	160,000	MPa	30, Table, Page 4-3	Typical properties for the coated material at 900°C
	147,000	MPa	30, Table, Page 4-3	Typical properties for the coated material at 1000°C
Elongation	22	%	29, Table 1, Page 3-5	Typical properties for IN-100 at 649°C (100hr)
Inelastic strain vs. cyclic life			29, Fig 11, Page 3-16	Graph shows PP and CP inelastic strain vs. cyclic life
Inelastic strain vs. life for TCSD cycle			29, Fig 3, Page 3-8	Graph shows the inelastic strain vs. life for TCSD cycle
Inelastic strain vs. life for THSC cycle			29, Fig 4, Page 3-9	Graph shows the inelastic strain vs. life for THSC cycle
Inelastic strain vs. life for HRSC cycle			29, Fig 5, Page 3-10	Graph show the inelastic strain vs. life for HRSC cycle
Inelastic strain ranges			30, Fig 10, Page 4-8	Graph shows the measured and calculated values of the stabilised inelastic strain ranges
Life			44, Fig 7, Page 452	Graph shows the variation of the fraction of life N_i/N_f spent in initiating a 0.25mm deep crack
Mechanical properties			31, Table 3, Page A1-8	Table shows the mechanical properties of 2 cast and 2 powder samples of IN 100 at various temperatures
Partitioning analysis			30, Tables 3 & 4, Page 4-11	Results of the partitioning analysis (tabulated)
RA	4	%	30, Table, Page 4-3	Typical properties for the coated material at 900°C
	12	%	30, Table, Page 4-3	Typical properties for the coated material at 1000°C
RA	12.1	-%	28, Table 3, Page 2-13	Mechanical properties (20°C)
	10.2	-%	28, Table 3, Page 2-13	Mechanical properties (925°C)
RA (creep)	10.3	-%	28, Table 3, Page 2-13	Creep rupture properties (10h)
	10.3	-%	28, Table 3, Page 2-13	Creep rupture properties (100h)
	10.3	-%	28, Table 3, Page 2-13	Creep rupture properties (1000h)
Rupture lifetime			42, Fig 21, Page 324	Rupture lifetime for IN 100 in different gases
Rupture stress	405	MPa	30, Table, Page 4-3	Typical properties for the coated material at 900°C

Mechanical Property	Value	Units	Reference	Notes
	198	MPa	30, Table, Page 4-3	Typical properties for the coated material at 1000°C
	280	MPa	30, Table, Page 4-3	Typical properties for the coated material at 900°C
	128	MPa	30, Table, Page 4-3	Typical properties for the coated material at 1000°C
	187	MPa	30, Table, Page 4-3	Typical properties for the coated material at 900°C
	82	MPa	30, Table, Page 4-3	Typical properties for the coated material at 1000°C
Strain range			29, Fig 2, Page 3-7	Graph shows the total strain range vs. cyclic life
Stress range			30, Fig 7, Page 4-7	Graph shows the effect of hold time and frequency on the relation between stress range and inelastic strain range
Stress rupture life	1020	MPa	29, Table 1, Page 3-5	Typical properties for IN-100 at 649°C (1000hr)
	880	MPa	29, Table 1, Page 3-5	Typical properties for IN-100 at 649°C
Strain range partitioning life			28, Fig 4, Page 2-10	Graph shows the strain range partitioning life relationships gatorised IN 100 in air at 760°C
			28, Fig 5, Page 2-11	Graph shows the strain range partitioning life relationships for cast IN 100 in air at 925°C
Temperature capability			9, Fig 2, Page 783	Graph shows the temperature capability of nickel superalloys for the turbine blades
THSC, TCSD and HRSC tests			29, Fig 6, Page 3-11	Graph shows a composite plot for THSC, TCSD and HRSC tests
Ultimate strength	890	MPa	30, Table, Page 4-3	Typical properties for the coated material at room temperature
	715	MPa	30, Table, Page 4-3	Typical properties for the coated material at 900°C
	470	MPa	30, Table, Page 4-3	Typical properties for the coated material at 1000°C
Ultimate strength	1040.0	MPa	28, Table 3, Page 2-13	Mechanical properties (20°C)
	622.0	MPa	28, Table 3, Page 2-13	Mechanical properties (925°C)
Ultimate tensile strength	1380	MPa	29, Table 1, Page 3-5	Typical properties for IN-100 at 649°C
Weight Gain			46, Fig 4, Page 8	Graph shows the weight gain of cast Ni-base alloys in HTGR environment at 900°C
Young's Modulus	205,500	MPa	28, Table 3, Page 2-13	Mechanical properties (20°C)
	155,100	MPa	28, Table 3, Page 2-13	Mechanical properties (925°C)

A5 Inconel MA6000

Mechanical Property	Value	Units	Reference	Notes
Coffin Manson			33, Fig 4, Page 1096	Graph shows the Coffin-Manson plots of MA 6000 at 850°C and 1050°C
	0.439		33, Table 3, Page 1097	Plastic strain amplitude k constant at T = 850°C
	1.706		33, Table 3, Page 1097	Plastic strain amplitude C constant at T = 850°C

Mechanical Property	Value	Units	Reference	Notes
	0.492		33, Table 3, Page 1097	Plastic strain amplitude k constant at T = 1050°C
	0.933		33, Table 3, Page 1097	Plastic strain amplitude C constant at T = 1050°C
	0.266		33, Table 3, Page 1097	Total strain amplitude k' constant at T = 850°C
	2.099		33, Table 3, Page 1097	Total strain amplitude C' constant at T = 850°C
	0.298		33, Table 3, Page 1097	Total strain amplitude k' constant at T = 1050°C
	0.875		33, Table 3, Page 1097	Total strain amplitude C' constant at T = 1050°C
CSS Curves			33, Figs 6 & 7, Pages 1097 & 1098	Graphs show the CSS curves of MA 6000 at 850°C and 1050°C
Cycles to failure	5123		33, Table 2, Page 1094	Tested at 850°C, 0.003 s^{-1}, 0.25% total strain amplitude
	72		33, Table 2, Page 1094	Tested at 850°C, 0.003 s^{-1}, 0.50% total strain amplitude
	4		33, Table 2, Page 1094	Tested at 850°C, 0.003 s^{-1}, 1.80% total strain amplitude
	>6800		33, Table 2, Page 1094	Tested at 1050°C, 2 x 10^{-5} s^{-1}, 0.10% total strain amplitude
	210		33, Table 2, Page 1094	Tested at 1050°C, 2 x 10^{-5} s^{-1}, 0.18% total strain amplitude
	122		33, Table 2, Page 1094	Tested at 1050°C, 2 x 10^{-5} s^{-1}, 0.22% total strain amplitude
	22		33, Table 2, Page 1094	Tested at 1050°C, 2 x 10^{-5} s^{-1}, 0.30% total strain amplitude
	8		33, Table 2, Page 1094	Tested at 1050°C, 2 x 10^{-5} s^{-1}, 0.52% total strain amplitude
Cyclic Deformation			32, Fig 1, Page 1070	Graph shows the cyclic deformation curves of MA 6000
Cyclic Hardening			33, Fig 2, Page 1095	Graph shows cyclic hardening curves of MA 6000 at 850°C
			33, Fig 3, Page 1095	Graph shows cyclic hardening curves of MA 6000 at 1050°C
Cyclic Lives			32, Fig 3, Page 1072	Graph shows the cyclic lives of MA 6000 at 850°C as a function of the total and of the plastic strain amplitude
Cyclic Stress/Strain Curves			32, Fig 2, Page 1071	Graph shows the cyclic stress-strain curves of MA 6000
Elastic Strain Amplitude	0.20	%	33, Table 2, Page 1094	Tested at 850°C, 0.003 s^{-1}, 0.25% total strain amplitude
	0.35	%	33, Table 2, Page 1094	Tested at 850°C, 0.003 s^{-1}, 0.50% total strain amplitude
	0.51	%	33, Table 2, Page 1094	Tested at 850°C, 0.003 s^{-1}, 1.80% total strain amplitude
	0.09	%	33, Table 2, Page 1094	Tested at 1050°C, 2 x 10^{-5} s^{-1}, 0.10% total strain amplitude
	0.11	%	33, Table 2, Page 1094	Tested at 1050°C, 2 x 10^{-5} s^{-1}, 0.18% total strain amplitude
	0.13	%	33, Table 2, Page 1094	Tested at 1050°C, 2 x 10^{-5} s^{-1}, 0.22% total strain amplitude
	0.13	%	33, Table 2, Page 1094	Tested at 1050°C, 2 x 10^{-5} s^{-1}, 0.30% total strain amplitude

Mechanical Property	Value	Units	Reference	Notes
	0.14	%	33, Table 2, Page 1094	Tested at 1050°C, 2 x 10^{-5} s^{-1}, 0.52% total strain amplitude
Hot Corrosion Resistance - Cyclic Oxidation - Descaled Mass Change	-1.205	g/m^2	13, Table 2, Page 76	504 h, 1100°C, Air + 5% H_2O, 24 h cycle to RT
Burner Rig Corrosion - Metal Loss	25.4	μm	13, Table 2, Page 76	504 h, 927°C, 1cycle/h (58 min. in flame, 2 min. out in air) 30:1 ratio of air + 5ppm sea water to fuel (0.3% S, JP-5)
Burner Rig Corrosion - Metal Attack	88.9	μm	13, Table 2, Page 76	504 h, 927°C, 1cycle/h (58 min. in flame, 2 min. out in air) 30:1 ratio of air + 5ppm sea water to fuel (0.3% S, JP-5)
Burner Rig Corrosion - Metal Loss	20.3	μm	13, Table 3, Page 78	1093°C 1cycle/hour (58 min. in flame, 2 min. out in air) 30:1 air to fuel (0.3%S in JP-5 fuel + 5ppm sea salt) ratio. Mass flow 5.5 ft^3/min.
Burner Rig Corrosion - Metal Loss	91.4	μm	13, Table 3, Page 78	1093°C 1cycle/hour (58 min. in flame, 2 min. out in air) 30:1 air to fuel (0.3%S in JP-5 fuel + 5ppm sea salt) ratio. Mass flow 5.5 ft^3/min.
Burner Rig Corrosion - Metal Attack	81.3	μm	13, Table 3, Page 78	1093°C 1cycle/hour (58 min. in flame, 2 min. out in air) 30:1 air to fuel (0.3%S in JP-5 fuel + 5ppm sea salt) ratio. Mass flow 5.5 ft^3/min.
Burner Rig Corrosion - Metal Attack	358.1	μm	13, Table 3, Page 78	1093°C 1cycle/hour (58 min. in flame, 2 min. out in air) 30:1 air to fuel (0.3%S in JP-5 fuel + 5ppm sea salt) ratio. Mass flow 5.5 ft^3/min.
Plastic Strain Amplitude	0.05	%	33, Table 2, Page 1094	Tested at 850°C, 0.003 s^{-1}, 0.25% total strain amplitude
	0.15	%	33, Table 2, Page 1094	Tested at 850°C, 0.003 s^{-1}, 0.50% total strain amplitude
	1.29	%	33, Table 2, Page 1094	Tested at 850°C, 0.003 s^{-1}, 1.80% total strain amplitude
	0.01	%	33, Table 2, Page 1094	Tested at 1050°C, 2 x 10^{-5} s^{-1}, 0.10% total strain amplitude
	0.07	%	33, Table 2, Page 1094	Tested at 1050°C, 2 x 10^{-5} s^{-1}, 0.18% total strain amplitude
	0.09	%	33, Table 2, Page 1094	Tested at 1050°C, 2 x 10^{-5} s^{-1}, 0.22% total strain amplitude
	0.17	%	33, Table 2, Page 1094	Tested at 1050°C, 2 x 10^{-5} s^{-1}, 0.30% total strain amplitude
	0.38	%	33, Table 2, Page 1094	Tested at 1050°C, 2 x 10^{-5} s^{-1}, 0.52% total strain amplitude
Saturation Stress Amplitude	358	MPa	33, Table 2, Page 1094	Tested at 850°C, 0.003 s^{-1}, 0.25% total strain amplitude
	632	MPa	33, Table 2, Page 1094	Tested at 850°C, 0.003 s^{-1}, 0.50% total strain amplitude
	830	MPa	33, Table 2, Page 1094	Tested at 850°C, 0.003 s^{-1}, 1.80% total strain amplitude
	150	MPa	33, Table 2, Page 1094	Tested at 1050°C, 2 x 10^{-5} s^{-1}, 0.10% total strain amplitude
	195	MPa	33, Table 2, Page 1094	Tested at 1050°C, 2 x 10^{-5} s^{-1}, 0.18% total strain amplitude

Mechanical Property	Value	Units	Reference	Notes
	220	MPa	33, Table 2, Page 1094	Tested at 1050°C, 2 x 10^{-5} s^{-1}, 0.22% total strain amplitude
	228	MPa	33, Table 2, Page 1094	Tested at 1050°C, 2 x 10^{-5} s^{-1}, 0.30% total strain amplitude
	235	MPa	33, Table 2, Page 1094	Tested at 1050°C, 2 x 10^{-5} s^{-1}, 0.52% total strain amplitude
Strain Rate			32, Fig 4, Page 1072	Graph shows the strain rate and temperature dependence of the cyclic life of MA 6000
Stress Rupture			13, Fig 2, Page 76	Graph shows a comparison of the stress rupture behaviour of experimental alloys vs. commercial alloys
			13, Fig 5, Page 79	Graph shows the preliminary stress rupture characteristics
Total Strain Amplitude			33, Fig 45, Page 1096	Graph shows the total strain amplitude vs. cycles to failure of MA 6000 at 850°C and 1050°C

A6 DS IN 792

Mechanical Property	Value	Units	Reference	Notes
Creep Crack Growth			17, Fig 9, Page 137	Graph shows the influence of the environment on the creep crack growth rate and a comparison with the fatigue crack growth rate
Fatigue Crack Growth			17, Fig 2, Page 134	Graph shows the fatigue crack growth rate in air and a vacuum
Temperature Capability			5, Fig 8, Page 1719	Graph shows the temperature capability of superalloys as a function of Chromium content

A7 DS CM 247 LC

Mechanical Property	Value	Units	Reference	Notes Sol = 2125°F/2h, DA = 1400°F/8h + 1200°C/24h
0.2% YS	115.7	ksi	19, Table 2, Page 48	70°F Tensile Test Results - DA only
	114.6	ksi	19, Table 2, Page 48	70°F Tensile Test Results - Sol and DA
	116.8	ksi	19, Table 2, Page 48	1200°F Tensile Test Results - DA only
	114.9	ksi	19, Table 2, Page 48	1200°F Tensile Test Results - Sol and DA
	108.4	ksi	19, Table 2, Page 48	1500°F Tensile Test Results - DA only
	116.6	ksi	19, Table 2, Page 48	1500°F Tensile Test Results - Sol and DA
	123.9	ksi	19, Table 4, Page 51	70°F - 2050°F HIP condition - Tensile Test Results
	120.2	ksi	19, Table 4, Page 51	70°F - 2165°F HIP condition - Tensile Test Results
	130.3	ksi	19, Table 4, Page 51	1200°F - 2050°F HIP condition - Tensile Test Results

Mechanical Property	Value	Units	Reference	Notes Sol = 2125°F/2h, DA = 1400°F/8h + 1200°C/24h
	129.6	ksi	19, Table 4, Page 51	1200°F - 2165°F HIP condition - Tensile Test Results
	117.4	ksi	19, Table 4, Page 51	1500°F - 2050°F HIP condition - Tensile Test Results
	114.4	ksi	19, Table 4, Page 51	1500°F - 2165°F HIP condition - Tensile Test Results
Density	8.54	Mg/m^3	5, Table 4, Page 1720	
EL (Creep)	4.1	%	19, Table 2, Page 48	1650°F/35 ksi Creep Rupture Test Results - DA only
	3.1	%	19, Table 2, Page 48	1650°F/35 ksi Creep Rupture Test Results - Sol and DA
	2.2	%	19, Table 4, Page 51	1300°F/100 ksi - 2050°F HIP condition Creep Rupture Test Results
	2.9	%	19, Table 4, Page 51	1300°F/100 ksi - 2165°F HIP condition Creep Rupture Test Results
	5.0	%	19, Table 4, Page 51	1650°F/35 ksi - 2050°F HIP condition Creep Rupture Test Results
	3.1	%	19, Table 4, Page 51	1650°F/35 ksi - 2165°F HIP condition Creep Rupture Test Results
EL (Tensile)	23.9	%	19, Table 2, Page 48	70°F Tensile Test Results - DA only
	18.2	%	19, Table 2, Page 48	70°F Tensile Test Results - Sol and DA
	25.2	%	19, Table 2, Page 48	1200°F Tensile Test Results - DA only
	19.0	%	19, Table 2, Page 48	1200°F Tensile Test Results - Sol and DA
	9.5	%	19, Table 2, Page 48	1500°F Tensile Test Results - DA only
	13.1	%	19, Table 2, Page 48	1500°F Tensile Test Results - Sol and DA
	21.3	%	19, Table 4, Page 51	70°F - 2050°F HIP condition - Tensile Test Results
	22.1	%	19, Table 4, Page 51	70°F - 2165°F HIP condition - Tensile Test Results
	17.1	%	19, Table 4, Page 51	1200°F - 2050°F HIP condition - Tensile Test Results
	17.1	%	19, Table 4, Page 51	1200°F - 2165°F HIP condition - Tensile Test Results
	5.3	%	19, Table 4, Page 51	1500°F - 2050°F HIP condition - Tensile Test Results
	4.4	%	19, Table 4, Page 51	1500°F - 2165°F HIP condition - Tensile Test Results
Failure	73.8	hr	19, Table 2, Page 48	1650°F/35 ksi Creep Rupture Test Results - DA only
	225.0	hr	19, Table 2, Page 48	1650°F/35 ksi Creep Rupture Test Results - Sol and DA
	599.8	hr	19, Table 4, Page 51	1300°F/100 ksi - 2050°F HIP condition Creep Rupture Test Results
	527.9	hr	19, Table 4, Page 51	1300°F/100 ksi - 2165°F HIP condition Creep Rupture Test Results
	59.0	hr	19, Table 4, Page 51	1650°F/35 ksi - 2050°F HIP condition Creep Rupture Test Results
	54.3	hr	19, Table 4, Page 51	1650°F/35 ksi - 2165°F HIP condition Creep Rupture Test Results

Mechanical Property	Value	Units	Reference	Notes Sol = 2125°F/2h, DA = 1400°F/8h + 1200°C/24h
Fatigue Lives			79, Figs 1 & 2, Pages 526 - 527	Graphs show the correlation of tension tortion multiaxial low-cycle fatigue lives with Mises strain at 1173K
Larson-Millar	46.1		19, Table 2, Page 48	1650°F/35 ksi Creep Rupture Test Results - DA only
	47.2		19, Table 2, Page 48	1650°F/35 ksi Creep Rupture Test Results - Sol and DA
	40.1		19, Table 4, Page 51	1300°F/100 ksi - 2050°F HIP condition Creep Rupture Test Results
	39.8		19, Table 4, Page 51	1300°F/100 ksi - 2165°F HIP condition Creep Rupture Test Results
	45.9		19, Table 4, Page 51	1650°F/35 ksi - 2050°F HIP condition Creep Rupture Test Results
	45.9		19, Table 4, Page 51	1650°F/35 ksi - 2165°F HIP condition Creep Rupture Test Results
Larson Millar Parameter			19, Fig 7, Page 47	Graph shows a Larson-Millar plot of creep rupture test results of Spraycast-X Mar-M247LC compared to other casting processes
LCF Data			79, Fig 7, Page 530	Graph shows the correlation of tension-tortion LCF data with anisotropic strain
Mach 1.0 Oxidation			36, Fig 7, Page 35	Graph shows the Mach 1.0 Oxidation at 1135°C
Stress-Rupture Strength			36, Fig 5, Page 35	Graph shows the stress-rupture strength of DS CM 247LC vs. DS and equiaxed Mar M 247
			36, Fig 6, Page 35	Graph shows 982°C stress-rupture for CMSX-4 vs. DS CM 247LC vs. equiaxed IN 738 LC
Temperature Capability			2, Fig 8, Page 1719	Graph shows the temperature capability of superalloys as a function of Chromium content.
Tensile Test Results			19, Fig 6, Page 47	Graph shows the tensile test results of Spraycast-X Mar-M247LC compared to other casting processes
UTS	199.7	ksi	19, Table 2, Page 48	70°F Tensile Test Results - DA only
	179.5	ksi	19, Table 2, Page 48	70°F Tensile Test Results - Sol and DA
	170.7	ksi	19, Table 2, Page 48	1200°F Tensile Test Results - DA only
	166.6	ksi	19, Table 2, Page 48	1200°F Tensile Test Results - Sol and DA
	138.3	ksi	19, Table 2, Page 48	1500°F Tensile Test Results - DA only
	136.9	ksi	19, Table 2, Page 48	1500°F Tensile Test Results - Sol and DA
	211.3	ksi	19, Table 4, Page 51	70°F - 2050°F HIP condition - Tensile Test Results
	213.6	ksi	19, Table 4, Page 51	70°F - 2165°F HIP condition - Tensile Test Results
	178.5	ksi	19, Table 4, Page 51	1200°F - 2050°F HIP condition - Tensile Test Results
	178.3	ksi	19, Table 4, Page 51	1200°F - 2165°F HIP condition - Tensile Test Results
	142.2	ksi	19, Table 4, Page 51	1500°F - 2050°F HIP condition - Tensile Test Results

Mechanical Property	Value	Units	Reference	Notes Sol = 2125°F/2h, DA = 1400°F/8h + 1200°C/24h
	138.5	ksi	19, Table 4, Page 51	1500°F - 2165°F HIP condition - Tensile Test Results

A8 L-TZM

Mechanical Property	Value	Units	Reference	Notes
0.2% yield strength	696	N mm^{-2}	12, Table 2, Page 135	T = 20°C prepared rod 1400°C 2h intermediate recrystalisation +
	751	N mm^{-2}	12, Table 2, Page 135	T = 20°C prepared rod 1700°C 5h +71% worked stress relieved
	416	N mm^{-2}	12, Table 2, Page 135	T = 20°C prepared rod 1400°C 2h intermediate recrystalisation +
	431	N mm^{-2}	12, Table 2, Page 135	T = 20°C prepared rod 1700°C 5h +71% worked stress relieved
	488	N mm^{-2}	12, Table 2, Page 135	T = 850°C prepared rod 1400°C 2h intermediate recrystalisation +
	537	N mm^{-2}	12, Table 2, Page 135	T = 850°C prepared rod 1700°C 5h +71% worked stress relieved
	262	N mm^{-2}	12, Table 2, Page 135	T = 850°C prepared rod 1400°C 2h intermediate recrystalisation +
	213	N mm^{-2}	12, Table 2, Page 135	T = 850°C prepared rod 1700°C 5h +71% worked stress relieved
Carburisation			10, Fig 6, Page 200	Graph shows carburisation of molybdenum TZM in HHT helium
Carburisation kinetics			58, Fig 8, Page O15	Graph shows the carburisation kinetics at 850°C
Creep rupture strength			8, Fig 4, Page 254	Graph shows the creep rupture of materials under consideration for advanced HTRs
Creep rupture strength			10, Fig 2, Page 198	Graph shows the creep rupture strength of different turbine blade materials at 850°C
Creep rupture strength			12, Fig 1, Page 133	Graph shows the creep rupture strength of some high temperature alloys at 1000°C
			12, Fig 8, Page 136	Graph shows the creep rupture strength at 850°C of PM Mo-TZM in different working conditions
			12, Fig 9, Page 136	Graph shows the creep rupture strength at 850°C of blades made of PM Mo-TZM produced in different ways
Creep rupture strength			46, Fig 2, Page 6	Graph shows the creep rupture strength of different turbine blade materials at 850°C
Creep rupture strength			58, Fig 7, Page O14	Graph shows the creep rupture strength of vacuum arc-melted TZM, 53% worked, at 850°C in helium

Mechanical Property	Value	Units	Reference	Notes
Elongation ($L_0 = 3d_0$)	28	%	12, Table 2, Page 135	T = 20°C prepared rod 1400°C 2h intermediate recrystalisation +
	18	%	12, Table 2, Page 135	T = 20°C prepared rod 1700°C 5h +71% worked stress relieved
	25	%	12, Table 2, Page 135	T = 20°C prepared rod 1400°C 2h intermediate recrystalisation +
	23	%	12, Table 2, Page 135	T = 20°C prepared rod 1700°C 5h +71% worked stress relieved
	15	%	12, Table 2, Page 135	T = 850°C prepared rod 1400°C 2h intermediate recrystalisation +
	17	%	12, Table 2, Page 135	T = 850°C prepared rod 1700°C 5h +71% worked stress relieved
	37	%	12, Table 2, Page 135	T = 850°C prepared rod 1400°C 2h intermediate recrystalisation +
	33	%	12, Table 2, Page 135	T = 850°C prepared rod 1700°C 5h +71% worked stress relieved
Fatigue behaviour			10, Fig 9, Page 201	Graph shows a comparison of the fatigue behaviour of alloy 713 LC and molybdenum TZM at 850°C
Fatigue strength			10, Fig 8, Page 201	Graph shows the fatigue strength of P/M molybdenum TZM at various positions in the air foil
Impact energy			12, Fig 7, Page 136	Graph shows curves for impact energy vs temperature
Impact test			152, Fig 4, Page 412	Graph shows the percentage of brittle fracture surface in impact test of arc cast TZM
Low cycle fatigue behaviour			10, Fig 10, Page 201	Graph shows the low cycle fatigue behaviour of alloy 713 LC and molybdenum TZM
Reduction of area	64	%	12, Table 2, Page 135	T = 20°C prepared rod 1400°C 2h intermediate recrystalisation +
	52	%	12, Table 2, Page 135	T = 20°C prepared rod 1700°C 5h +71% worked stress relieved
	23	%	12, Table 2, Page 135	T = 20°C prepared rod 1400°C 2h intermediate recrystalisation +
	23	%	12, Table 2, Page 135	T = 20°C prepared rod 1700°C 5h +71% worked stress relieved
	72	%	12, Table 2, Page 135	T = 850°C prepared rod 1400°C 2h intermediate recrystalisation +
	76	%	12, Table 2, Page 135	T = 850°C prepared rod 1700°C 5h +71% worked stress relieved
	81	%	12, Table 2, Page 135	T = 850°C prepared rod 1400°C 2h intermediate recrystalisation +
	85	%	12, Table 2, Page 135	T = 850°C prepared rod 1700°C 5h +71% worked stress relieved
Stress for rupture			12, Fig 1, Page 409	Graph shows the stress for rupture in 10^5 h vs. design temperature
Stress for rupture			46, Fig 3, Page 7	Graph shows the stress for rupture in 10^5 h vs. design temperature

Mechanical Property	Value	Units	Reference	Notes
Tensile strength	796	N mm^{-2}	12, Table 2, Page 135	T = 20°C prepared rod 1400°C 2h intermediate recrystalisation +
	826	N mm^{-2}	12, Table 2, Page 135	T = 20°C prepared rod 1700°C 5h +71% worked stress relieved
	581	N mm^{-2}	12, Table 2, Page 135	T = 20°C prepared rod 1400°C 2h intermediate recrystalisation +
	564	N mm^{-2}	12, Table 2, Page 135	T = 20°C prepared rod 1700°C 5h +71% worked stress relieved
	513	N mm^{-2}	12, Table 2, Page 135	T = 850°C prepared rod 1400°C 2h intermediate recrystalisation +
	570	N mm^{-2}	12, Table 2, Page 135	T = 850°C prepared rod 1700°C 5h +71% worked stress relieved
	301	N mm^{-2}	12, Table 2, Page 135	T = 850°C prepared rod 1400°C 2h intermediate recrystalisation +
	316	N mm^{-2}	12, Table 2, Page 135	T = 850°C prepared rod 1700°C 5h +71% worked stress relieved

A9 IN 713

Mechanical Property	Value	Units	Reference	Material	Notes
Bend fatigue			58, Fig 15, Page O19	IN 713 LC	Graph shows the push-pull bend fatigue of IN 713 LC
Carburisation			58, Fig 6, Page O14	IN 713 LC	Graph shows carburisation profiles
Creep behaviour			10, Fig 11, Page 202	alloy 713 LC	Graph shows the creep behaviour of alloy 713 LC at 850°C under cyclic loads
Creep curves			38, Fig 11, Page 74	alloy 713	Graph shows the creep curves for specimens machined from new, normal service exposed and over heated alloy 713 blades. Creep tests were conducted at 200MPa and 871°C
Creep rupture strength			10, Fig 1, Page 198	alloy 713 LC	Graph shows the creep rupture strength of alloy 713 LC in the 500 - 850°C temperature
Creep rupture strength			46, Fig 2, Page 6	alloy 713 LC	Graph shows the creep rupture strength of different turbine blade materials at 850°C
Creep rupture strength			58, Fig 1, Page O11	IN 713 LC	Graph shows the creep rupture strength of IN 713 LC at 850°C as a function of environmental conditions
Creep strain			10, Fig 3, Page 199	alloy 713 LC	Graph shows 1 % creep strain of alloy 713 LC at 850°C in air and HHT helium
Creep strength			58, Fig 2, Page O11	IN 713 LC	Creep strength of IN 713 LC at 1% elongation
Damage accumulation			10, Fig 12, Page 202	alloy 713 LC	Graph shows damage accumulation in creep cycle tests on alloy 713 LC
Decontamination factors			10, Fig 17, Page 205	alloy 713 LC	Graph shows the decontamination factors
Fatigue behaviour			10, Fig 9, Page 201	alloy 713 LC	Graph shows a comparison of the fatigue behaviour of alloy 713 LC and molybdenum TZM at 850°C
Fatigue tests			10, Fig 7, Page 201	alloy 713 LC	Graph shows fatigue tests on alloy 713 LC at elevated temperatures
Inoculation effects			16, Fig 14, Page 357	Inconel 713 C	Graph shows the effects of inoculation on creep curves
Larson Millar			16, Fig 6,	Inconel	Graph shows an example of Larson-Millar

Mechanical Property	Value	Units	Reference	Material	Notes
Parameter			Page 348	713 LC	parameter
Low cycle fatigue behaviour			10, Fig 10, Page 201	alloy 713 LC	Graph shows the low-cycle fatigue behaviour of alloy 713 LC
Low cycle fatigue behaviour			58, Fig 11, Page O17	IN 713 LC	Graph shows the influence of temperature on the low-cycle fatigue behaviour on IN 713 LC
			58, Fig 13, Page O18	IN 713 LC	Graph shows the influence of hold times on the low-cycle fatigue behaviour of IN 713 LC at 750°C
Rupture strength			16, Fig 7, Page 350	Inconel 713 C	Graph shows the correlation of 100,000h rupture strength with short time tensile strength at temperatures 800°C and 900°C
			16, Fig 9, Page 353	Inconel 713 C	Graph shows the temperature dependence of 100,000h rupture strength for various superalloys
Stress	338	MPa	16, Table 4, Page 349	Inconel 713 C	Comparison of short-time and long time strength, T = 850°C, t = 100h
	248	MPa	16, Table 4, Page 349	Inconel 713 C	Comparison of short-time and long time strength, T = 900°C, t = 100h
	181	MPa	16, Table 4, Page 349	Inconel 713 C	Comparison of short-time and long time strength, T = 950°C, t = 100h
	238	MPa	16, Table 4, Page 349	Inconel 713 C	Comparison of short-time and long time strength, T = 850°C, t = 1000h
	168	MPa	16, Table 4, Page 349	Inconel 713 C	Comparison of short-time and long time strength, T = 900°C, t = 1000h
	117	MPa	16, Table 4, Page 349	Inconel 713 C	Comparison of short-time and long time strength, T = 950°C, t = 1000h
	161	MPa	16, Table 4, Page 349	Inconel 713 C	Comparison of short-time and long time strength, T = 850°C, t = 10,000h
	107	MPa	16, Table 4, Page 349	Inconel 713 C	Comparison of short-time and long time strength, T = 900°C, t = 10,000h
	68	MPa	16, Table 4, Page 349	Inconel 713 C	Comparison of short-time and long time strength, T = 950°C, t = 10,000h
	101	MPa	16, Table 4, Page 349	Inconel 713 C	Comparison of short-time and long time strength, T = 850°C, t = 100,000h
	60	MPa	16, Table 4, Page 349	Inconel 713 C	Comparison of short-time and long time strength, T = 900°C, t = 100,000h
	30	MPa	16, Table 4, Page 349	Inconel 713 C	Comparison of short-time and long time strength, T = 950°C, t = 100,000h
Stress for rupture			15, Fig 1, Page 409	alloy 713 LC	Stress rupture in 10^5 h vs. design stress for HHT turbine blades
Stress for rupture			46, Fig 3, Page 7	alloy 713 LC	Graph shows the stress for rupture in 105 h vs. design temperature for HTGR turbine blade
Stress rupture			16, Fig 2, Page 342	alloy 713 LC	Graph shows stress rupture data for alloy 713 LC
			16, Fig 5, Page 346	Inconel 713 LC	Graph shows a comparison of TTP fit to stress rupture data
Stress-strain curve			58, Fig 12, Page O18	IN 713 LC	Graph shows the cyclic stress-strain curve for IN 713 LC at 750°C
Weight gain			11, Fig 6 Page 198	713 LC	Graph shows weight gain of cast high nickel alloys at 900°C
Weight gain			46, Fig 4, Page 8	713 LC	Graph shows the weight gain of cast Ni-base alloys in HTGR environment at 900°C

A10 IN 738

Mechanical Property	Value	Units	Material	Reference	Notes
Crack growth data			IN 738 LC	44, Fig 4-1, Page 508	Graph shows high temperature crack growth data for IN 738 LC
Creep crack growth rate			IN 738	17, Fig 8, Page 136	Graph shows the influence of environment on creep crack growth rate in IN-738 at 927°C
Creep crack growth rate			IN 738	43, Fig 17, Page 438	Graph shows creep crack growth rates as function of the stress intensity factor K
Creep behaviour			IN 738 LC	39, Fig 10, Page 80	Graph shows the creep behaviour of new and service exposed IN 738 LC tested at 90 MPa and 899°C
Creep curves			IN 738 LC	42, Fig 16, Page 322	Graph shows creep curves for IN 738 LC for different deposits and air
Creep fatigue data			IN 738 LC	31, Table 4, Page A135	Creep fatigue data (tabulated)
Creep properties			IN 738 LC	37, Fig 5, Page 55	Graph shows the creep properties tested at 850°C under stresses of 245 & 294 MPa in IN738 LC aged at 750°C-900°C up to 24000h
Creep rate			IN 738 LC	37, Fig 9, Page 57	Graph shows the changed in the minimum creep rate of IN 738 LC tested at 850°C under the stresses of 245 and 294 MPa
Creep rate			IN 738 LC	43, Figs 2 & 3, Page 429	Graphs show the dependence of steady state creep rate from applied stress
Creep rate			IN 738 LC	39, Fig 7, Page 79	Graph shows the minimum creep rate vs stress at 850°C
			IN 738 LC	39, Fig 8, Page 79	Graph shows the effect of service exposure on the minimum creep rate tested over a range of temperatures at 90MPa
Creep rupture tests			IN 738 LC	45, Fig 25, Page 617	Graph shows creep rupture tests at 650/850°C
Cycles to failure			IN 738 LC	27, Fig 4, Page …	Graph shows the number cycles to failure as a function of semi range of total stress for tests with load or strain cycling at 750 and 850°C
			IN 738 LC	27, Fig 6, Page …	Graph shows the number of cycles to failure as a function of inelastic strain range for tests with load or strain cycling at 750 and 850°C
			IN 738 LC	27, Fig 7, Page..	Graph shows the number of cycles to failure as a function of the semi range of total strain for tests with continuous strain cycling
			IN 738 LC	27, Fig 8, Page..	Graph shows the number of cycles to failure as a function of inelastic strain range for tests with continuous cycling
			IN 738 LC	27, Fig 9, Page..	Graph shows the number of cycles to failure as a function of the semi range of total strain for tests with continuous strain cycling
			IN 738 LC	27, Fig 11, Page..	Graphs show the number of cycles to failure as a function of inelastic strain range for tests with strain limited cycles
Cyclic and creep life			IN 738 LC	44, Fig 5-4, Page 532	Graph shows the relation and cyclic and creep life

Mechanical Property	Value	Units	Material	Reference	Notes
Cyclic hardening			IN 738 LC	44, Fig 3-2, Page 501	Graph shows the cyclic hardening in strain controlled tests at 850°C
Cyclic softening behaviour			IN 738 LC	76, Fig 2, Page 96	Graph shows the cyclic softening behaviour if IN 738 LC in a vacuum at different strain rates
Cyclic softening behaviour			IN 738 LC	7, Fig 3, Page 129	Graph shows the effect of hot corrosion and strain rate on the cyclic softening behaviour on IN 738 LC at 900°C
Cyclic stress response curves			IN 738 LC	25, Fig 1, Page 387	Graphs show cyclic stress response curves
Cyclic stress / strain behaviour			IN 738 LC	76, Fig 3, Page 96	Graph shows the cyclic stress / strain behaviour of IN 738 LC in a vacuum at 900°C
Cyclic stress / strain behaviour			IN 738 LC	7, Fig 4, Page 130	Graph shows the cyclic stress / strain behaviour of IN 738 LC in a vacuum at 900°C
Cyclic stress strain curves			IN 738 LC	25, Fig 2, Page 388	Graph shows cyclic stress strain curves
Cyclic stress strain curves			IN 738 LC	44, Fig 3-1, Page 501	Graph shows cyclic stress strain curves at 850°C
Elastic strain range			IN 738	23, Fig 7, Page 453	Graph shows the elastic strain range vs. life to failure
			IN 738	23, Fig 8, Page 453	Graph shows the elastic strain range vs. life to crack initiation
Elastic and plastic components			IN 738 LC	26, Fig 6, Page 796	Graph shows the elastic and plastic components vs. cycles to failure
			IN 738 LC	26, Fig 7, Page 797	Graph shows the elastic and plastic components vs. endurance
Fatigue crack growth rate			IN 738	17, Fig 1, Page 133	Fatigue crack growth rate as a function of ΔK in IN 738 at 927°C
Fatigue crack growth rate			IN 738 LC	44, Fig 12, Page 460	Graph shows the fatigue crack growth rates of long cracks in air at room temperature and at 850°C
Fatigue data			IN 738 LC	44, Fig 5-1, Page 525	Graph shows the fatigue data for IN 738 LC
Fatigue Lives			IN 738 LC	79, Figs 1 & 2, Pages 526 - 527	Graphs show the correlation of tension torsion multiaxial low-cycle fatigue lives with Mises strain at 1173K
Frequency strain rate			IN 738 LC	44, Fig 5-9, Page 539	Graph shows the frequency strain rate sensitivity
Image analysis results			IN 738 LC	37, Fig 2, Page 54	Graph shows image analysis results of IN 738 LC at 750°C - 900°C up to 24,000 h
Inelastic strain range			IN 738	23, Fig 9, Page 454	Graph shows the inelastic strain range vs. life to failure
			IN 738	23, Fig 10, Page 454	Graph shows the inelastic strain range vs. life to crack initiation
LCF behaviour			IN 738 LC	76, Fig 5, Page 97	Graph shows the LCF behaviour of IN738 LC in a vacuum at 900°C and 2 different strain rates
			IN 738 LC	76, Fig 6, Page 97	Graph shows the effect of the environment on the LCF behaviour of IN 738 LC at 900°C
LCF behaviour			IN 738 LC	7, Fig 2, Page 129	Graph shows the effect of hot corrosion on the LCF behaviour of IN 738 LC at different strain rates at 900°C

Mechanical Property	Value	Units	Material	Reference	Notes
LCF behaviour			IN 738 LC	24, Fig 5, Page 693	Graph shows the effect of environments on LCF behaviour of IN 738 LC at 900°C
Mechanical properties			IN 738 LC	37, Fig 4, Page 54	Graphs show mechanical properties art room temperature of IN 738 LC aged at 750°C - 900°C up to 24,000h
			IN 738 LC	37, Fig 6, Page 55	Graph shows the changes in the hardness, tensile strength and 0.2% yield stress in IN 738 LC with the density of precipitates
Partitioned strain ranges			IN 738	23, Table 1, Page 451	Typical test results and partitioned strain ranges
Plastic strain range			IN 738 LC	26, Fig 5, Page 796	Graph shows plastic strain range vs. endurance
Rupture life			IN 738 LC	39, Fig 6, Page 79	Graph shows the effect of artificial aging and service exposure on rupture life trend of IN 738 LC blades at 850°C
Rupture life			IN 738 LC	39, Fig 15, Page 83	Graph shows the effect of test temperature on the rupture life of new and service exposed blades at 90 MPa
Rupture lifetime			IN 738 LC	100 Fig 22, Page 324	Graph shows the rupture lifetime for IN 738 LC in different gases
Steady state creep rate			IN 738 LC	24, Fig 1, Page 691	Graph shows the effect of hot corrosion on the stress dependence of the steady creep rate at 850°C
			IN 738 LC	24, Fig 2, Page 691	Graph shows the effect of hot corrosion on the steady state creep rate at 307 MPa
Strains and failure data			IN 738 LC	31, Table 4, Page A135	Strains and failure data (tabulated)
Strain range partitioning			IN 738 LC	27, Fig 31, Page …	Graph shows the strain range partitioning - pp and derived cp, pc and cc lifetime relationships
Stress rupture			IN 738 LC	45, Fig 33, Page 622	Graph shows the influence of reheat treatment and HIP on stress rupture time of IN 738 LC
Stress rupture behaviour			IN 738 LC	43, Fig 8, Page 433	Graph shows the effect of HIP treatment on stress rupture behaviour of pre damaged IN 738 LC at 850°C
			IN 738 LC	43, Fig 9, Page 433	Graph shows the influence of corrosion on stress rupture of IN 738 LC at 850°C
			IN 738 LC	43, Fig 10, Page 434	Graph shows the effect of environment on stress rupture behaviour of IN 738 LC at 850°C
Stress rupture curves			IN 738 LC	43, Fig 1, Page 428	Graph shows stress rupture curves at 750, 850 and 900°C
Stress rupture life			IN 738 LC	37, Fig 10, Page 57	Graph shows changes in the stress rupture life of IN 738 LC tested at 850°C under the stresses of 245 and 294 MPa
Stress rupture results			IN 738 LC	22, Fig 6, Page 134	Graph shows IN 738 LC stress rupture results
Test results using various strain controlled cycles			IN 738 LC	27, Table 4, Page …	IN 738 LC test results using various strain controlled cycles (tabulated data)
Thermal expansion			IN 738	66, Fig 4, Page 728	Graph shows the thermal expansion as a function of temperature

Mechanical Property	Value	Units	Material	Reference	Notes
Time to fracture			IN 738 LC	24, Fig 3, Page 692	Graph shows the effect of hot corrosion on the stress dependence of the time to fracture for IN 738 LC at 850°C
			IN 738 LC	24, Fig 4, Page 692	Graph shows the effect of hot corrosion on the temperature dependence of the time to fracture for IN 738 LC at 307 MPa
Total strain range			IN 738	23, Fig 5, Page 452	Graph shows the total strain range vs. life to failure
			IN 738	23, Fig 6, Page 452	Graph shows the total strain range vs. life to crack initiation
Total strain range			IN 738 LC	26, Fig 4, Page 795	Graph shows the total strain range vs. endurance

A11 M 21

Mechanical Property	Value	Units	Reference	Notes
Weight Gain			11, Fig 6, Page 198	Graph shows the weight gain at 900°C
Weight Gain			46, Fig 4, Page 8	Graph shows the weight gain at 900°C

A12 SC 16

Mechanical Property	Value	Units	Reference	Notes
Density	8.21	Mg/m^3	5, Table 4, Page 1720	
Temperature Capability			5, Fig 8, Page 1719	Graph shows the Temperature Capability of Superalloys as a function of Chromium Content

A13 MAR M 004

Mechanical Property	Value	Units	Reference	Notes
Creep Rupture Strength			10, Fig 2, Page 198	Graph shows the creep rupture strength of different turbine blade materials at 850°C
Creep Rupture Strength			46, Fig 2, Page 6	Graph shows the creep rupture strength of different turbine blade materials at 850°C
Weight Gain			46, Fig 4, Page 8	Graph shows the weight gain of cast Ni-base alloys in the HTGR environment at 900°C

A14 Nimonic 80A

Mechanical Property	Value	Units	Reference	Notes
Creep rupture strength			10, Fig 2, Page 198	Graph shows the creep rupture strength of different turbine blade materials at 850°C
Creep rupture strength			46, Fig 2, Page 6	Graph shows the creep rupture strength of different turbine blade materials at 850°C
Density	8.2	$10^3 kgm^{-3}$	63, Table 1, Page 440	Measured at room temperature

Mechanical Property	Value	Units	Reference	Notes
Thermal conductivity	23	$Wm^{-1}K^{-1}$	63, Table 1, Page 440	Measured between 300 - 600K
Thermal expansion	8.1	$10^{-4}K^{-1}$	63, Table 1, Page 440	Measured between 300 - 600K
Young's modulus	340	$MNm^{3/2}$	63, Table 1, Page 440	Measured at room temperature

A15 Hastelloy X, Hastelloy XR & Hastelloy XR-II

Mechanical Property	Value	Units	Reference	Material	Notes
0.2% Yield strength	349.0	MPa	31, Table 3, Page A1-9	Hastelloy X	Wrought Hastelloy X, T = 20°C
	161.0	MPa	31, Table 3, Page A1-9	Hastelloy X	Wrought Hastelloy X, T = 871°C
Aging			59, Fig 2, Page R10	Hastelloy X	Graph shows the influence of aging on the yield and ultimate tensile stresses of Hastelloy X base metal.
			59, Fig 3, Page R10	Hastelloy X	Graph shows the influence of aging on the reduction in area of Hastelloy X
			59, Fig 4, Page R11	Hastelloy X	Graph shows the influence of aging on the Yield and Ultimate Tensile Stresses
			59, Fig 5, Page R11	Hastelloy X	Graph shows the influence of aging on the reduction in area
Carbon content	0.08	wt%	41, Table 3, Page 117	Hastelloy X	Results of bulk nitrogen and carbon analysis before testing
	0.01	wt%	41, Table 3, Page 117	Hastelloy X	Results of bulk nitrogen and carbon analysis after testing at 980°C for 1000h with 30 minute thermal cycling
Carbon content change			9, Fig 4, Page 95	Hastelloy X	Graph shows the change in bulk carbon content after in helium at 900°C
			9, Fig 5, Page 95	Hastelloy X	Graph shows the effect of exposure temperature on the change in carbon content
Carbon increase			56, Fig 4, Page J18	Hastelloy X	Graphs show the mass of carbon increase as a result of helium exposure
			56, Fig 7, Page J20	Hastelloy X	Graph shows the rates of carbon increase in Hastelloy X as a result of helium exposure
Corrosive wear			60, Fig 8, Page S11	Hastelloy X	Graph shows the corrosive wear of high temperature alloys in steam reformer atmosphere
Creep rupture properties	103.0	MPa	31, Table 3, Page A1-9	Hastelloy X	Wrought Hastelloy X, T = 871°C, t = 10h
	69.0	MPa	31, Table 3, Page A1-9	Hastelloy X	Wrought Hastelloy X, T = 871°C, t = 100h
	45.0	MPa	31, Table 3, Page A1-9	Hastelloy X	Wrought Hastelloy X, T = 871°C, t = 1000h
Creep rupture strength			11, Fig 4, Page 254	Hastelloy X	Graph shows the creep rupture strength of materials under consideration for advanced HTR's
Creep tests			55, Fig 15, Page B14	Hastelloy X	Graph shows the effect of thermal reactor irradiation on the onset of accelerated deformation in the post irradiation creep tests

Mechanical Property	Value	Units	Reference	Material	Notes
Cyclic crack growth			55, Fig 13, Page B14	Hastelloy X	Graph shows the cyclic crack growth of Hastelloy X measured in air and JAERI B helium environment
Dilation experiments			57, Table 2, Page L9	Hastelloy X	
Ductility			55, Fig 16, Page B14	Hastelloy X	Graph shows the effects of thermal neutron fluence and tensile test temperature on ductility of Hastelloy X
Fatigue behaviour			61, Fig 9, Page T14	Hastelloy X	Graph shows a comparison of the fatigue behaviour of several materials at 538°C
Fatigue crack growth rates			44, Fig 12, Page 460	Hastelloy X	Graphs show the fatigue crack growth rates of long cracks at RT and 850°C
Fatigue Data			61, Fig 4, Page T12	Hastelloy X	Graph shows a comparison of strain controlled fatigue data generated at 538°C in air and impure helium for Hastelloy X in several conditions
			61, Fig 5, Page T12	Hastelloy X	Graph shows a comparison of strain controlled fatigue data generated at 871°C in air for Hastelloy X in several conditions
Impact toughness	196	J	9, Table 3, Page 99	Hastelloy X	Room temperature CVN impact toughness properties
Internal Nitridation	>0.040	mm	41, Table 2, Page 117	Hastelloy X	Results of dynamic oxidation burner rig testing at 980°C for 1000h with 30 minute thermal cycling
Internal Oxidation	0.07	mm	41, Table 2, Page 117	Hastelloy X	Results of dynamic oxidation burner rig testing at 980°C for 1000h with 30 minute thermal cycling
LCF Behaviour			61, Fig 2, Page U8	Hastelloy X	Graph shows the LCF behaviour of different alloys at 850°C in air
Metal Loss	0.16	mm	41, Table 2, Page 117	Hastelloy X	Results of dynamic oxidation burner rig testing at 980°C for 1000h with 30minute thermal cycling
Minimum creep rates			59, Fig 7, Page R12	Hastelloy X	Graph shows the minimum creep rates of 3 Hastelloy X weldments
Minimum creep rates			11, Fig 8, Page 200	Hastelloy X	Graph shows the minimum creep rates vs. stress at 750°C
Mn			55, Fig 5, Page B12	Hastelloy X	Graph shows the effect of Mn in Hastelloy X based alloys on oxidation resistance to JAERI B helium
Nitrogen content	0.04	wt%	41, Table 3, Page 117	Hastelloy X	Results of bulk nitrogen and carbon analysis before testing
	0.57	wt%	41, Table 3, Page 117	Hastelloy X	Results of bulk nitrogen and carbon analysis after testing at 980°C for 1000h with 30 minute thermal cycling
Reduction in Area			61, Fig 1, Page T10	Hastelloy X	Tensile properties in solution annealed and aged conditions
Reduction in Area	59.0	%	31, Table 3, Page A1-9	Hastelloy X	Wrought Hastelloy X, T = 20°C
	89.0	%	31, Table 3, Page A1-9	Hastelloy X	Wrought Hastelloy X, T = 871°C
Strain range			61, Fig 2, Page T11	Hastelloy X	Graph shows a comparison of the data obtained from several heats, product forms and test techniques at RT
			61, Fig 3, Page T11	Hastelloy X	Graph shows the total strain range vs. cycles to failure tested in air
Stress			11, Fig 8,	Hastelloy X	Graph shows stress/log time plots at

Mechanical Property	Value	Units	Reference	Material	Notes
			Page 200		750°C
Stress rupture properties			59, Fig 6, Page R12	Hastelloy X	Graph shows the stress-rupture properties of 3 Hastelloy X weldments
Stress rupture tests			49, Fig 18, Page 90	Hastelloy X	Graph shows the stress-rupture test results on Hastelloy X and Alloy 800 before and after reactor irradiation at 900°C
Stress strain curves			61, Fig 10, Page T15	Hastelloy X	Graph shows the cyclic stress-strain curves for Hastelloy X and Inconel 617
Stress strain curves			11, Fig 7, Page 256	Hastelloy X	Graph shows the stress-strain curves for Hastelloy X
Surface oxide depth			11, Fig 1, Page 194	Hastelloy X	Graph shows the surface oxide depth vs. temperature
Tensile elongation			9, Fig 10, Page 98	Hastelloy X	Graph shows the tensile elongation in percent vs. temperature
Tensile ultimate strength			9, Fig 9, Page 98	Hastelloy X	Graphs shows the tensile ultimate strength vs. temperature
Tensile YS			9, Fig 8, Page 98	Hastelloy X	Graph shows the tensile YS (0.2%) vs. temperature
Total depth of attack	>0.56	mm	41, Table 2, Page 117	Hastelloy X	Results of dynamic oxidation burner rig testing at 980°C for 1000h with 30 minute thermal cycling
Total Elongation			61, Fig 1, Page T10	Hastelloy X	Tensile properties in solution annealed and aged conditions
Ultimate Tensile Strength			61, Fig 1, Page T10	Hastelloy X	Tensile properties in solution annealed and aged conditions
Ultimate Tensile Strength	764.0	MPa	31, Table 3, Page A1-9	Hastelloy X	Wrought Hastelloy X, T = 20°C
	165.0	MPa	31, Table 3, Page A1-9	Hastelloy X	Wrought Hastelloy X, T = 871°C
Uniform Elongation			61, Fig 1, Page T10	Hastelloy X	Tensile properties in solution annealed and aged conditions
Weight change	-107.1	mg/cm^2	41, Table 2, Page 117	Hastelloy X	Results of dynamic oxidation burner rig testing at 980°C for 1000h with 30 minute thermal cycling
Yield Strength			61, Fig 1, Page T10	Hastelloy X	Tensile properties in solution annealed and aged conditions
Young's Modulus	199.0	GPa	31, Table 3, Page A1-9	Hastelloy X	Wrought Hastelloy X, T = 20°C
	137.0	GPa	31, Table 3, Page A1-9	Hastelloy X	Wrought Hastelloy X, T = 871°C
Cr depleted zone			49, Fig 13, Page 87	Hastelloy X, Hastelloy XR	Graph shows the depth of the Cr depleted zone plotted against exposure time
Creep-rupture			55, Fig 11, Page B13	Hastelloy X, Hastelloy XR	Graph shows the trend of creep-rupture of Hastelloy XR in JAERI B helium
Minor element content			55, Fig 9, Page B13	Hastelloy X, Hastelloy XR	Graph shows the influence of minor element content in alloys on the incorporation of Co in loose corrosion products formed JAERI B helium

Mechanical Property	Value	Units	Reference	Material	Notes
Mn Cr evaporation loss			55, Fig 7, Page B12	Hastelloy X, Hastelloy XR	Graph shows the Mn, Cr evaporation loss after exposure of the alloy to JAERI-B helium for 1000hrs
Mn/Cr ratio			55, Fig 6, Page B12	Hastelloy X, Hastelloy XR	Graph shows the results of neutron activation analysis on the change of Mn/Cr ratio in the oxide film formed on the Hastelloy X and XR exposed to JAERI-B helium
Strain range			49, Fig 7, Page 85	Hastelloy X, Hastelloy XR	Graph shows the relation between total strain range and fatigue life under different strain rates at 900°C
Strain range			53, Fig 1, Page 117	Hastelloy X, Hastelloy XR	Graph shows the relation between the total strain range and fatigue life under different strain rates at 900°C
Stress strain curves			53, Fig 2, Page 118	Hastelloy X, Hastelloy XR	Graph shows the cyclic and monotonic stress-strain curves under different strain rates at 900 °C
0.2% PS	32.7	kg/mm^2	50, Table 1, Page 91	Hastelloy XR	Mechanical properties
0.2% PS	300	MPa	16, Table 1, Page 340	Hastelloy XR	Mechanical properties
Boron content effects			49, Fig 3, Page 83	Hastelloy XR	Graph shows the relation between the total boron content and the creep rupture strength
			49, Fig 4, Page 83	Hastelloy XR	Graph shows the effect of boron content on the number of cracks per one cross section
			49, Fig 5, Page 84	Hastelloy XR	Graph shows the effect of boron content on time to rupture for Hastelloy XR TIG weld metal and EB weld metal
Carbon content change			73, Fig 10, Page 101	Hastelloy XR	Graph shows the effects of Cr and Ti contents (wt%) on the change in carbon content after exposure at 900°C and 950°C in PNP-D for 3000h
			73, Fig 11, Page 101	Hastelloy XR	Graph shows the change in carbon content of the alloys tested at 950°C in PNP-S
			73, Fig 12, Page 101	Hastelloy XR	Graph shows the effects of Cr and Ti contents (wt%) on the change in carbon content after exposure at 900°C and 950°C in PNP-S for 3000h
			73, Fig 8, Page 100	Hastelloy XR	Graph shows the change in carbon content of the alloys tested at 900°C in PNP-D
			73, Fig 9, Page 101	Hastelloy XR	Graph shows the change in carbon content of the alloys tested at 950°C in PNP-D
Cr content			73, Fig 13, Page 102	Hastelloy XR	Graph shows the effect of Cr content (wt%) on the behaviour of the lower Ti content alloys
Creep buckling			35, Fig 3, Page 17	Hastelloy XR	Graph shows the safety design allowable time to creep buckling
Creep fatigue			50, Fig 7,	Hastelloy	Graph shows the Creep Fatigue

Mechanical Property	Value	Units	Reference	Material	Notes
interaction			Page 95	XR	Interaction damage diagram
Creep rate			55, Fig 10, Page B13	Hastelloy XR	Graph shows the influence if the specimen diameter on the secondary creep rate in JAERI B helium
Creep rupture data			49, Fig 1, Page 82	Hastelloy XR	Graph shows the creep rupture data for Hastelloy XR sampled from bar and tube in JAERI-type B helium
Creep rupture data (stress)	39	MPa	16, Table 2, Page 341	Hastelloy XR	Summary of creep rupture data (T = 800°C, rupture time = 23594h)
Creep rupture master curves			34, Fig 3, Page 78	Hastelloy XR	Graph shows simplified versions of the creep master rupture curves
Creep rupture property			55, Fig 3, Page B11	Hastelloy XR	Graph shows the influence of environment on creep rupture property
Creep rupture strength	3.6	kg_f/mm^2	34, Table 4, Page 83	Hastelloy XR	Measured value of creep rupture strength at T = 900°C, t_r = 1000h (air)
	1.5	kg_f/mm^2	34, Table 4, Page 83	Hastelloy XR	Measured value of creep rupture strength at T = 1000°C, t_r = 1000h (air)
	0.87	kg_f/mm^2	34, Table 4, Page 83	Hastelloy XR	Measured value of creep rupture strength at T = 1000°C, t_r = 10,000h (air)
	0.66	kg_f/mm^2	34, Table 4, Page 83	Hastelloy XR	Measured value of creep rupture strength at T = 1000°C, t_r = 50,000h (air)
	0.55	kg_f/mm^2	34, Table 4, Page 83	Hastelloy XR	Measured value of creep rupture strength at T = 1000°C, t_r = 100,000h (air)
	0.68	kg_f/mm^2	34, Table 4, Page 83	Hastelloy XR	Measured value of creep rupture strength at T = 1050°C, t_r = 10,000h (air)
	0.83	kg_f/mm^2	34, Table 4, Page 83	Hastelloy XR	Measured value of creep rupture strength at T = 1000°C, t_r = 1000h (no. 2 helium)
	1.3	kg_f/mm^2	34, Table 4, Page 83	Hastelloy XR	Measured value of creep rupture strength at T = 900°C, t_r = 1000h (PNP helium)
Creep rupture strength			35, Fig 5, Page 20	Hastelloy XR	Graph shows the creep rupture strength
Cyclic stress-relation			50, Fig 5, Page 94	Hastelloy XR	Graph shows the cyclic stress relation at $N_f/2$
Damage penetration curves			34, Fig 2, Page 77	Hastelloy XR	Graph shows a simplified version of the damage penetration curves due to surface oxidation
Depth of chromium-depleted layer	127	μm	34, Table 5, Page 84	Hastelloy XR	Changes after exposure to ERANS no. 2 simulated HTGR helium environment for 3000h
	174	μm	34, Table 5, Page 84	Hastelloy XR	Changes after exposure to ERANS no. 2 simulated HTGR helium environment for 5000h
Depth of internal oxidation	0	μm	34, Table 5, Page 84	Hastelloy XR	Changes after exposure to ERANS no. 2 simulated HTGR helium environment for 3000h
	0	μm	34, Table 5, Page 84	Hastelloy XR	Changes after exposure to ERANS no. 2 simulated HTGR helium environment for 5000h
Depth of microstructure change	0	μm	34, Table 5, Page 84	Hastelloy XR	Changes after exposure to ERANS no. 2 simulated HTGR helium environment for 3000h
	0	μm	34, Table 5, Page 84	Hastelloy XR	Changes after exposure to ERANS no. 2 simulated HTGR helium environment for 5000h
Ductility loss			55, Fig 14, Page B14	Hastelloy XR	Graph shows the ductility loss of a susceptible heat during aging under tensile stress

Mechanical Property	Value	Units	Reference	Material	Notes
ES	48.4	%	50, Table 1, Page 90	Hastelloy XR	Mechanical properties
Fatigue life			50, Fig 2, Page 92	Hastelloy XR	Graph shows the temperature effect on fatigue life
			50, Fig 3, Page 93	Hastelloy XR	Graph shows the environmental effect on fatigue life
			50, Fig 4, Page 93	Hastelloy XR	Graph shows the strain rate and hold time effect on fatigue life in He
			50, Fig 6, Page 94	Hastelloy XR	Graph shows a comparison of fatigue lives of Hastelloy XR and Hastelloy X at 900°C
Hold times			49, Fig 8, Page 85	Hastelloy XR	Graph shows the effect of hold time on low-cycle fatigue life for Hastelloy XR at 900°C
Hold times			53, Fig 3, Page 118	Hastelloy XR	Graph shows the effect of hold time on low-cycle fatigue life for Hastelloy XR at 900°C
			53, Fig 4, Page 118	Hastelloy XR	Graph shows the hold time dependence of the fatigue life in tensile hold-time experiments for Hastelloy XR at 700°C and 900°C
			53, Fig 5, Page 118	Hastelloy XR	Graph shows the hold time dependence of the ratio of the fatigue life in tensile hold time experiments
Impact value			49, Fig 15, Page 88	Hastelloy XR	Graph shows the RT impact value of Hastelloy XR after heating
Interaction with helium			55, Fig 18, Page B15	Hastelloy XR	Graph shows the interaction of the alloys and carbon bearing impurities in the HTR-helium as a function of temperature
Isothermal rupture curve			16, Fig 3 (b), Page 345	Hastelloy XR	Graph shows the Isothermal rupture Curves of Larson-Millar parameter for Hastelloy XR
Master rupture curve			16, Fig 3 (a), Page 344	Hastelloy XR	Graph shows the Master Rupture Curve of Larson-Millar paramater for Hastelloy XR
Oxidation kinetics			73, Fig 15, Page 103	Hastelloy XR	Graph shows the oxidation kinetics of the alloys tested at 950°C in PNP-S
Rupture strength			16, Fig 7, Page 350	Hastelloy XR	Graph shows the correlation of 100,000h rupture strength with short time tensile strength
Rupture strength			16, Fig 9, Page 353	Hastelloy XR	Graph shows the temperature dependence of 100,000h rupture strength for various superalloys
Stress	94	MPa	16, Table 4, Page 349	Hastelloy XR	Comparison of short-time and long time strength, T = 800°C, t = 100h
	51	MPa	16, Table 4, Page 349	Hastelloy XR	Comparison of short-time and long time strength, T = 900°C, t = 100h
	62	MPa	16, Table 4, Page 349	Hastelloy XR	Comparison of short-time and long time strength, T = 800°C, t = 1000h
	31	MPa	16, Table 4, Page 349	Hastelloy XR	Comparison of short-time and long time strength, T = 900°C, t = 1000h
	39	MPa	16, Table 4, Page 349	Hastelloy XR	Comparison of short-time and long time strength, T = 800°C, t = 10,000h
	17	MPa	16, Table 4, Page 349	Hastelloy XR	Comparison of short-time and long time strength, T = 900°C, t = 10,000h
	22	MPa	16, Table 4, Page 349	Hastelloy XR	Comparison of short-time and long time strength, T = 800°C, t = 100,000h

Mechanical Property	Value	Units	Reference	Material	Notes
	8	MPa	16, Table 4, Page 349	Hastelloy XR	Comparison of short-time and long time strength, T = 900°C, t = 100,000h
TS	73.6	kg/mm^2	50, Table 1, Page 91	Hastelloy XR	Mechanical properties
UTS	1000	MPa	16, Table 1, Page 340	Hastelloy XR	Mechanical properties
Weight gain (spalled oxide included)	1.355	mg/cm^2	34, Table 5, Page 84	Hastelloy XR	Changes after exposure to ERANS no. 2 simulated HTGR helium environment for 3000h
	1.832	mg/cm^2	34, Table 5, Page 84	Hastelloy XR	Changes after exposure to ERANS no. 2 simulated HTGR helium environment for 5000h
Creep rupture times			49, Fig 6, Page 84	Hastelloy XR, Hastelloy XR-II	Graph shows the comparison of creep rupture times of Hastelloy XR and XR-II under 26 MPa in different helium environments
Hold times			49, Fig 9, Page 86	Hastelloy XR, Hastelloy XR-II	Graph shows the hold time dependence of the fatigue life in tensile hold-time experiments for Hastelloy XR and XR-II at 900°C
0.2% proof stress and ultimate tensile stress			53, Fig 15, Page 122	Hastelloy XR-II	Graph shows the effect of test temperature on 0.2% proof stress and ultimate tensile strength
Fatigue life			49, Fig 12, Page 87	Hastelloy XR-II	Graph shows the fatigue life as a function of test temperature and total strain range
Fatigue life			53, Fig 18, Page 123	Hastelloy XR-II	Graph shows the fatigue life as functions of test temperature and total strain range for solution annealed Hastelloy XR-II and aged (900°C, 1000h) one
Fatigue test data			53, Fig 19, Page 124	Hastelloy XR-II	Graph shows a comparison of fatigue test data with fatigue curves predicted by the universal slope method and the 10% rule for solution annealed Hastelloy XR II
			53, Fig 20, Page 124	Hastelloy XR-II	Graph shows a comparison of fatigue test data with fatigue curves predicted by universal slope method and 10% rule for aged (900°C, 1000h) Hastelloy XR-II
Oxidation kinetics			49, Fig 14, Page 88	Hastelloy XR-II	Graph shows the oxidation kinetics of Hastelloy XR-II compared with Hastelloy XR in JAERI-type B helium
Strain range			49, Fig 10, Page 86	Hastelloy XR-II	Graph shows the total strain range vs. no. of cycles to failure
			49, Fig 11, Page 86	Hastelloy XR-II	Graph shows the relation between the normalised strain range vs. no. of cycles to failure
Strain range			53, Fig 17, Page 123	Hastelloy XR-II	Graph shows the relation between the total strain range and fatigue life for solution annealed Hastelloy XR-II and aged (900°C, 1000h) one
Total Elongation			53, Fig 16, Page 122	Hastelloy XR-II	Graph shows the effect of test temperature on total elongation and reduction in area

A16 IN 617

Mechanical Property	Value	Units	Reference	Notes
0.2 % PS			51, Fig 1, Page 97	Graph shows the 0.2% PS after thermal aging
0.2% proof stress			54, Fig 2, Page 160	Graph shows the 0.2% proof stress vs. temperature
Bulk carbon content change			9, Fig 4, Page 95	Graph shows the change in bulk carbon content after exposure on controlled impurity helium at 900°C
			9, Fig 5, Page 95	Graph shows the effect of exposure temperature on the change in bulk carbon content after exposure on controlled impurity helium
Carbon content	0.05	wt%	41, Table 3, Page 117	Results of bulk nitrogen and carbon analysis before testing
	0.04	wt%	41, Table 3, Page 117	Results of bulk nitrogen and carbon analysis after testing at 980°C for 1000h with 30 minute thermal cycling
Carbon content			54, Fig 6, Page 163	Graph shows the influence of corrosion time in PNP-helium on the variation of the carbon content near the surface of the alloy Inconel 617
Carbon content change			48, Fig 2, Page 74	Graphs show the change in carbon content of Inconel 617 during exposure in PNP helium
Carbon increase			56, Fig 6, Page J19	Graph shows the rates of carbon increase in Inconel 617 following exposure to helium
Corrosion kinetics			48, Fig 7, Page 77	Graph shows the corrosion kinetics of Inconel 617 at 950°C in impure helium
Corrosive wear			60, Fig 7, Page S11	Graph shows the corrosive wear of Inconel 717 in steam reformer atmosphere
Creep behaviour			9, Fig 11, Page 99	Graph shows a comparison of the 900°C creep behaviour
Creep crack growth behaviour			51, Fig 17, Page 104	Graph shows the creep crack growth behaviour
Creep curves			48, Fig 4, Page 75	Graph shows the creep curves for Inconel 617 in different environments showing the deleterious effect of decarburisation on creep strength
Creep fatigue damage			51, Fig 14, Page 102	Graph shows the creep fatigue damage
Creep properties			8, Fig 5, Page 255	Graphs show the creep properties of Inconel 617
Creep properties			54, Fig 3, Page 161	Graphs show the long time creep properties for 10^4 hrs
Creep rupture behaviour			58, Fig 10, Page O17	Graph shows a comparison of the creep rupture behaviour of IN 617 and Nimonic 86 at 850°C
Creep rupture strain limit data			51, Fig 7, Page 99	Graph shows 1% creep strain limit data
Creep rupture strength			8, Fig 4, Page 254	Graph show the creep rupture strength of materials under consideration for advanced HTRs
Creep rupture strength			51, Fig 11, Page 165	Graph shows the influence of the atmosphere on the creep rupture strength at 950°C
Creep rupture strength	1.02	kgf/mm^2	55, Table 7, Page B10	Creep rupture strength extrapolated (Larson-Millar method) to 50,000 hr at 1000°C

Mechanical Property	Value	Units	Reference	Notes
	0.88	kgf/mm^2	55, Table 7, Page B10	Creep rupture strength extrapolated (extrapolation method) to 50,000 hr at 1000°C
Creep rupture strength data			51, Fig 6, Page 99	Graph shows creep rupture strength data
Creep strength			40, Fig 1, Page 90	Graph shows the creep strength of solution annealed Inconel 617
Creep tests (stress)	51.4	N/mm^2	11, Table 7, Page 201	T = 800°C, t = 2000h, final strain = 0.30 - continuing (helium)
	51.2	N/mm^2	11, Table 7, Page 201	T = 800°C, t = 2000h, final strain = 0.09 % - continuing (helium)
	42.3	N/mm^2	11, Table 7, Page 201	T = 850°C, t = 2000h, final strain = 1.70 % - terminated (helium)
	42.2	N/mm^2	11, Table 7, Page 201	T = 850°C, t = 2000h, final strain = 2.31 % - continuing (helium)
	42.2	N/mm^2	11, Table 7, Page 201	T = 850°C, t = 2000h, final strain = 1.84 % - continuing (helium)
	37.0	N/mm^2	11, Table 7, Page 201	T = 850°C, t = 6000h, final strain = 0.52 % - continuing (helium)
	36.4	N/mm^2	11, Table 7, Page 201	T = 850°C, t = 2000h, final strain = 0.11 % - terminated (helium)
	36.4	N/mm^2	11, Table 7, Page 201	T = 850°C, t = 6000h, final strain = 0.66 % - continuing (helium)
	20.9	N/mm^2	11, Table 7, Page 201	T = 900°C, t = 3000h, final strain = 5.29 % - terminated (helium)
	20.9	N/mm^2	11, Table 7, Page 201	T = 900°C, t = 4000h, final strain = 4.76 % - continuing (helium)
	42.3	N/mm^2	11, Table 7, Page 201	T = 850°C, t = 3000h, final strain = 0.89 % - continuing (air)
	42.2	N/mm^2	11, Table 7, Page 201	T = 850°C, t = 3000h, final strain = 1.60 % - continuing (air)
	36.4	N/mm^2	11, Table 7, Page 201	T = 850°C, t = 2000h, final strain = 0.18 % - terminated (air)
	36.4	N/mm^2	11, Table 7, Page 201	T = 850°C, t = 10,000h, final strain = 2.23 % - continuing (air)
	36.5	N/mm^2	11, Table 7, Page 201	T = 850°C, t = 10,000h, final strain = 2.12 % - continuing (air)
Cyclic stress / strain curves			61, Fig 10, Page T15	Graph show the cyclic stress / strain curves for Hastelloy X and Inconel 617
Cyclic stress responses			51, Fig 12, Page 101	Graph shows the cyclic stress responses
Depth of max attack	53	μm	40, Table 3, Page 93	Burner rig tests - air to fuel ratio 25:1
Elongation	68	%	40, Table 4, Page 94	no exposure
	69	%	40, Table 4, Page 94	T = 595°C t = 100h
	67	%	40, Table 4, Page 94	T = 595°C t = 1000h
	67	%	40, Table 4, Page 94	T = 595°C t = 4000h
	61	%	40, Table 4, Page 94	T = 595°C t = 8000h
	34	%	40, Table 4, Page 94	T = 595°C t = 12,000h
	69	%	40, Table 4, Page 94	T = 650°C t = 100h

Mechanical Property	Value	Units	Reference	Notes
	37	%	40, Table 4, Page 94	T = 650°C t = 1000h
	33	%	40, Table 4, Page 94	T = 650°C t = 4000h
	28	%	40, Table 4, Page 94	T = 650°C t = 8000h
	32	%	40, Table 4, Page 94	T = 650°C t = 12,000h
	38	%	40, Table 4, Page 94	T = 705°C t = 100h
	33	%	40, Table 4, Page 94	T = 705°C t = 1000h
	36	%	40, Table 4, Page 94	T = 705°C t = 4000h
	35	%	40, Table 4, Page 94	T = 760°C t = 100h
	37	%	40, Table 4, Page 94	T = 760°C t = 1000h
	38	%	40, Table 4, Page 94	T = 760°C t = 4000h
	40	%	40, Table 4, Page 94	T = 760°C t = 8000h
	38	%	40, Table 4, Page 94	T = 760°C t = 12,000h
Elongation			51, Fig 3, Page 98	Graph shows the elongation after thermal aging
Elongation after rupture			54, Fig 2, Page 160	Graph shows the elongation after rupture
Fatigue behaviour			61, Fig 9, Page T14	Graph shows a comparison of the fatigue behaviour at 538°C
Fatigue behaviour			62, Fig 5, Page U10	Graph shows the influence on temperature and environment on the fatigue behaviour of Inconel 617
Fatigue crack growth behaviour			51, Fig 16, Page 102	Graph shows the fatigue crack growth behaviour
Fatigue crack growth rates			44, Fig 12, Page 460	Graphs show fatigue crack growth rates of long cracks for various high temperature alloys in air at room temperature and at 850°C
Fatigue life			51, Fig 10, Page 101	Graph shows the fatigue life in air and HTGR-helium
Impact energy			14, Fig 11, Page 258	Graph shows the impact energy after isothermal exposure at 900°C
Impact energy			47, Fig 1, Page 68	Graph shows the effect of exposures for 1000 to 15000h at 650 to 950°C on the RT impact energy
			47, Fig 2, Page 68	Graph shows the effect of exposures for 1000 and 3000h at 650 to 950°C on the RT impact energy
Impact energy			51, Fig 4, Page 98	Graph shows the impact energy at aging temperature after thermal aging
			51, Fig 5, Page 98	Graph shows the RT-impact energy after thermal aging
Impact strength	232	J	40, Table 4, Page 94	no exposure
	289	J	40, Table 4, Page 94	T = 595°C t = 100h

Mechanical Property	Value	Units	Reference	Notes
	302	J	40, Table 4, Page 94	T = 595°C t = 1000h
	245	J	40, Table 4, Page 94	T = 595°C t = 4000h
	133	J	40, Table 4, Page 94	T = 595°C t = 8000h
	94	J	40, Table 4, Page 94	T = 595°C t = 12,000h
	259	J	40, Table 4, Page 94	T = 650°C t = 100h
	47	J	40, Table 4, Page 94	T = 650°C t = 1000h
	47	J	40, Table 4, Page 94	T = 650°C t = 4000h
	54	J	40, Table 4, Page 94	T = 650°C t = 8000h
	52	J	40, Table 4, Page 94	T = 650°C t = 12,000h
	77	J	40, Table 4, Page 94	T = 705°C t = 100h
	65	J	40, Table 4, Page 94	T = 705°C t = 1000h
	65	J	40, Table 4, Page 94	T = 705°C t = 4000h
	76	J	40, Table 4, Page 94	T = 760°C t = 100h
	85	J	40, Table 4, Page 94	T = 760°C t = 1000h
	85	J	40, Table 4, Page 94	T = 760°C t = 4000h
	87	J	40, Table 4, Page 94	T = 760°C t = 8000h
	91	J	40, Table 4, Page 94	T = 760°C t = 12,000h
Impact toughness	229	J	9, Table 3, Page 99	Room temperature CVN impact toughness properties
Internal nitridation	>0.41	mm	41, Table 2, Page 117	Results of dynamic oxidation burner rig testing at 980°C for 1000h with 30 minute thermal cycling
Internal oxidation	0.07	mm	41, Table 2, Page 117	Results of dynamic oxidation burner rig testing at 980°C for 1000h with 30 minute thermal cycling
LCF results			14, Fig 8, Page 256	Graph shows the LCF results for Inconel 617
Linear damage accumulation			14, Fig 20, Page 263	Graph shows the linear damage accumulation for creep fatigue interaction
Low cycle fatigue behaviour			58, Fig 14, Page O19	Graph shows the influence of temperature on the low-cycle fatigue behaviour of IN 617
Low cycle fatigue behaviour			61, Fig 6, Page T13	Graph shows a comparison of the LCF behaviour of Inconel 617 in air and impure helium at 538°C
			61, Fig 7, Page T13	Graph shows a comparison of the LCF behaviour of Inconel 617 in air and impure helium at 704°C
			61, Fig 8, Page T14	Graph shows a comparison of the LCF behaviour of Inconel 617 in air and impure helium at 871°C

Mechanical Property	Value	Units	Reference	Notes
Mass change			40, Fig 2, Page 91	Graph shows the mass change vs. exposure time in air plus 5% water vapour at 1000°C
			40, Fig 3, Page 91	Graph shows the mass change vs. exposure time in air plus 20% water vapour at 1000°C
			40, Fig 4, Page 91	Graph shows the mass change in cyclic oxidation test at 1093°C vs. exposure time
			40, Fig 5, Page 92	Graph shows the mass change vs. exposure time for alloys exposed at 704°C in oxygen plus 4% sulphur dioxide
			40, Fig 6, Page 92	Graph shows the mass change vs. exposure time for alloys exposed to H_2-1%CH_4 at 1000°C for ~ 1000h
			40, Fig 7, Page 92	Graph shows the mass change vs. exposure time for alloys exposed to H_2-5.5%CH_4 - 4.5% CO_2 at 1000°C for ~ 1000h
Max tensile stress			8, Fig 10, Page 257	Graph shows the max. tensile stress at cycle nr. 200 vs. strain rate
Metal loss	24	μm	40, Table 3, Page 93	Burner rig tests - air to fuel ratio 25:1
Metal loss	0.17	mm	41, Table 2, Page 117	Results of dynamic oxidation burner rig testing at 980°C for 1000h with 30 minute thermal cycling
Nitrogen content	0.03	wt%	41, Table 3, Page 117	Results of bulk nitrogen and carbon analysis before testing
	0.52	wt%	41, Table 3, Page 117	Results of bulk nitrogen and carbon analysis after testing at 980°C for 1000h with 30 minute thermal cycling
Reduction in area			61, Fig 1, Page T10	Graph shows a comparison on the tensile properties of Hastelloy X and Inconel 617 in both solution annealed and aged conditions
Stationary creep rate			52, Fig 2, Page 106	Graph shows the stationary creep rate of Inconel 617 dependant on the uniaxial stress
Stress (ultimate), T_u	40	ksi	22, Table 2, Page 132	Nominal mechanical properties at 1600°F
Stress (yield), T_y	28	ksi	22, Table 2, Page 132	Nominal mechanical properties at 1600°F
Stress for rupture			15, Fig 2, Page 409	Graph shows the stress for rupture
Stress relaxation behaviour			51, Fig 13, Page 102	Graph shows the stress relaxation behaviour
Surface oxide depth			14, Fig 1, Page 194	Graph shows the surface oxide depth vs. temperature
Tensile elongation			9, Fig 10, Page 98	Graph shows the tensile elongation vs. temperature
Tensile strength	769	MPa	40, Table 4, Page 94	no exposure
	769	MPa	40, Table 4, Page 94	T = 595°C t = 100h
	803	MPa	40, Table 4, Page 94	T = 595°C t = 1000h
	810	MPa	40, Table 4, Page 94	T = 595°C t = 4000h
	838	MPa	40, Table 4, Page 94	T = 595°C t = 8000h
	910	MPa	40, Table 4, Page 94	T = 595°C t = 12,000h

Mechanical Property	Value	Units	Reference	Notes
	989	MPa	40, Table 4, Page 94	T = 650°C t = 100h
	920	MPa	40, Table 4, Page 94	T = 650°C t = 1000h
	979	MPa	40, Table 4, Page 94	T = 650°C t = 4000h
	993	MPa	40, Table 4, Page 94	T = 650°C t = 8000h
	993	MPa	40, Table 4, Page 94	T = 650°C t = 12,000h
	872	MPa	40, Table 4, Page 94	T = 705°C t = 100h
	952	MPa	40, Table 4, Page 94	T = 705°C t = 1000h
	952	MPa	40, Table 4, Page 94	T = 705°C t = 4000h
	872	MPa	40, Table 4, Page 94	T = 760°C t = 100h
	869	MPa	40, Table 4, Page 94	T = 760°C t = 1000h
	886	MPa	40, Table 4, Page 94	T = 760°C t = 4000h
	897	MPa	40, Table 4, Page 94	T = 760°C t = 8000h
	893	MPa	40, Table 4, Page 94	T = 760°C t = 12,000h
Tensile strength			54, Fig 2, Page 160	Graph shows the tensile strength vs. temperature
Tensile ultimate strength			9, Fig 9, Page 98	Graph shows the tensile ultimate strength vs. temperature
Tensile YS (0.2%)			9, Fig 8, Page 98	Graph shows the tensile YS (0.2%) vs. temperature
Tension-tension axial stress			40, Fig 11, Page 96	Graph shows the effect of grain size on the tension-tension axial stress controlled LCF properties of alloy 617
			40, Fig 12, Page 96	Graph shows the effect of temperature on the tension-tension axial stress controlled fatigue strength of alloy 617
	500	34.5 - 413.7 MPa cycles to failure	40, Table 6, Page 97	Effect of grain size (2.5) on tension-tension axial stress controlled LCF properties of alloy 617 at 760°C
	64,391	34.5 - 413.7 MPa cycles to failure	40, Table 6, Page 97	Effect of grain size (5.0) on tension-tension axial stress controlled LCF properties of alloy 617 at 760°C
	40,440	34.5 - 413.7 MPa cycles to failure	40, Table 6, Page 97	Effect of grain size (9.5) on tension-tension axial stress controlled LCF properties of alloy 617 at 760°C
Thermal gravimetric analysis			60, Fig 6, Page S10	Graph shows the thermal gravimetric analysis of corrosion in steam reformer atmosphere
Total depth of attack	>0.58	mm	41, Table 2, Page 117	Results of dynamic oxidation burner rig testing at 980°C for 1000h with 30 minute thermal cycling
Total elongation			61, Fig 1, Page T10	Graph shows a comparison on the tensile properties of Hastelloy X and Inconel 617 in both solution annealed and aged conditions

Mechanical Property	Value	Units	Reference	Notes
Ultimate tensile strength			61, Fig 1, Page T10	Graph shows a comparison on the tensile properties of Hastelloy X and Inconel 617 in both solution annealed and aged conditions
Uniform elongation			61, Fig 1, Page T10	Graph shows a comparison on the tensile properties of Hastelloy X and Inconel 617 in both solution annealed and aged conditions
UTS			51, Fig 2, Page 97	Graph shows UTS after thermal aging
Weight change	- 80.1	mg/cm^2	41, Table 2, Page 117	Results of dynamic oxidation burner rig testing at 980°C for 1000h with 30 minute thermal cycling
Weight change			51, Fig 8, Page 164	Graph shows the specific weight change at 950°C as a function of corrosion time
Yield strength			61, Fig 1, Page T10	Graph shows a comparison on the tensile properties of Hastelloy X and Inconel 617 in both solution annealed and aged conditions
Yield strength (0.2%)	319	MPa	40, Table 4, Page 94	no exposure
	321	MPa	40, Table 4, Page 94	T = 595°C t = 100h
	357	MPa	40, Table 4, Page 94	T = 595°C t = 1000h
	384	MPa	40, Table 4, Page 94	T = 595°C t = 4000h
	410	MPa	40, Table 4, Page 94	T = 595°C t = 8000h
	466	MPa	40, Table 4, Page 94	T = 595°C t = 12,000h
	357	MPa	40, Table 4, Page 94	T = 650°C t = 100h
	459	MPa	40, Table 4, Page 94	T = 650°C t = 1000h
	526	MPa	40, Table 4, Page 94	T = 650°C t = 4000h
	527	MPa	40, Table 4, Page 94	T = 650°C t = 8000h
	534	MPa	40, Table 4, Page 94	T = 650°C t = 12,000h
	405	MPa	40, Table 4, Page 94	T = 705°C t = 100h
	486	MPa	40, Table 4, Page 94	T = 705°C t = 1000h
	487	MPa	40, Table 4, Page 94	T = 705°C t = 4000h
	402	MPa	40, Table 4, Page 94	T = 760°C t = 100h
	388	MPa	40, Table 4, Page 94	T = 760°C t = 1000h
	401	MPa	40, Table 4, Page 94	T = 760°C t = 4000h
	403	MPa	40, Table 4, Page 94	T = 760°C t = 8000h
	389	MPa	40, Table 4, Page 94	T = 760°C t = 12,000h
			40, Fig 13, Page 96	Graphs show the effect of cold work and subsequent annealing temperature on the yield strength and grain size of alloy 617

Appendix B - Published Document Summaries

Reference 5: Advance Materials and Processes for Land-Based Gas Turbines (CMS X4, IN 792, MA M247 & SC 16)

This document reviews present research on materials technology for blade applications such as single crystal and directionally solidified superalloys, oxide dispersion strengthened superalloys, intermetallics, thermal barrier coatings and ceramics.

Reference 6: The Contribution of Advanced Materials to Future Aeroengines (CMSX4 & IN 100)

This document contains information on advanced materials for gas turbine engines. The alloy CMSX4 is one of the alloys under consideration for the tile material for the lining of the combustor wall.

The need to increase engine combustion temperatures to raise the efficiency and thrust if new engines has resulted in an enormous increase in the turbine efficiency temperature. It has therefore been necessary to develop alloys with greater temperature capabilities.

Reference 7: Low Cycle Fatigue Behaviour of Cast Nickel-base Superalloy IN-738LC in Air and in Hot Corrosive Environments

The low-cycle fatigue behaviour of as-heat treated IN738 LC is studied in this document in air and hot corrosive environments at 900°C and two different strain rates. The fatigue life was found to decrease as the environment became more severe and as the strain rate increased.

Reference 8: Evaluation of Alloys for Advanced High Temperature Reactor Systems (TZM, Inconel 617 & Hastelloy)

This document contains a review of alloy improvement and the development of new alloys to resist the effects of helium on the mechanical properties. The influence of neutron irradiation on the hot tensile and creep properties of absorber rod materials is also investigated.

Reference 9: Design of Wrought Nickel-Base Alloys for Advanced High Temperature Gas Cooled Rector Applications (IN 100, Inconel 617 & Hastelloy)

Alloys used for components in the High Temperature Gas Cooled Reactor (HTGR) are required to operate at temperatures of up to 1000°C for times approaching 30yrs. The alloys must withstand the corrosive effects of the impure helium environment and maintain elevated temperature strength. This document reviews the programme to develop wrought alloys having a better combination of corrosion resistance and high temperature strength. Ten Ni-Cr-Mo-W-Al-Ti-Zr-C alloys were fabricated, one of which showing significantly better properties than those of the commercial alloy Inconel 617.

The document also contains graphical data on Hastelloy X as a comparison.

Reference 10: Evaluation of High Temperature Alloys for Helium Gas Turbines (TZM, IN 713, MAR M004 & Nimonic 80A)

An extensive alloys development programme has been undertaken for materials for the HTR helium turbine. This is because of the high thermal and mechanical stresses the components are subjected to. The candidate alloys for turbine blades and hot ducts (nickel and molybdenum-base alloys) and for rotors (1% CrMoV and 12% chromium steels) have been tested under the expected services conditions.

The results of creep/rupture, fatigue, and fracture mechanics tests on turbine blades and rotor materials are presented in this document. Gas/metal reactions that occur in the simulated reactor coolant gas and the decontamination behaviour of components are also discussed. Also, the development of a molybdenum-base alloy for turbine blades is discussed in this document.

Other possibilities for blade materials and various tests are also covered in this document.

Reference 11: Materials for Advanced High Temperature Reactors (IN 713, M21, Inconel 617 & Hastelloy)

This document contains information about materials selection for high temperature reactors. The engineering development of reactors has been heavily dependent on materials innovation. The document contains irradiated mechanical data for various alloys including Hastelloy X.

Reference 12: PM Mo-TZM Turbine Blades - Demands on Mechanical Properties

This document contains information on the long term and short term mechanical properties of PM Mo-TZM. The properties investigated are: hardness and microstructure, tensile strength and ductility at 20°C, 850°C and 1000°C, impact energy, creep rupture behaviour and reversed bending fatigue.

Reference 13: The Development of ODS Superalloys for Industrial Gas Turbines (Inconel MA 6000)

Oxide Dispersion Strengthened (ODS) alloys retain useful strengths up to a relatively high fraction of their melting points. At the higher operating temperatures of advanced gas turbine engines, these alloys display long-term strength beyond the capabilities of conventional superalloys. Commercial alloys such as INCONEL alloy MA 6000 possess unique stress rupture behaviour characteristics. Two distinct regions of the rupture stress vs. time curves have been identified which together show that the higher design stresses for long-term service can be realised than predicted from only short term data.

INCONEL MA 6000 has excellent corrosion resistance in aerospace applications, however new ODS superalloys for industrial applications require extremely high corrosion resistance typical of IN939. Cyclic and isothermal oxidation tests were run at 1100°C on the prepared samples as well as burner rig hot corrosion tests at 927°C and 1097°C.

The results are discussed at length in this document.

Reference 14: Corrosion of Metallic Materials in HTR Helium Environments (Inconel 617)

This document summarises the main corrosion effects found in HTR-helium environments, especially those which could change the mechanical properties of component materials. It is shown that corrosion phenomena derive from the presence of low concentrations of the impurities H_2O, CO, CH_4 and H_2 in the helium which can produce oxidation, decarburisation and carburisation depending on the relative and absolute partial pressures of the impurities and the temperature.

Reference 15: High Temperature Alloys for the Power Conversion Loops of Advanced HTRs (TZM, IN 713 & Inconel 617)

This document surveys the high temperature alloys nuclear process heat plants in Germany and corresponding efforts for the gas turbine HTR in Germany and Switzerland. The service conditions in the different components are outlined and a survey of the candidate alloys for use at high temperatures is given. Alloys developed specifically for the HTR are also mentioned. The nature and extent if the work needed to select and characterise the alloys for the different applications are summarised in this document.

Reference 16: Creep and Stress Rupture – Long Term (IN 713 & Hastelloy)

This document contains evaluation of the creep rupture data of various superalloys. Time-Temperature Parameter (TTP) methods based on the theory of the thermally activated rate process are used to evaluate previously collected creep data from various sources. These sources include NRIM and JAERI. The data is also evaluated using strain-time behaviour.

Reference 17: Creep and Fatigue Crack Growth Behaviour of Some Cast Nickel-Base Alloys (IN 792 & IN 738)

The crack growth in various nickel-base alloys, IN792, IN738 and Rene 80 under cyclic and static loads are investigated using fracture mechanics type specimens. The influence of the environment (air, vacuum and impure helium) is also considered.

The chemical compositions of the investigated alloys and the standard heat treatments are listed in Tables 1 and 2 respectively. IN792 was developed for higher strength at the expense of corrosion resistance. Compared with IN738, IN792 contains higher amounts of niobium, tantalum, cobalt, tungsten and titanium, a lower amount of chromium and in addition hafnium. Rene 80 is similar to IN792 but contains more carbon and chromium but no niobium, tantalum or hafnium.

The results of the tests and analysis of the figures are discussed at length in this document. The results of the tests of IN792 are compared to those performed on IN738 and Rene 80.

Reference 18: **The Effect of Oxygen and Water Vapour on Time Dependent Crack Propagation and Crack Tip Oxide Scale Formation in Nickel Base Gas Turbine Disk Alloys (IN718)**

In this document, high temperature sustained load crack propagation testing was performed, under controlled oxygen and water vapour partial pressures, on specimens taken from Alloy 718 and Rene 88DT forgings. The document contains graphical data on the crack propagation rate and crack growth rate.

Reference 19: **Sprayformed Materials for Disc Applications (MA M247 & Udimet 720)**

This document specifically relates to the utilisation of MAR M247 and Udimet 720 as disc materials. MAR M247 is not selected as a disc material for this turbine but some of the general tests on the material performed in this study may be relevant to this project. Udimet 720 is selected as a disc material for this turbine.

Reference 20: **High Temperature Static and Fatigue Crack Growth of INCONEL Alloy 706**

In this study, static and fatigue crack growth rates of alloy 706 were determined at 538°C and 649°C. The test material was produced by two different heat treatments. The static and fatigue crack growth resistance of alloy 706 was found to be comparable to alloy 718. Materials were examined using optical metallography, scanning electron and transmission electron spectroscopy and the crack growth behaviour was correlated to the microstructure.

Reference 21: **The Effect of Intergranular Eta Phase on LCF in Alloy 706**

This document looks at possible mechanisms of intergranular h phase precipitation in very large forgings which alloy 706 is typically used for. A range of aging heat treatments are examined and their impact on 399°C LCF evaluated. In addition, subscale forgings that stimulate heat-up and post solution cooling rates found in full scale forgings were used to generate test materials for tensile and LCF evaluation. The effect of the environment was evaluated through comparisons of 399°C LCF tests conducted in air and in a vacuum.

This document contains extensive mechanical properties data on Alloy 706 at various temperatures.

Reference 22: **Extending the Limits of Welding Nickel-based Superalloys (IN738 & Inconel 617)**

This document contains a welding study on “serviced” turbine blades in restrained conditions performed and evaluated by stress rupture, impact, cyclic oxidation and thermal mechanical fatigue (TMF) testing. Commonly used base materials for large gas turbine blades (U520, IN738 LC and GTD 111 DS) were chosen for this welding study.

Reference 23: **High Temperature Low Cycle Fatigue of IN738 and Application of Strain Range Partitioning**

This document investigates the effect of strain rate and strain wave shape on high temperature low-cycle fatigue life of cast IN738 nickel base superalloy at 1123K. The test results were analysed by the SRP method.

Reference 24: **The Effect of Hot Corrosion on Creep and Low-Cycle Fatigue in the Cast Nickel-Base Superalloy IN738 LC**

This document contains a study on the creep and low-cycle fatigue of IN738 as a function of the environment. Creep tests were conducted in air, both with and without a deposited layer of 25%NaCl 75%Na2SO4 between 850°C and 950°C and 275 – 375 MPa.

Reference 25: **Deformation Behaviour and Microstructural Evolution in IN738 LC Under LCF Loading**

This document contains the results of low cycle fatigue (LCF) tests conducted on the nickel-base superalloy IN738 LC at 10-3s-1 and 10-5s-1 strain rates at 950°C. Two unimodal γ' distributions in the material with an average size of 80nm and 450nm, respectively, were used in the work. The implications for mechanical properties and dislocation structure are discussed.

Reference 26: **High Temperature Low-Cycle Fatigue Behaviour of IN738 LC Alloy in Air and in a Vacuum**

This document contains the results of high temperature low-cycle fatigue tests carried out on alloy IN738 LC in air and in a vacuum. Optical and scanning electron microscopy observations were used to determine the results. The fatigue life was found to be longer in tests carried out under vacuum conditions than on tests carried out in air.

Reference 27: **Prediction of Intergranular Failure in NiCr based Alloys in Low Cycle Fatigue at High Temperatures (IN738)**

Specimens of IN597 and IN738 LC were tested mainly at 850°C using various strain-limited cycles including those with dwell periods in tension, compression or both. Post-test metallographic examination including measurements of damage due to cracks and cavities was carried out. The aims of this work were to characterise the low-cycle fatigue (LCF) behaviour of the cast IN738 LC alloy, assess predictive schemes for LCF performance and to examine the accumulation of microstructural damage during LCF deformation in IN597 and IN738 LC.

Reference 28: **Strain Range Partitioning Behaviour of the Nickel-Base Superalloys, Rene' 80 and IN100**

This document assesses the ability of the method of Strainrange Partitioning (SRP) to both correlate and predict high-temperature, low-cycle fatigue lives of nickel base superalloys for gas turbine applications.

Reference 29: Low-Cycle Fatigue Behaviour of IN100: Strainrange Partitioning Method

The elevated temperature, low cycle fatigue behaviour of the gas turbine disk alloy IN100 is evaluated in this document using the Strainrange Partitioning method. In this investigation, PP and CP curves were developed for gatorised IN100 at 649°C, mean strain equal to half maximum strain.

Reference 30: Applicability of the SRP Method and Creep-Fatigue Damage Approach to the LCHTF Life Prediction of IN100 Alloy

This document contains a comparison of the actual capabilities of two life prediction methods in the low cycle high temperature regime. These methods are; the strain range partitioning method and the continuous damage approach which are evaluated for IN100 alloy at 900°C and 1000°C.

Reference 31: Appendix A1 of AGARD Conference Proceedings No. 243, Characterization of Low Cycle High Temperature Fatigue by the Strain Range Partitioning Method (IN700, IN738 & Hastelloy)

This document contains a tabulation of the high-temperature, low-cycle, creep fatigue results generated by the laboratories participating in the SRP evaluation program. Also contained are the chemical compositions, material processing and heat treatments and the conventional mechanical properties for each alloy tested.

Reference 32: High Temperature Low-Cycle Fatigue of Inconel MA 6000

This document contains information about the fatigue behaviour of Inconel MA 6000. The document also contains cyclic deformation curves, cyclic stress-strain curves and cyclic life data as a function of the applied strain rate for a temperature range 760°C–1050°C. At 850°C the high strain fatigue results are correlated with high cycle fatigue data and compared to the performance of IN738 LC. Microstructural analysis is also recorded in this document.

Inconel MA 6000 is a candidate material for demanding high-temperature environments (such as HTRM).

The data collected is discussed at length in this document.

Reference 33: High Temperature Low Cycle Fatigue Properties of Superalloy MA 6000

This document contains the low cycle high temperature fatigue properties of oxide dispersion strengthened superalloy MA 6000 studied at 850°C and 1050°C at different strain amplitudes and strain rates. The cyclic hardening curves, Coffin-Manson plots and CSS-curves are determined at both temperatures and are presented with SEM and TEM analysis.

Reference 34: Research and Development on Heat Resistant Alloys for Nuclear Process Heating in Japan (Hastelloy)

This document reviews the developments of the last decade for heat resistant alloys in application to the high temperature structural components of the process heating high temperature gas cooled reactor. One of the alloys reviewed is Hastelloy XR.

Hastelloy XR was subjected to a series if engineering tests for the preparation of a design database. The tests, which were carried out in a reactor environment were corrosion and carbon transfer, corrosion product transfer and radioactivation, creep and rupture properties, low cycle fatigue and crack growth and toughness after aging under isothermal or cyclic heating conditions, with or without sustained stress. These results were obtained other sources and analysed in this document.

The data was evaluated to determine it's chemical compatibility and it's high temperature mechanical properties. The results are discussed at length in the document.

The creep rupture performance if the candidate alloys is investigated as is the corrosion resistance and the corrosion in a reducing gas.

Reference 35: Application of New Design Methodologies to Very High Temperature Metallic Components of the HTTR (Hastelloy)

This document covers the design methodologies for an HTTR which can separate the heat-resistant function from the pressure retaining functions and allow them to expend freely. The Japan Atomic Energy Research Institute (JAERI) has been performing design and research works on their verifications.

Some design methodologies have been applied to the very high temperature components of the HTTR so as to reduce mechanical and thermal loads or to lower their service temperatures. The service conditions of the components are now categorised as a) low temperature / high pressure or b) high temperature / low pressure. Hastelloy XR is a high temperature / low pressure material.

The mechanical properties of Hastelloy XR have been characterised from a large amount of material testing and structural mechanics testing data. Design allowable limits for Hastelloy XR have been specified in the high temperature structural design code for class 1 components for the HTTR.

Reference 36: Superalloy Developments for Aero and Industrial Gas Turbines (CMS X4 & MA M247)

This document discusses selected Ni-based alloy development activity which is primarily undertaken for the specific materials requirements identified for emerging civil aero engine turbines and industrial engines.

The alloy CM 247 LC is derived from MA M247. This document compares the properties of the two alloys.

CMS X4 is a re-containing modification of the CMS X2 alloy. CMS X4 has reduced Cr and W content and increased Co content. This alloy exhibits the improved properties desired for advanced turbine blade and vane requirements.

The document concludes that superalloy development will continue to provide the turbine and engine industries with new materials which will in turn improve turbine and engine efficiency.

Reference 37: Effect of Material Degradation on Mechanical Properties of Cast Ni-Base Superalloy IN738 LC

As a basis of developing a materials degradation assessment system for gas turbine buckets, the effects of materials degradation on the mechanical properties of a gas turbine bucket alloy IN738 LC were investigated by evaluating the long time aged materials at 850°C - 900°C. This document contains data on changes in the hardness, tensile strength , 0.2% yield stress, diameter, density, creep rate and rupture life.

Reference 38: Degradation of High Performance Aero-Engine Turbine Blades (IN713)

This document reviews common forms of damage incurred by cast turbine blades in high performance aero engines. The document reviews thermal fatigue damage, oxidation damage, hot corrosion damage and over temperature damage.

Reference 39: Creep Behaviour of Industrial Turbine Blade Materials (IN738)

This document reviews the creep behaviour of blade materials such as cast IN738 LC.

Reference 40: Recent Advances in the Enhancement of Inconel Alloy 617 Properties to Meet the Needs of the Land Based Gas Turbine Industry

This document reviews the improvements in high temperature strength, LCF behaviour and cyclic oxidation resistance available from Inconel alloy 617. Tests performed include oxidation tests, oxygen-sulphur dioxide tests, carburisation tests, burner rig tests, metallurgical stability, weldability and formability. The document also contains data on the mechanical properties before and after exposure to elevated temperatures.

Reference 41: Nitridation of Several Combustor Alloys in a Simulated Gas Turbine Combustion Environment (Inconel 617 & Hastelloy)

This document contains an investigation of Ni base combustor alloys in a simulated gas turbine combustion atmosphere generated by a dynamic oxidation burner rig (980°C, 1000h & 30 minute thermal cycling). Internal nitridation was found to be a predominant type of attack for Inconel 617, Haynes 263 alloy and Hastelloy X. Haynes 230 alloy exhibited little nitridation attack. Other types of attack such as oxide spallation, metal loss and other internal oxidation are also discussed.

Reference 42: Interactions of Corrosion and Mechanical Properties (IN100 & IN738)

This document contains a review of investigations into corrosion/creep interactions in high temperature alloys exposed to corrosive environments. After a brief consideration of some essential problems met in creep testing in aggressive environments, the influence of oxidising, carburising and sulphidising conditions encountered in either single or multi-component environments is discussed.

Reference 43: Creep Dominated Damage Processes (IN738)

This document contains creep and stress rupture properties investigated in various COST-programs. The main emphasis is put on the cast superalloys IN738 LC and IN939. The effects of the microstructure, pre-treatments and the environment on the above mentioned properties are investigated.

Reference 44: Fatigue Dominated Damage Processes (IN100, IN738, Inconel 617 & Hastelloy)

This document reviews the damage processes in high temperature engineering alloys at elevated temperatures, drawing where possible on results obtained in the framework of COST 50 and COST 501. This paper considers the bulk and localised damage modes which consecutively appear with evolving life fraction, including dislocation substructures, microcrack nucleation, microcrack extension and microcrack growth.

The paper also reviews the effect of time dependant deformation, environmental attack and microstructural instabilities on the deformation mechanisms, the damage modes and the damage rates.

Reference 45: Effect of Fabrication and Repair Procedures on the Performance of IN738 LC and IN939

This document describes the results of a collaborative programme in COST 50 to establish a database in order to compare the properties of IN738 LC or IN939 after welding and joining. Properties investigated include hot corrosion resistance, fatigue behaviour, creep and stress rupture properties.

Reference 46: High Temperature Alloys for the HTGR Gas Turbine: Required Properties and Development Needs (TZM, IN100, IN713, M 21, MAR M004 & Nimonic 80A)

This document contains information on criteria for materials selection for the HTGR. Creep fatigue, fatigue and environment effect and creep-fatigue and environment effect are considered. The document then considers materials for the turbine disks and the turbine blades. The effect of the environment and the long term materials properties are also reviewed.

Reference 47: Thermal Stability and Environmental Compatibility (Inconel 617)

The thermal stability and environmental compatibility of Inconel 617, a prime nuclear process heat steam reformer candidate alloy, are described in this paper. Room temperature tensile and toughness data and microstructural information for Inconel 617 specimens at elevated temperature are presented. The document also contains the results of gas corrosion experiments. The results include carbon analyses and optical and scanning electron microscopy.

Reference 48: Corrosion Behaviour of High Temperature Alloys in the Cooling Gas of High Temperature Reactors (Inconel 617)

Reactive impurities in the primary cooling helium of advanced high temperature gas cooled reactors (HTGR) can cause oxidation, carburisation or decarburisation of the heat exchanging metallic components. This document reviews extensive test programmes with exposure times if up to 30,000 hours which have been used to construct a database which allows a reliable extrapolation of the corrosion effects up to the envisaged service lives of the heat exchanging components.

Reference 49: Current Status of Studies on High Temperature Metallic Materials for HTGR Applications in JAERI (Hastelloy)

The target alloys for applications in the High Temperature Engineering Test Reactor (HTTR) require comprehensive qualification tests on properties such as creep, fatigue, corrosion resistance and other fracture relevant properties. These tests have been carried out on Hastelloy XR, which is a modified version of Hastelloy X, have been carried out to accumulate the data for structural design and safety evaluation.

The items of research activities carried out are classified into three different categories; near-term target structural alloys, long-term target heavy duty structural alloys and cladding materials of neutron absorber rods.

The document concludes that for the near term target alloy for the HTTR, Hastelloy XR-II will replace the present Hastelloy XR gradually for future comprehensive qualification tests.

Reference 50: High Temperature Low-Cycle Fatigue Strength of Hastelloy XR

This document describes the low-cycle fatigue and creep fatigue interaction properties of Hastelloy XR in air and helium containing a small quantity of impurity gas. The test results are compared with the fatigue property of Hastelloy X which is the original alloy of Hastelloy XR

Hastelloy XR is an improvement of Hastelloy X developed by JAERI. At present, Hastelloy XR is the leading structural material for the HTGR in Japan.

The results and analysis are discussed at length in this document.

Reference 51: **Evaluation of Mechanical Properties of the Alloy NiCr22Co12Mo (alloy 617) for Heat Exchanging Components of HTGRs**

This document contains the following experimental results performed on alloy 617:

creep and creep rupture tests
fatigue and creep/fatigue tests
short term mechanical tests after thermal aging

Additional creep and fatigue crack growth experiments were carried out for leak before break argumentations.

Reference 52: **Multiaxial Creep of Tubes of Alloy 800 and Alloy 617 at High Temperature**

This document contains a mathematical description of the creep deformation of a multiaxial loaded component of alloy 800 and alloy 617. The document contains information about uniaxial creep, multiaxial creep, lifetime estimation and deformation behaviour.

Reference 53: **Fatigue Properties of Nickel-Base High Temperature Alloys for HTGRs (Hastelloy)**

This document details a series of strain controlled low-cycle fatigue tests conducted at temperatures ranging from room temperature (RT) to 900°C on nickel-base high-temperature alloys, namely Hastelloy XR and Hastelloy XR-II, which are candidate alloys for HTGR applications. Tests were conducted in a simulated HTGR environment with the exception of those conducted in air at room temperature (RT). The effects of strain rate, hold time, aging and test temperature on the fatigue properties were investigated.

The results of the tests and analysis and comparisons between Hastelloy X, Hastelloy XR and Hastelloy XR II are discussed at length in this document.

Reference 54: **The New Alloy Thermon 1492 (NiCr22W12Fe) for High Temperature Reactors (Inconel 617)**

This document contains experimental test results carried out in PNP helium for durations up to 2000 h in the temperature range 750 – 950°C for the new alloy Thermon 1492. The mechanical and creep-rupture properties are compared to those of Inconel 617.

Reference 55: **Development and Testing of Alloys for Primary Circuit Structures of a VHTR (Inconel 617 & Hastelloy)**

This document contains information on commercially available high temperature alloys such as Hastelloy XR. The topics involved are; corrosion and carburisation, evaporation, creep and fatigue, radioactivity generation by corrosion, microstructural stability and age embrittlement and the effects of thermal neutron irradiation on the mechanical properties at elevated temperatures.

These results are discussed at length in this document. The document concludes that there is a necessity to establish a reasonable common methodology basis on conducting tests in well-defined environment conditions

Reference 56: Interaction of Metals with Primary Coolant Impurities: Comparison of Steam Cycle and Advanced HTGRs (Inconel 617 & Hastelloy)

This document contains a study of the carburisation behaviour of Incoloy 800H, Inconel 617 and Hastelloy X in helium containing various amounts of H_2, CO, CH_4, H_2O and CO_2. Corrosion tests were conducted in a temperature range from 649°C to 1000°C for exposure times of up to 10,000h. Thermodynamic analyses were also performed. The results suggested that controlling the oxygen potential of the service environment can be an effective means of reducing the carburisation of alloys.

Reference 57: Relationship Between Carburization and Zero-Applied-Stress Creep Dilation in Alloy 800H and Hastelloy X

Typical candidate alloys can carburise when exposed to simulated service environments. The carbon concentration gradients so formed give rise to internal stresses which could cause dilation. Studies performed with Hastelloy X and Alloy 800 H showed that dilations of up to almost 1% can occur at 1000°C when carbon pickup is high. Dilation was normally observed only when the carbon increase was >1000 µg/cm2 and ceased when the diffusing carbon reached the centre of the specimen.

Reference 58: Properties of Materials for the High Temperature Helium Turbine Under Mechanical and Thermal Loading (TZM, IN713 & Inconel 617)

This document contains controlled impurity helium, air creep rupture and fatigue test results of candidate blade and linear materials for application in the HTGR direct cycle helium gas turbine.

Reference 59: Weldability Evaluations and Weldment Properties of Hastelloy X

This document contains studies of weldability and weldment properties on commercial heats of Hastelloy X. Evaluation methods employed included hot cracking susceptibility and tensile and creep properties measured both before and after aging at 593 to 871°C for up to 10,000h.

Reference 60: Materials Behaviour in Methane Reforming Gas (Inconel 617 & Hastelloy)

This document contains the following evaluation tests in process gas in the temperature range of 800 – 950°C:

- Corrosion tests up to 20,000h
- Thermogravimetric evaluations
- Creep rupture tests to be continued up to 30,000h in single and multi-specimen creep machines
- Component tests in a high temperature tube test facility at high pressure

The test materials are solid solution hardening steels and nickel base alloys which are available or will be available in the near future as wrought and cast reformer tubes.

Reference 61: High Temperature Low-Cycle Fatigue and Tensile Properties of Hastelloy X and Alloy 617 in Air and HTGR-Helium

This document contains the results of strain controlled fatigue and tensile tests for two nickel base solution hardened alloys (Hastelloy X and Inconel 617). These materials were tested at temperatures ranging from room temperature to 871°C in air and impure helium. The samples were tested on the solution annealed as well as in the pre-aged condition. Comparisons are given between the strain controlled fatigue lives of these alloys and several other commonly used alloys all tested at 538°C.

Reference 62: Fatigue and Creep-Fatigue Behaviour of high-Temperature Alloys for HTR-Application (Inconel 617 & Hastelloy)

The development of High Temperature Gas-Cooled Reactors requires the evaluation of the fatigue behaviour of those alloys which have been taken into account for possible use as structural materials. This document contains the results of fatigue tests of 6 wrought alloys including Inconel 617 and Hastelloy at 850°C.

Reference 63: Turbines for Motor Vehicles (Nimonic 80A)

This document contains a review of the metallic turbine materials available for motor vehicle turbines. The properties of various superalloys are compared to some silicon based engineering ceramics.

Reference 64: Materials Advancements in Land-Based Gas Turbines (CMSX4)

This document reviews the evolution of materials technology and the bill of materials in the current generation of turbines along with remaining concerns about their reliability from a user perspective.

This document does not greatly detail in the context of turbine blades which is what they are all selected for in the HTRM turbine. However the document does provide general materials information on CMS X4 among others.

Reference 65: Ballistic Penetration Testing of the Contaminant Wall of a Marine Gas Turbine (IN718)

This paper considers alternative gas turbine containment designs for the prevention of consequential damage in the event of turbine disk failure. The data in this document includes calculation of the fracture energies of turbine casing (IN718) and external bandage.

Reference 66: Development of Diffusion Barriers for the Superalloy Blades of Gas Turbine Blades (IN738)

This document reviews the development of diffusion barriers for nickel base superalloys for the temperature range of 1000-1100°C. The document contains data on the thermal expansion and melting points of various materials including Inconel 738. Also presented are the tensile test results for coated samples.

Reference 67: Development of Brazing Techniques for the Joining of Single Crystal Components (CMS X4)

This document details the differences in the strength of the joints between CMS X4 components and those between MAR M002. The joints between MAR M002 components are found to be significantly stronger despite using the same braze alloy and conditions.

Reference 68: Precipitation and Deformation Behaviour of Cast 718 During Creep and Thermal Exposure (IN718)

This document contains an investigation of precipitation, deformation and fracture behaviour of cast alloy 718 during creep-rupture tests in comparison with thermal exposure tests. The creep tests were performed between 704°C and 871°C in the stress range 80 – 520 MPa. The thermal exposure tests were performed at the same temperatures for 50, 300, and 500 hrs in air.

Reference 69: A Study of the Role of (Nb, Ti)C Carbides in Fatigue Crack Initiation in Inconel 718 at 20°C and 600°C

This document contains the results of testing U-notch specimens of IN718 taken from an extruded bar and tested at 600°C in air using trapezoidal waveforms with 1 and 30 second dwells at maximum dwell. Additional tests were performed on plain bend bars at room temperature, comparing as-polished specimens with specimens thermally exposed at 600°C to promote oxidation of primary carbides.

Reference 70: Description of the Mechanical Behaviour of the Single Crystal Alloy CMSX4

This document derives equations to explain the deformation behaviour of anisotropic single-crystal blades taking into account the modifications to the deformation processes caused evolution of the microstructure during service. The viscoplastic deformation is divided into two temperature regimes; low temperatures below 800°C and high temperatures >850°C.

Reference 71: Constitutive Modelling of the Single Crystal Superalloy CMS X4 for Industrial Gas Turbine Applications

This document examines a model to predict the anisotropic deformation behaviour of the commercially available alloy CMS X4. The model is based on a crystallographic slip formulation. The model was adjusted to uniaxial deformation data and verified by comparing with experimental data for multiaxial stress rates.

The deformation modelling activities presented in this document concentrate on the aspects of deformation of CMS X4 that are relevant to industrial gas turbine blades.

Reference 72: High Temperature Creep of CMS X4 Effect of Precipitate Orientation and Morphology

This document contains investigations of the anisotropy of single crystal deformation in turbine blades. For the temperatures at which the turbine blades operate the g'-precipitates within the g–matrix are known to directionally coarsen. Microstructural examination showed that the coarsening in the low stresses and orientated specimens eventually led to the g' precipitates becoming the continuous phase.

As the initial stress is reduced, the anisotropy of the orientations is increased with regard to creep rupture life for CMS X4 at 1223 K.

Reference 73: Corrosion Behaviour of High Temperature Alloys in Impure Helium Environments (Hastelloy)

This document contains the results of corrosion tests with Ni-base high temperature alloys carried out at 900 and 950°C in simulated high temperature reactor helium environments. It is shown that the carburisation and decarburisation behaviour is strongly affected by the Cr and Ti (Al) contents of the alloys. The experimental results obtained are compared with a recently developed theory describing corrosion of high temperature alloys in high temperature reactor helium environments.

Reference 74: Corrosion of High Temperature Alloys in the Primary Circuit Helium of High Temperature Gas Cooled Reactors: Part II: Experimental Results (Hastelloy)

This document shows how a stability diagram for a commercial alloy can be constructed and how this can be used to correlate the corrosion results with the main experimental parameters, temperature, gas and alloy composition.

Reference 75: ATS Land Based Turbine Casting Initiative (CMS X4)

As the casting size increases, the total number of defects and variation in properties increase with the surface area and volume of the material.. These property variations have been shown to impart additional cost and performance penalties. This document contains mechanical test results on CMSX-4.

Reference 76: Environmental Effect on the Low-Cycle Fatigue Behaviour of Cast Nickel-Base Superalloy IN738 LC

The effect of the environment on the high temperature low-cycle fatigue (LCF) of superalloys is very severe. In this document, the LCF of IN738 LC is studied at 900°C in a vacuum and compared with the results of tests carried out in air and on specimens coated with a layer of NaCl + Na2SO4 .

Reference 77: Design Criteria for High Temperature Metallic and Ceramic Components as well as for Pre-Stressed Concrete Pressure Vessels of Future HTR-Plants

The text in this document is entirely in German. However the document does contain information on specific materials used in the German HTR Programme.

Reference 79: High Temperature Multiaxial Low-Cycle Fatigue of Nickel Base Superalloys

This document describes the tension-torsion multiaxial low cycle fatigue of conventional cast, directionally solidified and single crystal superalloys.